LARGE SCALE CARBOTHERMAL SYNTHESIS OF SUBMICRON SILICON NITRIDE POWDER

Serge Grenier

Department of Mining and Metallurgical Engineering
McGill University,
Montreal, Canada.

May 1992

A Thesis submitted to the Faculty of
Graduate Studies and Research
in partial fulfillment of the
requirements for the degree of
Master of Engineering

Ã ma mère...pour avoir eu la patience de m'élever,

Ã mon père...pour avoir eu la patience de m'écouter,

Ã ma soeur...pour m'avoir appris à aimer les femmes à leur juste valeur,

Ã Mathieu...pour m'avoir appris à aimer les bébés,

Au 12 janvier 1991 !!!

ABSTRACT

The synthesis of silicon nitride (Si_3N_4) by carbothermal reduction of silica was found to be very sensitive to the processing steps used for the starting materials (SiO_2, C) and to the reaction conditions. It was found that a good degree of intimacy between the starting materials was required in order to obtain fine ceramic powders. This was best achieved by attrition milling the precursors with ZrO_2 media for 0.5 to 4 hours. Due to its lower wear rate, ZrO_2 media proved to be superior to both Si_3N_4 and Al_2O_3 media.

The formation of Si_3N_4 was known to occur over a narrow temperature range (1450-1550°C). Experiments showed that, indeed, full conversion of SiO_2 occurs only in this temperature range. Below 1450°C the reaction proceeds at an extremely slow rate, while above 1550°C, silicon carbide forms. The morphology of the silicon nitride powder produced was also shown to vary widely depending on the reaction temperature. The silicon nitride grains synthesized at 1490°C were equiaxed, while those produced at a slightly higher temperature, 1540°C, were acicular.

The amount and morphology of the silicon carbide formed proved to be very sensitive to impurities present in the precursors prior to the reaction. The nitrogen flow rate during reaction as well as the position of pellets in the reactor played a key role in the final SiC content of the powder.

The addition of 5 weight % UBE silicon nitride powder (0.2 μm) as seed in the starting materials resulted in a definite decrease in the overall grain size of the silicon nitride powder produced. Also, seeding the precursors resulted in silicon nitride powders with narrow size distribution, as opposed to a bimodal size distribution for the unseeded ones.

One of the best commercially available Si_3N_4 powder (UBE) together with two large batches of silicon nitride powder made by carbothermal reduction were pressed and sintered into bars. The bars were then broken and their bend strengths were evaluated. The results showed that, although not as high as UBE (637 MPa), the strength values of the two carbothermal powders were excellent (507 and 577 MPa) considering their lower sintered densities which was the result of residual carbon present in the powder.

RÉSUMÉ

Il est démontré que la synthèse du nitrure de silice (Si_3N_4) par la réduction carbothermique de la silice est très sensible aux différentes étapes de préparation des réactifs (SiO_2, C) ainsi qu'aux conditions de réaction. Un excellent degré de mélange du carbone et de la silice s'est avéré essentiel afin d'obtenir une fine poudre de nitrure de silicium. Ceci a été réalisé en mélangeant les réactifs par attrition avec des billes d'oxyde de zirconium (ZrO_2) pour une durée de 0.5 à 4 heures. A cause de leur faible taux d'usure, les billes de ZrO_2 se sont avérées supérieures à celles en oxyde d'aluminium (Al_2O_3) ou encore, à celles en Si_3N_4.

Il avait précédement été démontré que la formation de Si_3N_4 a lieu seulement entre 1450 et 1550°C. Les expériences effectuées dans cette thèse ont corroboré que la conversion complète de la silice en nitrure de silicium n'a lieu que dans ce mince intervale de température. Sous 1450°C la cinétique de formation du nitrure de silicium est extrêmement lente, alors qu'au-dessus de 1550°C, le carbure de silicium (SiC) commence à se former. La morphologie des grains de Si_3N_4 formés à 1490°C s'est avérée équiaxiale (sphérique) alors qu'à 1540°C, les grains ont adopté une morphologie nettement aciculaire.

L'ensemencement par addition de 5 % par masse de fines particules (0.2 μm) de Si_3N_4 (UBE) s'est traduit par un net décroissement de la taille des grains de nitrure de silicium produits. Une autre conséquence de l'ensemencement a été d'uniformiser la distribution de la taille des grains; comparativement à une distribution bimodale pour les poudres de nitrure de silicium produites sans

ensemencement.

Deux poudres de nitrure de silicium synthétisées par réduction carbothermique, ainsi que l'une des meilleures poudres présentement disponible sur le marché (UBE) ont été compactées et frittées sous forme de barres. Les barres ont ensuite été brisées afin de mesurer la force de pliage (bend strength). Les résultats indiquent une force de rupture légèrement inférieure pour les poudres carbothermiques (507 et 577 MPa) comparativement à UBE (637 MPa). Ces résultats sont excellent si l'on tient compte des densités finales inférieures des poudres carbothermiques causées par un traitement de décarburisation non-optimisé.

ACKNOWLEDGEMENTS

I would like to express my sincere gratitude to Professor R.A.L. Drew for his supervision and encouragements throughout the course of this thesis, and to Dr. K. Shanker for his advice, assistance and expert opinion.

Special thanks goes to J.R. McDermid for ideas and suggestions, as well as to Dr. M.D. Pugh for technical advice.

I would also like to show my appreciation to Martin Knoepfel and Bruno Grondin for their instruction and guidance in the construction of several pieces of equipment.

Thank you also to Dr. Tilley of Sherritt Gordon Laboratories for performing XRF analysis and to *Fonds pour la Formation de Chercheurs et l'Aide à la Recherche* (FCAR) for providing a scholarship to help support this thesis.

Last, but certainly not least, I would like to thank E. Benguerel and D. Filippou from the hydrometallurgy group and all my colleagues in the ceramics group, in particular Y. Baik, D. Muscat, A. Hadian, L. Edovas and M. Xun, for their contribution by way of help, support and personal expertise.

TABLE OF CONTENTS

LIST OF FIGURES

LIST OF TABLES

1. INTRODUCTION

Advanced ceramics include a wide variety of materials based on silicon carbide, silicon nitride, zirconia, and alumina. These materials combine the traditional advantages of ceramics, such as high hardness, good heat resistance, and chemical inertness, with the ability to withstand a significant tensile stress. While fabricated in a manner similar to that for traditional ceramics, the higher performance of advanced ceramics is a result of strict control of purity, composition, microstructure, and processing.

Advanced ceramics can be separated into two categories; those used for electronic applications which make up >84% of the world ceramics market, and those used for structural applications sharing the remainder of the market. Electronic applications range from SiC resistors, to AlN substrates and from $BaTiO_3$ ferroelectrics to ZrO_2 oxygen sensors, while the structural applications include TiC coated machining tools, Si_3N_4 valves, and SiC turbocharger rotors to name a few.

The commercialization of advanced structural ceramics has not occurred as rapidly as anticipated. The slower growth in development is directly related to technical problems associated with the production of reliable, reproducible, and cost-competitive ceramic products. These problems stem from the inherent brittleness of ceramics and their sensitivity to small flaws introduced during processing and in service[1]. With a conservative estimate of the potential market of between $1 billion and $5 billion by the year 2000[2] and a more optimistic potential market of $24.5 billion by 1995[3], solutions to these problems

are the focus of intense research worldwide.

Because the starting powder determines the ultimate quality of a ceramic part, there is a need to develop improved starting powders with high chemical purity and controlled particle sizes. Ceramic powders should be very fine (<1μm) in order to have good sinterability and, at the same time, the grains should be equiaxed in order to improve the green density (better packing) and hence, increase the particle-particle contacts before sintering.

For Si_3N_4 powders, not only should the above requirements be fulfilled but also, since Si_3N_4 is a non-oxide ceramic, its oxygen content should be carefully controlled. Oxygen compounds such as SiO_2 (melting point of silica = 1728°C) present with the Si_3N_4 at the sintering temperature (1650-1800°C) will melt and surround the Si_3N_4 grains by forming a liquid (or glassy) phase, particularly in conjunction with other oxide sintering aids. A small amount of oxygen is, however, desirable (<5 weight %) since the oxygen-based glassy phase that will form at the sintering temperature is instrumental in helping the Si_3N_4 densification. This increases the mass transfer rates of Si and N atoms (otherwise slow since Si and N atoms are strongly bonded together with covalent bonds), and also provides a medium into which α-Si_3N_4 grains can dissolve and reprecipitate as β-Si_3N_4 grains (section 2.1.2.2). On the other hand, excessive amounts of oxygen will result in a glassy phase occupying a large volume fraction of a dense Si_3N_4 component. This will in turn translate into a deterioration of the high temperature mechanical properties of that component. Other impurities such as iron, sodium or calcium can

also be very detrimental by reducing the melting point of the liquid phase through the formation of low melting eutectics[4].

A whole variety of processes are available to synthesize Si_3N_4 powders. The most widely used are the imide process, direct nitridation, laser and plasma techniques, and the carbothermal reduction of SiO_2 (section 2.1.4.4) to name a few. The latter, due its obvious economic benefits (cheap and abundant starting materials - SiO_2, C, N_2), has been chosen to be the object of study of this thesis. The next chapter will discuss the structure of Si_3N_4, its applications, how it can be densified, as well as the most common ways to synthesize Si_3N_4 powders.

2. LITERATURE REVIEW

2.1 SILICON NITRIDE

Nitride ceramics are not naturally occurring materials, and the only native nitrides which have been found were in meteorites[5]. Silicon nitride (Si_3N_4) must therefore be synthesized. This was first accomplished by Wöhler and Deville[6] in 1857 by using silicon tetrachloride and ammonia. However, it was not until the early 1950's that silicon nitride was rediscovered as a potentially good candidate for engineering applications[7]. Table 2.1 lists some of the unique properties that have made monolithic Si_3N_4 so interesting then and now, and compares these properties with those of well-known materials.

Table 2.1 : Comparison of properties of various materials[1,8-10].

Material	Density (g/cm^3)	Melting point (°C)	Tensile strength (MPa)	Elong. (%)	Hardness (kg/mm^2)	Toughness ($MPa/m^{\frac{1}{2}}$)
Sintered Si_3N_4	3.19	1900 (decompose)	300-500	—	2200	4-6
Dense Al_2O_3 (α)	3.95	2050	200-300	—	2370	3-5
Gray cast iron	6.95-7.35	1170-1290	200	—	230	37-45
Stainless steel (304)	8.0	1400-1450	500-600	30-40	170	150-250
Copper	9.0	1080	200	18	110	250-350
Aluminum	2.7	660	40-50	55	140	23-45

As can be seen in Table 2.1, silicon nitride has a high decomposition

temperature and a high strength to density ratio compared to stainless steel[11]. Also, in contrast to metals, which tend to soften at high temperatures, Si_3N_4 still demonstrates excellent strength at elevated temperatures with a modulus of rupture (MOR) of ~350 MPa at 1300°C[12].

Silicon nitride is also well known for its wear resistance, excellent thermal shock properties (due to its relatively low coefficient of thermal expansion), resistance to corrosive environments, and hot hardness. These all make silicon nitride the ideal engineering ceramic for tribological applications such as bearings and cutting tools[13,14], and high temperature applications[15,16] like turbine blades or valves for diesel engines[17,18]. In gas-turbine engines, the use of silicon nitride allows engines to operate at higher temperatures without the need for cooling, thus enabling a more efficient thermodynamic cycle[19] and eliminating mechanical losses resulting from the need to pump cooling air. While the efficiency of diesel engines does not increase with operating temperature, the use of silicon nitride still eliminates the need for water cooling, thus reducing friction by eliminating the fan and the water pump. In spark-ignited engines, ceramics reduce friction, rotating inertia, and the increased operating temperature also results in a more complete burning of the fuel, as well as a reduction in CO emissions. For example, recent studies[20] showed that the use of silicon nitride valves in a 5.8L Chevrolet V-8 engine increased its power by 6 to 7%.

The structure of Si_3N_4 responsible for these unique properties will be discussed in the following section.

2.1.1 THE STRUCTURE OF SILICON NITRIDE

Silicon nitride is a highly covalent compound. It is composed of ~ 70% covalent bonds, the remaining 30% being ionic bonds[21]. The strong and directional nature of covalent bonds accounts for the hardness of silicon nitride, its high melting (decomposition) temperature, its high strength even at elevated temperatures, and its low thermal expansion coefficient.

A little more than 20 years ago, Vassiliou and Wild[22] identified for the first time two forms of Si_3N_4, designated as α and β. These α and β phases observed by Ruddlesden and Popper[23] were first thought to be orthorhombic and rhombohedral respectively. Soon after, a study done by Turkdogan et al.[24] resolved some of the previous anomalies, and established that both the α and β phases were hexagonal with the α-Si_3N_4 unit cell having a c-axis twice as long as the β-Si_3N_4 cell (Table 2.2).

Table 2.2 : Si_3N_4 unit cell dimensions (Å)

AXIS	α-Si_3N_4[25]	β-Si_3N_4[26]
a	7.765 ± 0.001	7.608 ± 0.001
b	5.622 ± 0.001	2.911 ± 0.001

It was originally proposed that α-silicon nitride was actually an oxynitride of approximate composition $Si_{11.5}N_{15}O_{0.5}$[27-31], however, recent observations do not support this conclusion[25,32-34]. It therefore appears that α and β are true polymorphs of silicon nitride.

The crystal structure of both α and β-Si_3N_4 are composed of tetrahedra of four nitrogen atoms with a Si atom in the center. The α unit cell ($Si_{12}N_{16}$) has a stacking sequence ABCD...with CD being the mirror image of AB, whereas the β unit cell (Si_6N_8) has a stacking sequence ABAB...(Fig. 2.1)[12].

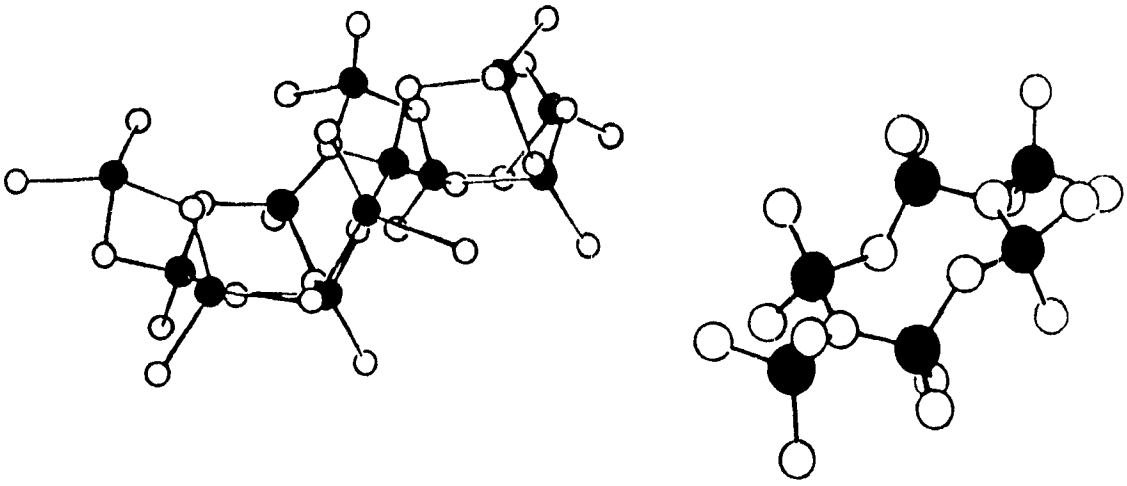

(a) (b)

Figure 2.1 : Crystal structures of a) α-Si_3N_4 and b) β-Si_3N_4.

Both phases of Si_3N_4 have approximately the same density (~3.19g/cm^3). α-Si_3N_4 is known as the low-temperature phase, and given enough time and the proper means of mass transport, it will transform to β-Si_3N_4 at around 1500°C[35,36]. The understanding of these two phases is paramount in the Si_3N_4 system since, during sintering, α-Si_3N_4 grains will dissolve in the liquid phase (see 2.1.2.1) and reprecipitate as fiber-like β-Si_3N_4 grains. The presence of these intertwined elongated β-Si_3N_4 grains in the final sintered product is in good part

responsible for the high strength and toughness of Si_3N_4 products.

2.1.2 DENSIFICATION OF SILICON NITRIDE

Silicon nitride components must be densified in order to have useful mechanical properties. Three main processing routes can be used to achieve this, namely sintering (SSN), reaction-bonding (RBSN), or hot-pressing (HPSN). Section 2.1.2.2 will deal with the basic mechanisms behind sintering.

The component to be sintered is usually a powder compact (premixed with suitable additives), or green body, made by various methods such as slip casting, injection molding, uniaxial-pressing, and/or isostatic-pressing, as described in the following section.

2.1.2.1 Compaction Processes

The main purposes of forming a compact prior to sintering is to increase the particle-particle contact which is essential for proper mass transport, to increase capillary pressure of the liquid phase (at sintering temperature) and to form a green body into the desired shape so that a minimum amount of machining will be required after sintering.

A green body can contain anywhere from 25% to 60% porosity and the powder is held together by weak van der Waal forces and mechanical interlocking.

Powders can be compacted by various pressing methods. The most common is uniaxial pressing, where the powder is placed in a die and pressure is applied in one direction (uniaxially). This compaction method is, however, limited

to simple geometries and the green bodies compacted with uniaxial-pressing usually have nonuniform densities[37-39] which will in turn cause the densification or shrinkage to be nonuniform.

Isostatic pressing[40] involves the concurrent application of pressure on the powder from all sides. The powder is placed in a rubber mold, sealed (most of the air inside the rubber mold has been evacuated), and it is then placed in a fluid (H_2O/oil). Pressure is applied (35-1380MPa) on the fluid and transferred uniformally to the rubber mold containing the powder.

An alternate compaction method is slip casting, where a liquid containing ceramic particles is poured into a porous mold (usually plaster[41]) which removes the liquid, leaving behind a particulate compact along mold walls. The compaction is provided by the capillary pressure of the liquid entering the fine porous structure of the mold. Slip casting is usually done at room temperature. This process allows the fabrication of complex objects such as gas turbine stator, turbine blades, and fuel injection nozzles. However, careful control of several parameters[42] must be exerted. These include viscosity of slip, freedom from air bubbles, and mold release properties to name a few.

In injection molding, the ceramic powder is mixed with a thermoplastic resin, wax, plasticizer, or solvent and then kneaded under heat[43]. A molding machine then pressure-injects the mixture into a mold through a nozzle. The organics in the molded part are then burned out, after which the compact is sintered[44,45]. This technique is suitable for manufacturing in large quantities,

products of complicated shapes requiring dimensional accuracy and surface smoothness such as heat engines ceramic parts.

2.1.2.2 Sintering Mechanisms

Sintering is essentially a heat-treatment process by which fine particles, which are in contact with each other, agglomerate when heated to a suitable temperature, this agglomeration being accompanied usually by a decrease in the porosity and an increase in the bulk density of the mass[46]. During this process the surface area decreases so that the surface free energy, and hence the total free energy of the system decreases. In other words, the system eliminates the high surface free energy solid-vapour interfaces in favor of the lower free energy solid-solid interfaces.

In order for sintering to take place, three things must be considered:

1 - A driving force for densification such as the reduction of surface area (the smaller the particles, the higher this driving force).

2 - A source of energy (usually heat) to activate this process.

3 - A means of material transport.

Material transport can take place in a number of ways, as shown in Figure 2.2. Each one involves the transport of material from a source at the grain boundary to a sink or the neck between particles. The smaller the particles are, the

greater is the difference in curvature between the surface area and neck, and the greater is the driving force.

The self-diffusion coefficient, D, of N in β-Si_3N_4 at 1400°C is $1x10^{-16}$ cm^2/sec. This low self-diffusion coefficient can be attributed to the covalent nature (strong and directional bonds) of Si_3N_4 and its short interatomic distances. This fact makes densification of pure Si_3N_4 by solid-state sintering a highly impractical and slow process. The introduction of a liquid phase during sintering of Si_3N_4 can enhance material transport, and hence enable densification to occur without the help of very high external pressures, a costly alternative[47,48]. The better densification that is achieved during liquid phase sintering can also be attributed to the enhanced

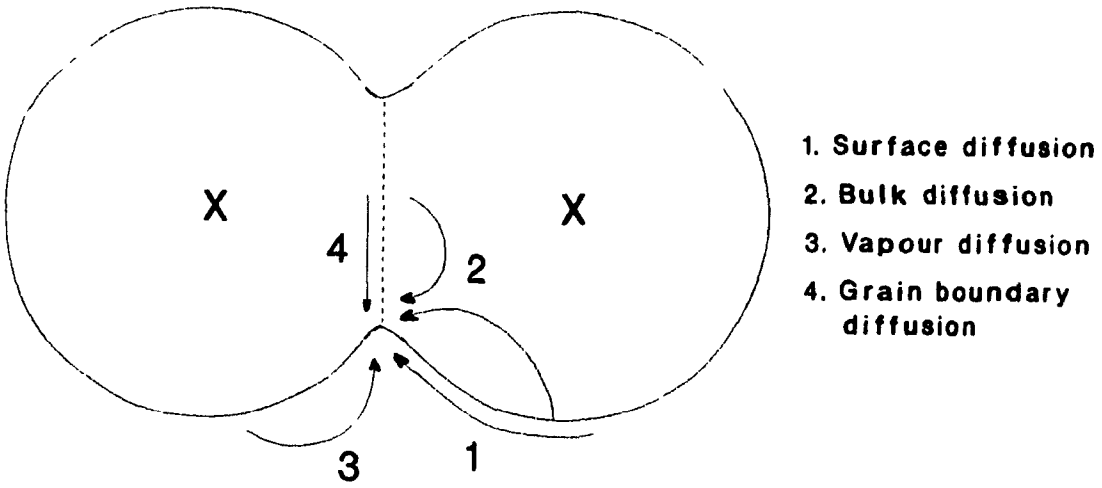

Figure 2.2 : Material transport path during solid-state sintering.

rearrangement of the particles by creep, and capillary pressure which brings the particles closer together.

2.1.2.3 Sintering of Silicon Nitride

In general, sintering of silicon nitride can be done with the help of external pressure (*hot-pressed silicon nitride* - HPSN) or alternatively, without (*sintered silicon nitride* - SSN).

The expression *sintered silicon nitride* is usually reserved for Si_3N_4 which has been densified at atmospheric pressure (also termed *pressureless sintering*) with the help of additives which react and melt to form a liquid phase below the sintering temperature (1650-1850°C). The liquid phase not only enhances material transport, but also by wetting the Si_3N_4 grains, it enables the particles to rearrange themselves into a denser body. For Si_3N_4, the additives (about 5-10 weight %) that are usually used are AlN, Al_2O_3, MgO and Y_2O_3, although many other additives and additive combinations have been reported.

SSN components generally have high relative densities (~ 95-99%) which give them very good strengths (bend strength ~ 400-1000 MPa). This pressureless sintering process does not require sophisticated high-pressure, high-temperature equipment, and hence offers the possibility to manufacture complex-shaped Si_3N_4 articles at a low cost.

Hot-pressing is analogous to sintering except that pressure and temperature are applied simultaneously[49]. Hot pressing is typically conducted at

approximately half the absolute melting temperature of the material[50], which is usually a lower temperature than that at which the material can be densified by pressureless sintering. In a hot press, pressures of up to 35 MPa can be applied uniaxially by a graphite die[21]. However, the pressure used is usually much lower. This external pressure is often used in conjunction with sintering aids to improve the densification kinetics.

This process offers several advantages such as reduced densification time, lower densification temperature (less grain growth, hence higher strengths), and near-theoretical density can be achieved (very low residual porosity). The major limitation of hot pressing is shape capability. Nonuniform cross-sections, and intricate or contoured shapes are difficult and often impossible to fabricate by conventional uniaxial techniques. Another drawback of this process is the high cost, as well as the difficulty involved in mass-producing Si_3N_4 components. Table 2.3 compares the densities and strength obtained by hot pressing and sintering at 1700°C.

In order to eliminate the shape limitation problems involved with the hot pressing technique, a similar process was developed where the pressure is applied isostatically by a gas during sintering. This process is named *Hot-Isostatic Pressing* (HIPping). The apparatus for HIPping consists of a high-temperature furnace enclosed in a water-cooled autoclave capable of withstanding pressures up to 300 MPa and providing a uniform hot-zone temperature of up to 2000°C[52]. To achieve densification of a ceramic preform, it must first be evacuated and then

Table 2.3 : Comparison of strength and densities obtained by different densification methods[51].

Material	Sintering aid	Density (% theoritical)	MOR (at room temp.) (MPa)
Sintered Si_3N_4 (SSN)	5% MgO	~ 90	483
Hot-Pressed Si_3N_4 (HPSN)	5% MgO	> 98	587

sealed in a gas-impermeable envelope (usually Ta or SiO_2). When pressure is applied at high temperatures, the envelope deforms as the compact shrinks. Although this process solves some of the shape-limitation problems associated with the hot-pressing (uniaxial) technique, it is still a complex and costly alternative.

2.1.3 THE INFLUENCE OF POWDER CHARACTERISTICS ON SINTERING AND MECHANICAL PROPERTIES

Purity, particle size distribution, reactivity, and polymorphic form (α and β content) of the starting Si_3N_4 powder can all affect the final properties of sintered components. Therefore, a thorough knowledge of a powder's characteristics prior to sintering is an essential part of any advanced ceramic processing operation.

2.1.3.1 The Ideal Powder

One approach to develop ceramic materials with enhanced strength and toughness involves the synthesis of ideal powders for sintering. These powders are often considered to have a small particle size (see section 2.1.2.1), a narrow

range of sizes to avoid excessive grain growth, an absence of aggregates, equiaxed morphology for improved powder packing and a controlled chemical purity.

2.1.3.2 Particle Size

In general, the finer the powder and the greater its surface area, the lower is the temperature and time required for densification. This is shown in Equation 2.1[53] which summarizes the various parameters that have a direct influence on the sintering rate (linear shrinkage).

$$\frac{\Delta L}{L_0} = \left(\frac{20\,\gamma\,a^3\,D}{\sqrt{2}\,k\,T} \right)^{2/5} r^{-6/5}\, t^{2/5} \qquad (2.1)$$

$\Delta L/L_0$ = Linear shrinkage
γ = Surface energy
a^3 = Atomic volume of the diffusing vacancies
t = Time
D = Self-diffusion coefficient
k = Boltzmann constant
T = Temperature
r = Particle radius

For example, for a given sintering time and temperature, Si_3N_4 starting powder of ~ 2μm average particle size sinters to only about 90% of theoretical density. While, with the same sintering cycle, submicron Si_3N_4 powder with a surface area greater than ~10 m^2/g sinters to more than 95% of theoretical density[54].

Given enough time at high temperature, even the coarser powder (2 - 5μm) would sinter to > 95% of theoritical density. However, long times at sintering temperature should be avoided since excessive grain growth would occur, and hence the large grains formed would result in a lower strength of the sintered product[55].

2.1.3.3 Particle Size Distribution

There is still a debate as to which is better; a narrow, or a broad size distribution. A broad particle size distribution will result in a higher green density and a lower, although not necessarily uniform, shrinkage upon firing. On the other hand, a narrow particle size distribution will yield a lower green density but its shrinkage during sintering will be uniform and much more pronounced[56].

The difference in shrinkage is related to the packing efficiency of the two powders. A monosized powder can have a maximum packing density of ≈ 74%[57]. In the broad particle size distribution, the smaller grains can fill the voids between larger particles and hence attain a much higher maximum packing density. Table 2.4 shows that, for example, for a powder with a trimodal size distribution, the theoretical packing density (assuming spheres) can reach up to 95%[58].

Table 2.4 : Optimized trimodal packing of spheres[59-61].

Volume % of particle size			
Small (0.1μm)	Medium (0.7μm)	Large (4.9μm)	Fractional density
13.2	20.7	66.1	0.878
11.0	14.0	75.0	0.950

In general, a narrow size distribution is the preferred alternative, since during firing, the larger grains present in the broad size distribution will tend to grow at the expense of the smaller ones, resulting in a fined-grained microstructure with several large grains imbedded in it. These large grains can then act as stress

concentrators, and hence lower the strength. For the densification of silicon nitride the presence of a liquid phase is usually required for particle rearrangement, improved mass transfer rates, and also for dissolution of α-Si_3N_4 grains and precipitation of β-Si_3N_4 grains. However, because of the dissolution of the α-Si_3N_4 grains there may, in fact, be little advantage of using monosized powder.

2.1.3.4 Effect of Impurities

Depending on the powder synthesis method and the subsequent milling and purification steps used, various types of impurities can find their way into the powder prior to sintering. The most common impurities are oxygen, C, Fe, Ca, F, Cl, and Al. As these impurities tend to migrate to the liquid phase they have an effect, alone or grouped, on both the densification behaviour and the high temperature mechanical properties of Si_3N_4[62]. For example, Cl, an impurity commonly found in powders produced by the imide process (if $SiCl_4$ is used as a starting material - section 2.1.4.2), has been found to be detrimental in establishing a creep-resistant glassy phase as it reduces the solubility of nitrogen in the glassy phase[63,64].

Individually Al and Fe seem to have only a minor effect on high-temperature strength, but in combination, especially with Ca, a strong decrease in the glassy phase viscosity is observed[65,66].

For the carbothermal reduction process, the use of high purity starting materials limits the presence of metallic impurities in the final powder. For this process the most common impurities found are oxygen and carbon. Their effect on

the high-temperature mechanical properties and densification behaviour is discussed in section 2.1.4.4.

2.1.4 SILICON NITRIDE POWDER PRODUCTION ROUTES

As mentioned in section 2.1.3, the mechanical properties of a densified Si_3N_4 component are strongly dependent upon the starting powder characteristics. For example, particle size, purity, morphology, and the size distribution of a powder have a strong influence on the properties and densification behaviour of the final product.

There is several methods by which Si_3N_4 powder can be synthesized. Each method offers a unique set of advantages and disadvantages. The following sections deal with some of the Si_3N_4 powder synthesis processes currently available.

2.1.4.1 Direct Nitridation

Silicon nitride powders can be synthesized by direct nitridation[67,68], with controlled bed-depth of chemically pure Si powder (less than 10μm diameter) at between 1473 and 1723K in an atmosphere of NH_3, N_2/H_2 or N_2[69] according to the overall reaction :

$$3Si + 2N_2 \longrightarrow Si_3N_4 \qquad (2.1)$$

Due to the formation of a protective layer of Si_3N_4 on the outside of

the Si powder, the nitridation reaction generally requires a long period of time (5-20 hours)[70,71]. This reaction is exothermic, therefore, precautions have to be taken in order to avoid melting the Si powder, or forming β-Si_3N_4 (high-temperature phase).

The direct nitridation of Si is a fairly simple method to synthesize Si_3N_4 powder. The reaction can be conducted in a conventional resistance furnace, and this process can easily be adapted for batch or continuous production. However, it has several associated problems. Since the nitridation product is usually strongly agglomerated, a milling stage is necessary for the production of fine Si_3N_4 powders[72]. A final chemical purification step is also required to remove impurities due to mill wear, and residual metallic Si (typically 0.2-1 weight%)[73].

2.1.4.2 Imide Process

This process is termed the "imide" or "diimide" process because of the formation of the intermediate product silicon diimide ($Si(NH)_2$), according to the reaction:

$$SiCl_4 + 6NH_3 \text{ --> } Si(NH)_{2\,(s)} + 4NH_4Cl_{\,(s)} \quad (2.2)$$

The reactants can be either both liquid, or one of them can be a gas, and the other a liquid[71]. In all cases an intimate mixture of fine particulate silicon diimide and ammonium chloride is formed. The reaction usually takes place at a low temperature (-40°C to 0°C).

The NH_4Cl can be removed by washing with liquid ammonia or thermal treatment in an inert gas stream at about 900°C. The final step is the pyrolysis of $Si(NH)_2$ according to the following reaction[74]:

$$3Si(NH)_{2\,(s)} \xrightarrow{1200°C} Si_3N_{4\,(s)} + 2NH_{3\,(g)} \qquad (2.3)$$

The Si_3N_4 powder produced is amorphous. A crystallization treatment (>1300°C) is therefore required to transform the amorphous Si_3N_4 into α-Si_3N_4 powder. This heat treatment results in the formation of hard agglomerates, which are then broken down by milling. A final chemical purification stage is performed to remove the impurities from milling, as well as the residual amount of chlorine present.

The imide process offers the advantage of producing a relatively fine α-Si_3N_4 powder (~ 10 m^2/g) with high purity. However, this process also has several disadvantages such as the problems associated with the corrosive nature of NH_3, $SiCl_4$ and HCl (a by-product from the decomposition of NH_4Cl which is recycled).

2.1.4.3 Plasma and Laser Synthesis Process

In recent years, much attention has been given to ultra fine powders. To synthesize such powders, direct current (d.c.), alternating current (a.c.) and radio-frequency (r.f.) thermal plasma reactors have been developed[69]. For these techniques, a highly ionized gas is used as a heat source. The plasma gas can be either pure Ar, or mixtures of Ar/N_2, or Ar/H_2[71,75].

Si_3N_4 powder is synthesized by introducing gaseous, liquid or finely dispersed solid reactants into the plasma torch (temperature up to ~ 6000K) together with ammonia, according to reactions 2.4-6.

$$3SiCl_{4\ (l)} + 4NH_{3\ (g)} \longrightarrow Si_3N_{4\ (s)} + 12\ HCl_{\ (g)} \qquad (2.4)$$

$$3SiH_{4\ (g)} + 4NH_{3\ (g)} \longrightarrow Si_3N_{4\ (s)} + 12H_{2\ (g)} \qquad (2.5)$$

$$3\ Si_{(s)} + 4NH_{3\ (g)} \longrightarrow Si_3N_{4\ (s)} + 6H_{2\ (g)} \qquad (2.6)$$

Problems are associated with each of these routes. The use of $SiCl_4$ leads to corrosive by-products, whereas SiH_4 is chemically more dangerous than the tetrachloride because of its spontaneous flammability in air. When metallic Si is used as a reactant, a significant amount of unreacted Si can end up in the Si_3N_4 powder.

The Si_3N_4 powders produced by the plasma method are usually amorphous and extremely fine (10-20 nm). After heat treatment (>1300°C), the final size of the crystalline powder is usually in the 0.2-0.3 μm range. A laser can also be used as a heat source by orthogonally intersecting with the reactant gas stream (silane-ammonia-mixtures)[76] and heating up the gas up to approximately 1000°C with a heating rate of 10^6°C/second. The Si_3N_4 powder synthesized by this method is also extremely fine (15-20 nm), amorphous, and contains considerable amounts of free silicon (~ 2 %).

These methods have the advantage of producing fine powders of very

high purity. This is especially true for the laser and r.f. plasma[77] techniques where there is no contamination from the electrodes. There are, however, several drawbacks associated with these methods in that the reactors are usually complex and have high energy requirements. More importantly, the very fine Si_3N_4 powders are extremely sensitive to humidity and will oxidize readily in air. Oxygen impurities in the order of a few percent are the consequence.

2.1.4.4 Carbothermal Reduction of Silica

The previous sections dealt with various methods to synthesize silicon nitride powders. All have at least one drawback associated with them such as complexity of reactor, corrosion problems, cost, powder purity, fineness and crystallinity of powder. The choice of a process depends on the application of the powder, the subsequent densification process (pressureless-sintering, hot-pressing, etc.), as well as the cost of the powder with a given series of properties. The cost of advanced ceramics is an important factor when considering the replacement of their metallic counterparts.

Carbothermal reduction is a very cost-effective process since the high purity starting materials required (C, SiO_2, and N_2) are cheap and abundant. Reactio 2.7 describes the general form of the carbothermal reduction process where an oxide is reduced by carbon, and then subsequently nitrided.

$$\text{OXIDE}_{(s)} + \text{C}_{(s)} + \text{N}_{2\,(g)} \xrightarrow{1350\text{-}1600^\circ\text{C}} \text{NITRIDE}_{(s)} + \text{CO}_{(g)} \qquad (2.7)$$

The carbothermal reduction process is not limited to the synthesis of silicon nitride. Other oxides such as Al_2O_3, TiO_2, ZrO_2, and B_2O_3 can also be reduced and transformed into their nitrides, or even carbides[78]. Also, the total energy cost of synthesizing compounds by carbothermal reduction is lower than other processes. Table 2.5 compares the energy requirements for the synthesis of Si_3N_4 and SiC by both carbothermal reduction and from metallic Si[79].

Table 2.5 : Energy requirements for the synthesis of Si_3N_4 and SiC.

	Energy requirements (kWh/kg) for the synthesis of:	
	Si_3N_4	SiC
From SiO_2	2.60	4.20
From Si	4.03	4.70

Carbothermal reduction of silica was among the first methods used to make silicon nitride.The first patent was granted to Mehnar in 1895[80], followed by a series of patents at the beginning of this century[81-84]. Currently, Toshiba (Japan) is the only company that commercially produces silicon nitride powder by carbothermal reduction. Other companies, such as Atochem (France), and DOW (USA) are also interested in the process and are presently at the pilot plant level.

The overall reaction for the carbothermal reduction of silica is

described as follows:

$$3SiO_{2\ (s)} + 6C_{(s)} + 2N_{2\ (g)} \text{----->} Si_3N_{4\ (s)} + 6CO_{(g)} \qquad (2.8)$$

In this relatively simple equation, SiO_2 is reduced by carbon, and then nitrided to form silicon nitride. However, in practice, stoichiometric amounts of starting materials do not guarantee completion of the reaction. Excess amounts of C (molar ratio > 3:1, C:SiO_2) are normally used to ensure full conversion of SiO_2, and to dilute the CO product gas present in the reaction bed, and hence avoid the formation of SiC (see section 4.1.5), flowing N_2 is usually preferred over a static N_2 atmosphere.

The overall reaction is believed to follow several steps[85-87]:

$$SiO_{2\ (s)} + C_{(s)} \text{----->} SiO_{(g)} + CO_{(g)} \qquad (2.9)$$

and $$3SiO_{(g)} + 3C_{(s)} + 2N_{2\ (g)} \text{----->} Si_3N_{4\ (s)} + 3CO_{(g)} \qquad (2.10)$$

and/or $$3SiO_{(g)} + 3CO_{(g)} + 2N_{2\ (g)} \text{----->} Si_3N_{4\ (s)} + 3CO_{2\ (g)} \qquad (2.11)$$

The first reaction (2.9) is a solid-solid reaction between silica and carbon that results in the formation of SiO and CO gases[87,88]. More silica is then reduced by carbon monoxide in the reaction:

$$SiO_{2\ (s)} + CO_{(g)} \text{----->} SiO_{(g)} + CO_{2\ (g)} \qquad (2.12)$$

with carbon monoxide being regenerated by the following reaction:

$$C_{(s)} + CO_{2\,(g)} \text{ ----> } 2CO_{(g)} \qquad (2.13)$$

It has been suggested that nuclei of Si_3N_4 are produced by the reaction of SiO and N_2 with C[89] (equation 2.10). The growth of these nuclei via the gas phase reaction[90] (equation 2.11) and the formation of new nuclei of Si_3N_4 will occur with time (at the reaction temperature) until all the SiO_2 is converted to SiO gas[86].

Like all synthesis methods, carbothermal reduction of SiO_2 has associated drawbacks. The main problem is related to the removal of the excess amount of carbon used to ensure full conversion of SiO_2 to Si_3N_4. After reaction, the Si_3N_4 powder and the remaining C (30-50 wt%) are intimately mixed together, rendering separation by physical or mechanical means virtually impossible. The most common way to eliminate the carbon is to simply oxidize it in air at a temperature of 650-800°C for several hours.

After C removal, the Si_3N_4 powder can still contain levels of C between 0.7 and 1.0 % by weight[71]. This residual C can react with the silicon oxynitride liquid phase during sintering, and therefore result in a compositional shift of the liquid[4], as well as a porous final product (from SiO and CO evolution). The removal of C in an oxidizing environment also partially oxidizes Si_3N_4 to SiO_2[78]. The high levels of oxygen sometimes found in Si_3N_4 powders produced by

carbothermal reduction can have a deleterious effect on the high temperature mechanical properties of a component. The presence of excessive amounts of oxygen (>5 weight %) will result in the formation of a large volume fraction of intergranular glassy phase in the final dense Si_3N_4 part. Although the densification behavior of such a compound would be excellent due to improved mass transfer rates and larger medium into which α grains can dissolve and reprecipitate as β grains, its high temperature strength and creep resistance would be strongly affected in a negative way; the intergranular phase softening at a relatively low temperature (≈ 1000°C). To limit the amount of oxygen, methods for the elimination of C in oxygen-free atmospheres (NH_3, H_2/NH_3) can be used as an alternative[91] decarburization method.

Another problem that has traditionally been associated with the carbothermal reduction process is the morphology of the Si_3N_4 powder produced. Although usually fully crystalline (with high α contents), the powder produced has a tendency to be agglomerated and have a large particle size (typically 1-5 μm). This meant that a final milling or "deagglomeration" step had to be performed to make the Si_3N_4 powder suitable for sintering.

2.1.5 OBJECTIVES OF THESIS

The goal of this thesis was to study and identify the parameters influencing the powder morphology, particle size, size distribution and composition (α-Si_3N_4, β-Si_3N_4, SiC) of Si_3N_4 powders produced by the carbothermal reduction

process and then produce a Si_3N_4 powder with optimized properties for sintering.

A further objective was to characterize the powders in terms of their sinterability and mechanical properties.

3. EXPERIMENTAL PROCEDURE

3.1 STARTING MATERIALS

The raw materials used in this study were high surface area, high purity fumed SiO_2, and carbon black. This choice was based on previous work[92] that showed that very fine starting materials were necessary to achieve full conversion of SiO_2 to Si_3N_4. For experiments with seeded raw materials, a sub-micron, high purity α-Si_3N_4 powder was used. This is a commercial powder produced by the imide process. Table 3.1 summarizes the specifications of these powders. Fig. 3.1 is a secondary

Table 3.1 : Specifications of starting materials.

POWDER	FUMED SILICA	CARBON BLACK	α-Si_3N_4 (SEED)
GRADE	EH-5 (Cabot Corp.)	M-1300 (Cabot Corp.)	SN-E-10 (UBE Industries Ltd.)
PARTICLE SIZE	~0.010μm	0.010-0.020μm	0.1-0.2μm
SPECIFIC SURFACE AREA	400 m^2/g	500 m^2/g	10-11 m^2/g
MAJOR IMPURITIES	H_2O ~ 1% Al < 5ppm Fe < 2ppm Ca < 2ppm	ASH ~ 0.24% CYANIDES<7ppm Ni < 17ppm Cr < 12ppm Fe < 10ppm	O < 2.0% C < 0.2% Cl < 100ppm Fe < 100ppm Ca < 50ppm Al < 50ppm
COMMENTS	AMORPHOUS	AMORPHOUS	CRYSTALLINE α-Phase=95% β-Phase=5%

electron micrograph of the seed material, showing an average particle size of ~ 0.2 μm.

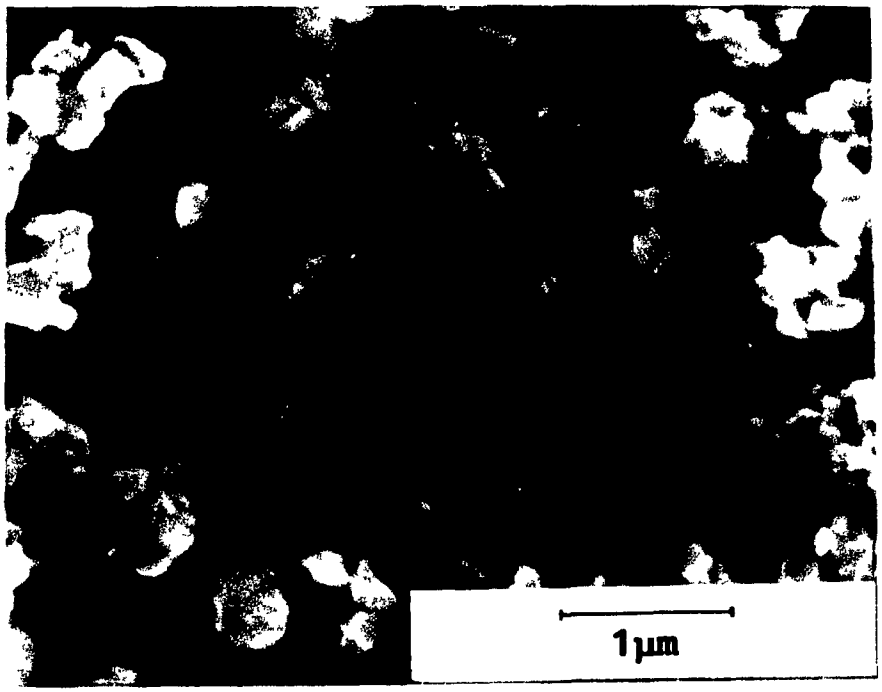

Fig. 3.1: α-Si_3N_4 seed material (UBE SN-E-10)

3.2 MIXING OF PRECURSORS

The starting materials were mixed in a 7:1 C:SiO_2 molar ratio by a sol-gel processing technique. This ratio was previously determined to be optimum for full conversion of SiO_2 to Si_3N_4[92]. The solids were either ball milled or attrition milled (200 rpm) with distilled water in a 6:1 wt H_2O:weight solids ratio with 5mm ϕ Si_3N_4[+], Al_2O_3[+] or ZrO_2[++] media. The media : solids ratio ranged from 1.5:1 to 13.4:1.

[+] Union Process

[++] Toyo Soda

After blending, the mixture was dried in a microwave oven, and then, dried further in a convection oven at 140°C for 24 hours. Before the nitridation, a final H_2O removal step was done in a furnace at 300°C for 2 hours. Fig.3.2 is a photograph of the "lumps" of starting materials which are ready to be reacted, while Fig.3.3 is a flowchart summarizing the mixing procedure.

Fig. 3.2 : "Lumps" of starting materials ready to be reacted.

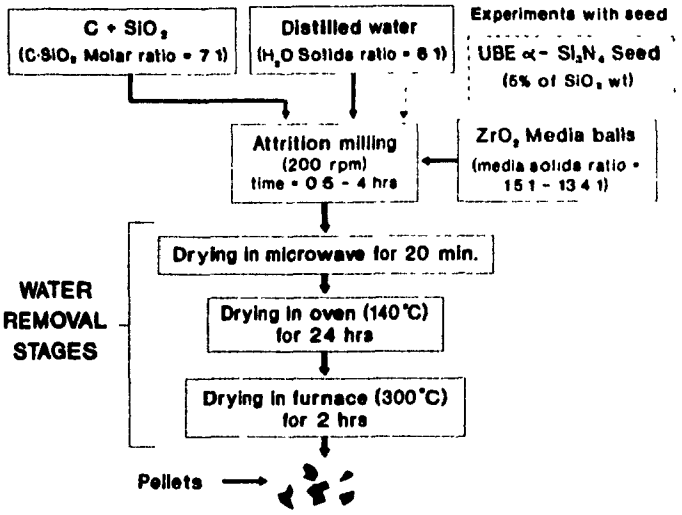

Fig. 3.3 : Flowchart of mixing and drying of precursors.

3.3 NITRIDATION

The pellets were put onto a perforated graphite plate, inside a large cylindrical graphite reactor (ϕ~16cm, height~18cm) (Fig.3.4). A layer of carbon felt was placed between the pellets and the perforated plate in order to provide a more uniform N_2 flow through the reactants, and also, to prevent the smaller pellets from falling out of the reactor. The design of the reactor was such, that preheated flowing N_2 gas entered the bottom of the reactor, passed over the reactants and exited the reactor at the top. In most experiments, a N_2 gas flow rate of 1900cc/min at STP (linear flow = 0.2 cm/sec) was used. In order to study the importance of gas flow rate, several experiments were conducted with lower and

higher flow rates 950 cc/min (0.1 cm/s at STP) and 3800 cc/min (0.4 cm/s

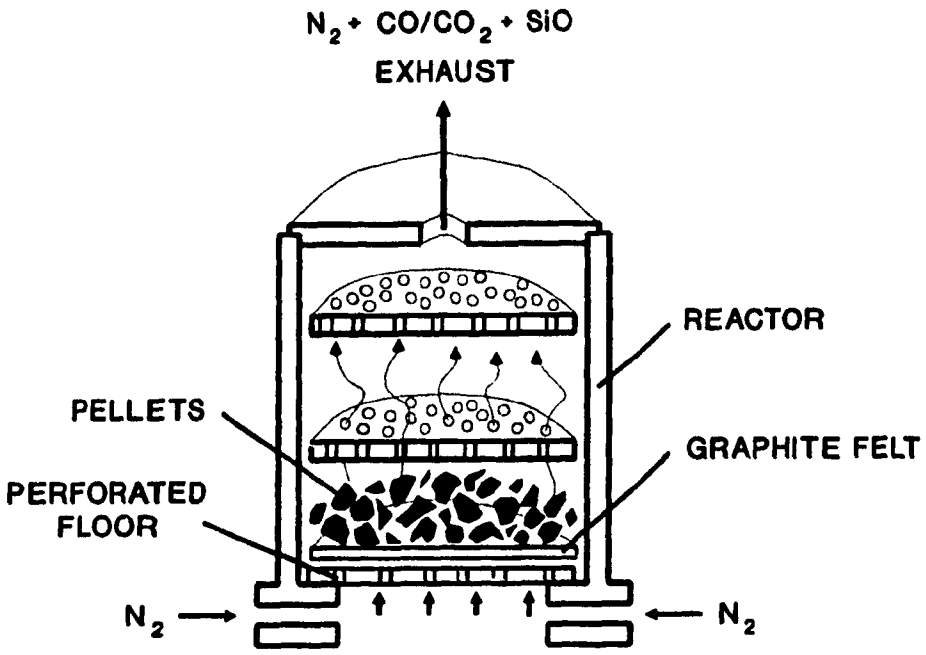

Fig. 3.4: Schematic view of graphite reactor.

at STP) respectively. Relatively low linear flow rates were used in order to avoid excessive loss of SiO gas.

The reaction took place in a graphite resistance furnace (Fig.3.5) with a rectangular hot zone (25cmX30cmX35cm) at the back of which, a W5%Re-W26%Re thermocouple monitored the temperature. Calibration of the furnace temperature was done using the melting points of pure metal powders (Co, Ni, and Fe) placed in small BN crucibles inside an empty reactor. The accuracy of the temperature resulting from the calibration procedure is estimated to be ± 10°C. The furnace temperature was regulated by a controller which received the signal from the thermocouple, and sent an appropriate signal to the SCR (Silicon Control Rectifier),

which in turn dictated to the transformer the current to be sent to the elements.

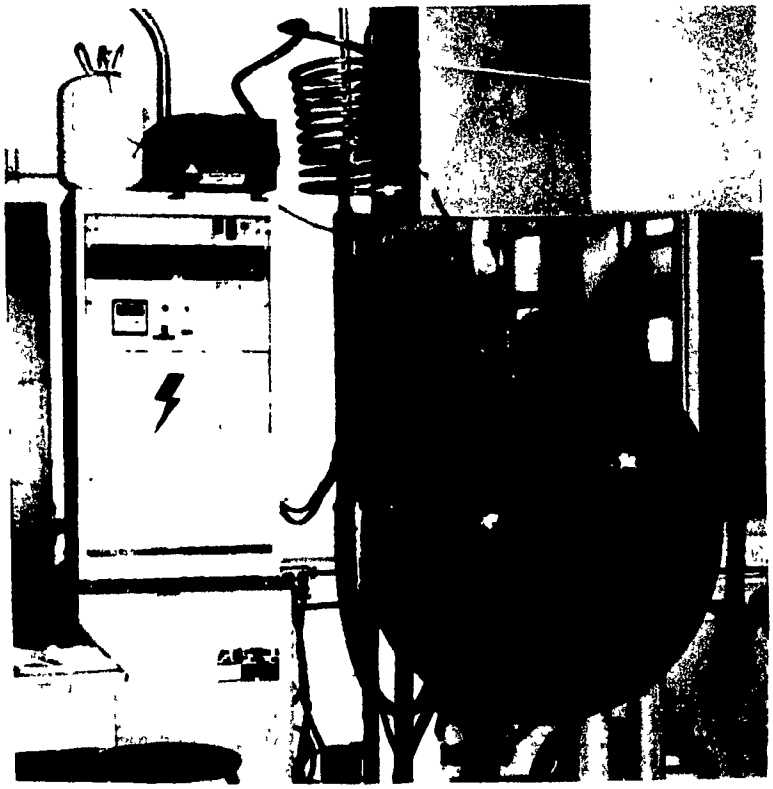

Figure 3.5: High temperature graphite electric resistance furnace.

The reactions took place at various temperatures, ranging from 1450°C to 1600°C. While the time of experiments was varied. The CO analyzer can be seen in Figure 3.5 above the controller panel.

3.4 ANALYSIS

3.4.1 X-RAY DIFFRACTION (XRD)

X-ray diffraction was used both to identify and quantify the phases present after reaction. An American Instruments X-ray generator was used to provide CuKα radiation, with an accelerating voltage of 40kV (±0.1%) and a beam

current of 20mA (±0.1%). A Philips Automatic Powder Diffractometer system was used to produce XRD patterns over a scan range of 2θ from 15^{o} to 45^{o}, at a rate of 1^{o}/minute. This range was chosen so that the strongest peaks from all the possible phases could be detected.

The identification of the phases present in the nitrided powders was done by comparing their patterns to JCPDS reference patterns stored in the memory of a Philips APD 1700 computer system (Digital Micro-PDP II).

Quantitative analysis using XRD patterns was done with the help of two calibration curves (Appendix I). With these, it was possible to quantify the amount of α-SiC in α-Si_3N_4 and, the amount of β-Si_3N_4 in α-Si_3N_4 within an estimated accuracy of ± 2%.

The β-Si_3N_4/α-Si_3N_4 calibration curve (in Appendix I) showed good agreement with a similar curve drawn by Gazzara et al.[93]. Although different peaks for α and β-Si_3N_4 were selected for their calibration curve, by using the diffraction patterns that were generated in this study, it was possible to compare the curves. This comparison yielded maximum differences of 4% for mixtures containing around 50-60 weight% β-Si_3N_4.

3.4.2 CHEMICAL ANALYSIS

As mentioned in section 2.1.4.4, the main impurities present in a silicon nitride powder produced by the carbothermal reduction process are oxygen and carbon. Hence, most of the chemical analysis was focussed on these two

elements. The total nitrogen content of the powders was also evaluated as a mean of estimating the actual amount of silicon nitride in the powders, and hence determine the degree of conversion of SiO_2 to Si_3N_4.

The total oxygen (SiO_2, Si_2N_2O, and various oxides) as well as the total nitrogen content of the powders were analyzed by ELKEM Metals in Niagara Falls (New-York) using a TC136 LECO EF100 electrode furnace and associated analyzer. In this method, between 20-25 mg of the ceramic powder is placed into a tin capsule, which is then placed into a nickel basket. This basket is then put into a graphite crucible, together with a small amount of graphite powder and ~ 0.5 g of tin. The whole assembly is then burned (~ 2700°C) under a flowing He (carrier gas) atmosphere to release the oxygen and nitrogen in the sample. The oxygen present in the sample reacts with the graphite crucible forming carbon monoxide. The gas to be analyzed together with the carrier gas flow first through an infrared (IR) analyzer. The IR detector responds selectively to carbon monoxide and produces a signal proportional to the concentration. This signal is integrated over a period of time and forms a unique measure of the carbon monoxide quantity and therefore of the oxygen content of the sample. After passing through the IR analyzer, the gases are filtered, leaving only nitrogen and the helium carrier gas. This mixture passes into a thermal conductivity cell where nitrogen produces a change in the output signal due to its appreciably lower thermal conductivity compared with pure helium. The time integral of this signal is then interpreted as a unique measure of the nitrogen content of the sample.

The carbon content of the decarburized silicon nitride powders was evaluated at McGill University using a LECO WR12 (model 761-100) carbon analyzer. Carbon is analyzed in a very similar manner to oxygen. About 0.05-0.2 g of ceramic powder is placed in a relatively porous clay crucible together with 0.5 - 1 g of copper chips used as an accelerator. The assembly is then placed in a small induction furnace where it is burned (1350°C) in a dry air environment. The carbon present in the sample reacts with the oxygen, forming carbon dioxide. This gas then passes in a thermal conductivity cell where its reading is compared with two reference gases (O_2 and dry air). This comparison enables the total amount of carbon dioxide in the gas to be found, and therefore the initial carbon content in the powder can be estimated.

X-Ray Fluorescence analysis were also done on Si_3N_4 powders to establish the presence of various cations (Mg, Zr, Fe, Na, Al, K, Ca, and Y). The analysis were performed at the Sherritt Gordon Laboratories on a Siemens XRF 303 instrument. The powder samples were pressed into pellets and placed in a cup where X-rays from a Rh target were focussed. The X-rays emitted by the sample then passed through a LiF analyzing crystal attached to a goniometer. Using Bragg's law, a computer system analyzed the information (wavelength of radiation of interest, angle, d spacing) and yielded the content (wt%) of the cations.

3.4.3 PARTICLE SIZE ANALYSIS

As mentioned in section 2.1.3, the average particle size as well as the

size distribution of powders have tremendous effects on the sintering behaviour[94,95], and hence the mechanical properties of the final product. It is therefore very important to clearly identify these parameters before sintering.

To do so, three methods have been used; surface area measurements (BET), particle sizing by Dynamic Light Scattering (DLS), and visual examination with a Scanning Electron Microscope (SEM).

3.4.3.1 Surface Area Measurements (BET)

The surface area measurements of the nitrided powders were carried out using a Quantasorb area-meter. The measurement of the specific surface area is based upon the theory of Brunauer, Emmett, and Teller[96] (BET theory), and is usually expressed in m^2/g. The surface area is inferred from the differential thermal conductivity of a He/N_2 mixture before and after adsorption of a monolayer of N_2[97,98] onto the surface of the powders at 77K.

Equivalent spherical particle sizes can be calculated from the specific surface, but will be influenced by particle shape (whiskers as opposed to equiaxed grains), surface roughness, surface phases like amorphous SiO_2-layers or absorbed chemical residues from the powder production, and degree of agglomeration[71]. More importantly, since one of the driving forces of sintering is the reduction of surface energy (decrease of the area of the solid-gas phase interfaces)[21,99], this value gives a direct indication of a powder's sinterability.

3.4.3.2 Dynamic Light Scattering (DLS)

The particle sizing of the powders was carried out using a submicron particle size analyzer, a NICOMP 370, from Pacific Scientific Instruments. It uses the principle of Dynamic Light Scattering to obtain a size distribution. The light from a laser is focussed into a glass tube containing a dilute suspension of particles. The suspended particles are not stationary; rather, they move about, or diffuse, in random-walk fashion by the process known as Brownian motion (caused by collisions of neighbouring solvent molecules). Each of these particles scatters light in all directions. The intensity of this scattered light is then related to the particles equivalent diameter. Small particles will "jitter" about in solution relatively rapidly, resulting in a rapidly fluctuating intensity signal; by contrast, larger ones will diffuse more slowly, resulting in a more slowly varying intensity.

The samples were prepared by dispersing ~ 0.1g of powder in 50 ml of distilled water with an ultrasonic horn for 5 minutes. After the ultrasonic dispersion, about 1ml of a dispersant (DARVAN 821*) was added to keep the dispersion stable. With a syringe, this dispersion was then injected in the NICOMP through a "luer" connection.

Every 15 seconds, the machine automatically generated particle size distribution graphs on a % number or a % volume basis, as well as an average diameter. The analysis was stopped, and the results were retrieved, when enough

* Vanderbilt Corp., Norwalk, CT.

data had been collected and the statistical parameters (chi-squared, fit error) indicated a good fit for the particle distribution curves.

3.4.4 SCANNING ELECTRON MICROSCOPE (SEM)

Particle sizing as well as powder morphology observations were done with the aid of Scanning Electron Microscopy (JEOL 840 and JEOL T300). The samples were prepared by dispersing ~ 0.05g of powder in 50ml of isopropanol with an ultrasonic horn for 10 minutes. A few drops of the dispersion were then deposited on an aluminum stub where upon the isopropanol was allowed to evaporate. A thin coating (a few nanometers) of gold-platinum was sputtered onto the sample to avoid charging.

The particle size distributions were obtained by taking several micrographs of a given powder at high magnification, and then, manually measuring the diameter of several hundred grains. For each grain, an average diameter was calculated by measuring the width and the length of the grain on the micrograph, and taking an average. The results obtained with this method proved to be very close to those obtained with the DLS technique (see Appendix II).

3.5 SINTERING OF SYNTHESIZED POWDERS

3.5.1 SELECTION OF POWDERS AND ADDITIVES

To study the sinterability of the silicon nitride powders synthesized in this work, two powders were selected and compared with UBE SN-E10 (imide process), one of the best quality commercial silicon nitride powders presently

available on the market. The two carbothermally produced powders were made with reactants (7:1 carbon black:fumed silica ratio, 5 weight% seed) attrition milled with a ZrO_2 media:solids ratio of 13.4:1, for 0.5 and 4 hours respectively (see section 4.3).

In this study, the sintering additives that were used were Al_2O_3* (4 weight%) and Y_2O_3+ (6 weight%), two commonly used additives[100-102]. The amount of sintering aids used was slightly higher than the AY6 composition[103,104] developed by GTE (2 weight% Al_2O_3, 6 weight% Y_2O_3) to compensate for the presence of residual C in the Si_3N_4 powder which acts as a reducing agent.

The silicon nitride powders and the additives were attrition milled and processed according to the overall flowchart presented in Figure 3.6.

* A16 AG, Alcoa Corp.
+ MOLYCORP Corp.

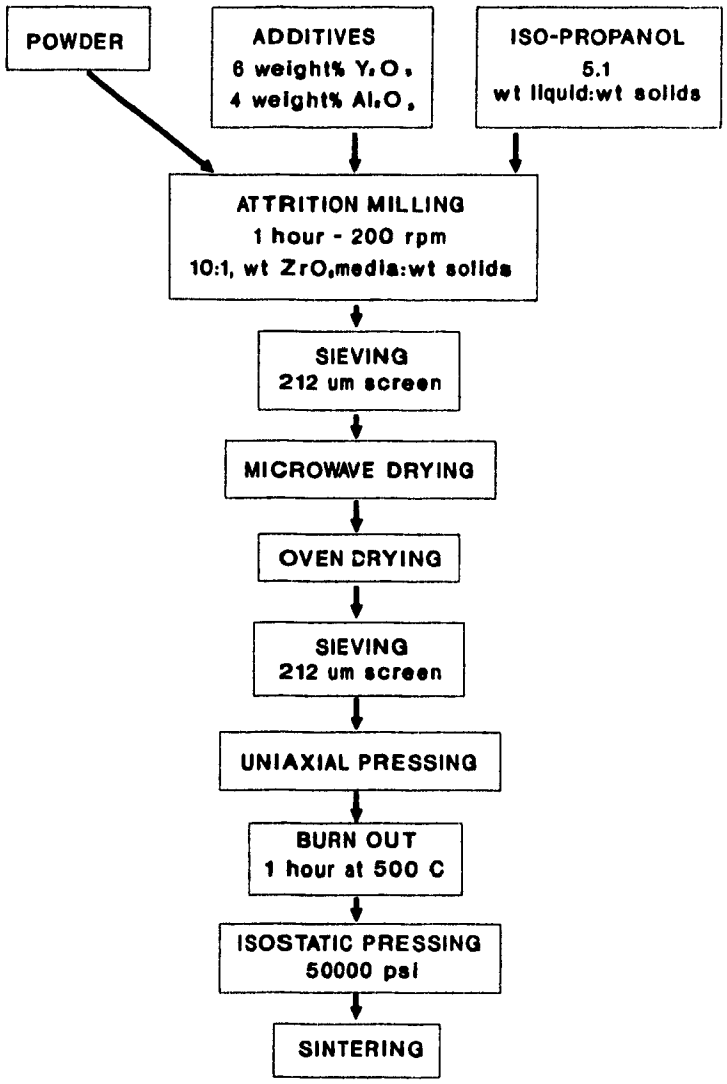

Figure 3.6 : Overall flowchart of powder processing scheme.

3.5.2 PRESSING & SINTERING OF Si_3N_4 BARS

After the second sieving step the powders (4.5 - 5.5 grams) were isostatically pressed into rectangular bars (60 mm x 10 mm x 5-7 mm). The bars were then placed in a graphite crucible filled with a powder made up of 40 weight% BN and 60 weight% silicon nitride powder and additives (90 weight% Si_3N_4, 4

weight% Al_2O_3, 6 weight% Y_2O_3). The bars, surrounded by the powder bed material, were sintered for 2 hours at 1800°C according to the following temperature cycle.

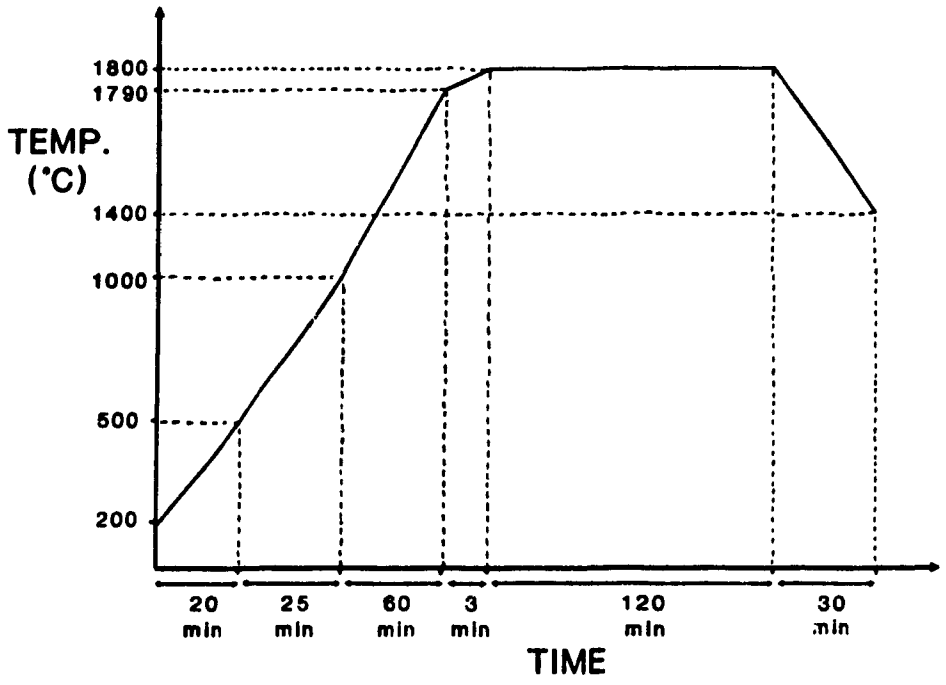

Figure 3.7 : Sintering cycle of the bars.

After sintering, the surfaces of the bars were machined with a 240 grit diamond wheel (60 - 80 μm finish) to ensure flat, parallel surfaces and the edges were bevelled to remove stress concentration features that would negatively influence the strength of the bars.

Densities were measured at various points in the process. The tap density of the powders was measured prior to the uniaxial pressing step, the green density of the bars was measured both before and after the isostatic pressing stage and the final sintered density was evaluated using the Archimedian method in water (ASTM C373).

3.5.3 EVALUATION OF MECHANICAL PROPERTIES

The bars were placed in a 4-point bend apparatus (Figure 3.8) where a load was applied until fracture. Knowing this load, the cross-sectional dimensions of the bars, and the dimensions of the jig, it was possible to evaluate the Modulus of Rupture (bend strength) of the bars (equation 3.1).

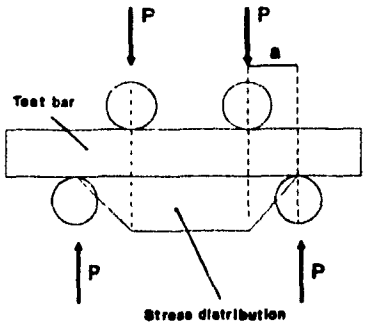

Figure 3.8[105] : 4-point bend testing of ceramic samples.

$$M.O.R. = \frac{3\,P\,a}{b\,d^2} \qquad 3.1$$

Where M.O.R. = Modulus of Rupture (Pa)
P = Load (N)
a = Constant related to the jig's geometry (here 0.010 m)
b = Width of bar (in m)
d = Thickness of bar (in m)

The machine used to supply the load was an universal testing machine*. The deformation was done at a rate of 0.5 mm/min.

The toughness of the bars was evaluated by randomly selecting four

bars from each of the three groups (1/2 hour attrition milling (A.M.), 4 hours A.M., UBE) and polishing them to a 1 μm finish. The samples were then tested with a diamond indentor* using a 50 kg load. The K_{Ic} was measured using the following equation[106]:

$$K_{Ic} = 0.015\ ((c-a)/a)^{-1/2}(E/H)^{2/3}(P/c^{3/2}) \qquad 3.2$$

Where E = Young's Modulus
H = Hardness
P = Load
c = Length of crack
a = size of indent

* INSTRON 1362
* Vicker's Indentation

4. RESULTS & DISCUSSION

4.1 SELECTION OF PRECURSOR PREPARATION METHOD

The mixing/milling of the precursors (C, SiO_2 and maybe Si_3N_4 seed) is a crucial step in determining the final characteristics of the Si_3N_4 powder produced. The objective of the mixing/milling step is to increase the intimacy between C and SiO_2 particles which will ultimately result in a finer Si_3N_4 powder (section 4.2) and while doing so, introduce minimal impurities which could promote the formation of other phases (e.g. SiC - section 4.1.2).

The efficiency of various mixing methods as well as the resulting contamination have been investigated. The outcome of this study is presented in the following sections, together with the influence of various reaction conditions (temperature, location of pellets in reactor, N_2 gas flow) on the formation of SiC.

4.1.1 PRECURSOR MIXING EFFICIENCY

Both carbon and silica particles are extremely fine (10-40 nm) but tend to form soft agglomerates. In order to break down these agglomerates and bring about good contact between the silica and carbon particles, various mixing/milling methods were investigated. The first mixing method studied was blending, where upon the starting materials together with water were placed into a 4 liter commercial stainless steel blender for up to 1/2 hour at high speed. However, blending did not succeed in breaking down the agglomerates and also, iron contamination from the blades and the walls of the blender, resulting from

prolonged blending time, was a strong possibility and a major concern. The lack of efficiency of blending in breaking down agglomerates was indirectly evaluated by looking at the final Si_3N_4 particle size. The blended precursors (with seed) yielded Si_3N_4 powders with large average grain sizes of 0.9 - 1.2 μm. As will be shown in sections 4.2.1 and 4.3, large Si_3N_4 grain sizes (> 0.5 μm) are the result of poor intimacy between C and SiO_2.

The more aggressive nature of attrition milling, on the other hand, proved to be a very efficient way of breaking down the precursor agglomerates. This method also offered the advantage that the amount of milling energy put toward mixing the carbon and silica could be easily controlled via the attrition milling time, the volume of media used, and the rotational speed of the attrition milling arms. In this work, the rotational speed was kept constant at 200 rpm, while changes in the amount of media, the type of media, and the milling time were all studied. Three different types of milling media balls were used; hot-pressed Si_3N_4, Al_2O_3, and ZrO_2.

The efficiency of ball milling as a mixing method was also studied. However, as will be shown in the following section, ball milling proved to be much less efficient when compared to attrition milling.

The pick up of impurities during the milling operation (from media wear) is a major concern. Section 4.1.2 will deal with the source, the nature, as well as with the effects of such contaminants on the formation of by-products other than Si_3N_4 (SiC, AlN, SiO_2-Al_2O_3 compounds).

4.1.2 MEDIA CONTAMINATION

Impurities can be either present in the starting materials (e.g. iron in silica, or organics in carbon black) or can be introduced during the different processing steps (handling, mixing/milling, drying) required for the preparation of the precursors. As mentioned in section 3.1, the starting materials used in this work contain very low levels of impurities and pick up of impurities during the various processing steps (mainly media wear during attrition or ball milling) prior to the reaction determines the quality of the end product. A study of the wear of the different types of milling media as a function of attrition milling time was therefore undertaken. This was compared with ball milling using Si_3N_4 media. The results are presented in Figure 4.1.

Figure 4.1 shows that the amount of contamination that can result from attrition or ball milling of the starting materials can be surprisingly high, depending on the media used. For example, attrition milling 100 g of silica together with 140 g of carbon for 4 hours with hot-pressed Si_3N_4 media balls resulted in a media wear of about 8 g. It can also be seen that attrition milling is much more efficient than ball milling, since one day of ball milling was found to be roughly equivalent to 2 hours of attrition milling. Hence, in order to make the starting materials processing stage as short as possible, attrition milling was chosen over ball milling.

Of the three different types of media balls studied, after 4 hours of attrition milling the Al_2O_3 media (7:1 media weight:solids weight) showed the most

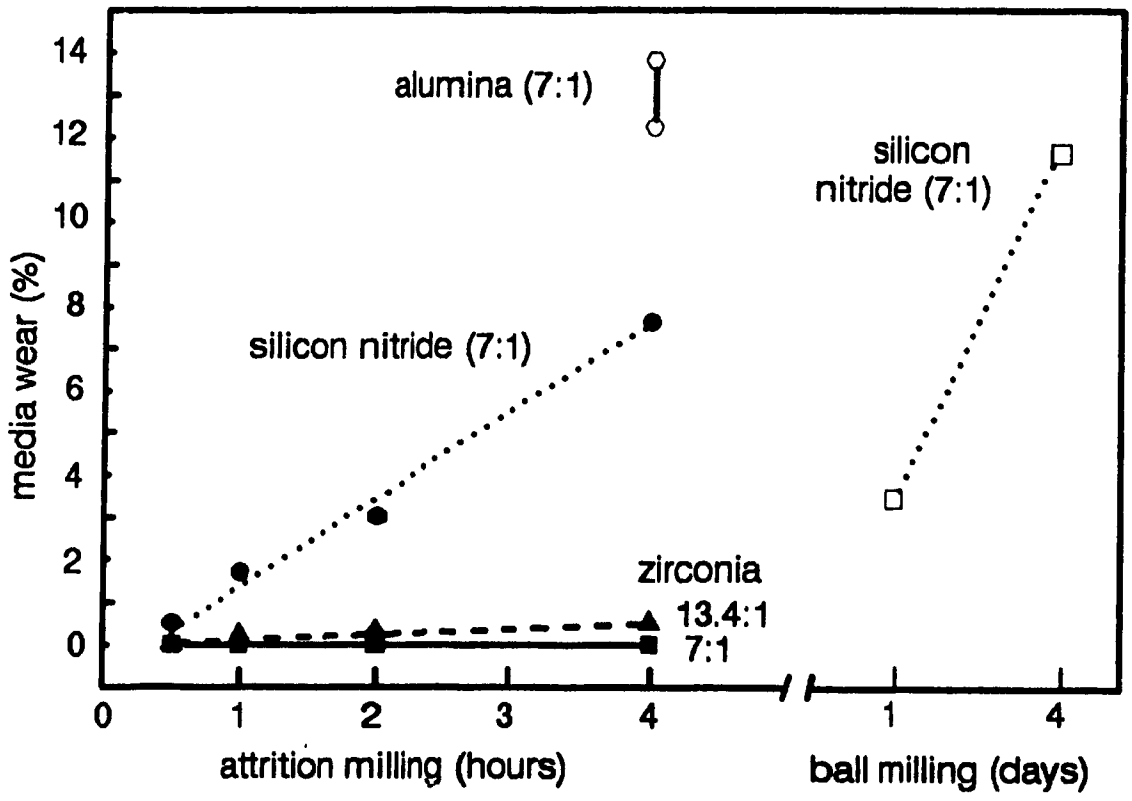

Figure 4.1 : Wear behaviour of Al_2O_3, Si_3N_4, and ZrO_2 media as a function of milling time.

wear, losing between 12 and 14 g of its weight for every 100 g of SiO_2 milled. This Al_2O_3 present in the starting materials resulted in the synthesis of a "silicon nitride" powder which contained 5-15 weight% AlN, 15-25 weight% SiC, and 35-45 weight% β-Si_3N_4 the balance being α-Si_3N_4. Figure 4.2 is the X-ray diffraction pattern of this powder. Although not clearly identified on the diffraction patterns, large globules which are believed to be alumino-silicates could be clearly seen with the aid of the SEM (Figure 4.3). These alumino-silicate globules are believed to be the result of alumina "chips" (from alumina media wear) which have reacted with SiO_2 prior to nitridation, and sintered together. Because of their smooth features these

globules are thought to have been a viscous liquid at the synthesis temperature (1510°C). This liquid phase is in turn believed to be in part responsible for the formation of silicon carbide and β-silicon nitride at such a low temperature (section 4.1.5).

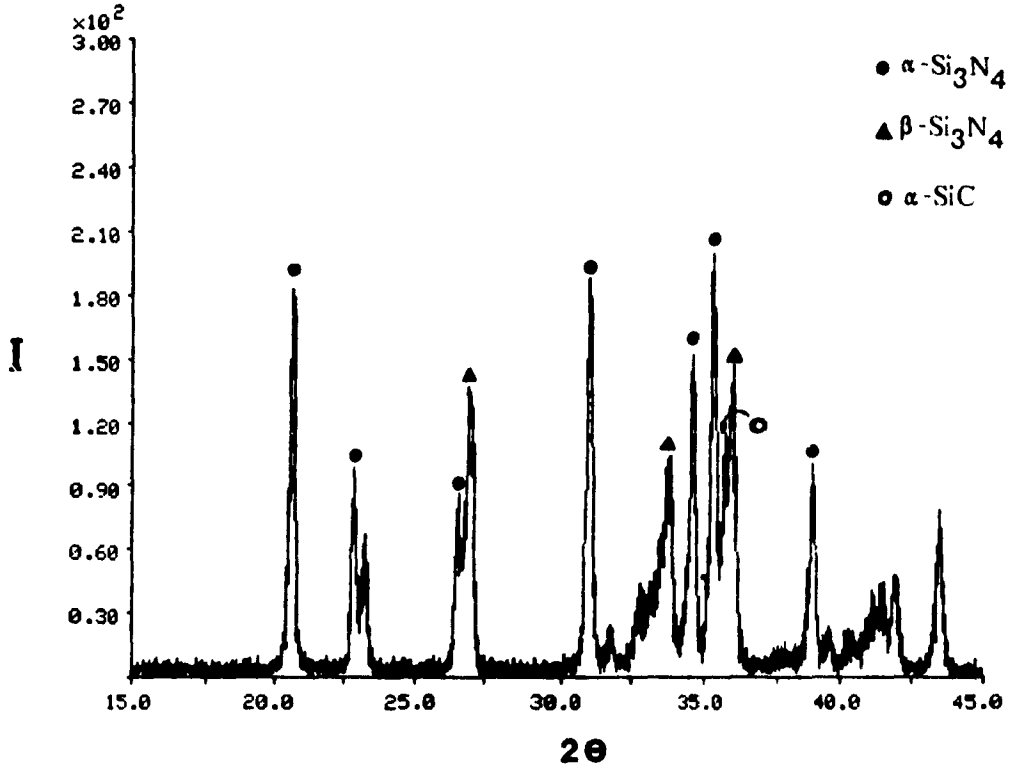

Figure 4.2 : X-ray diffraction pattern of powder produced from starting materials (5 weight% seed) attrition milled for 4 hours with Al_2O_3 media (7:1 weight of media:weight of solids).

For the same amount of materials milled and with the same weight of media to solids (7:1), the silicon nitride media showed a slight improvement, losing around 8 g after 4 hours of attrition milling. Besides the obvious contamination problems, the wear of silicon nitride media poses another threat to the mechanical properties of the final product, i.e. the introduction of large (10-100μm) β-Si_3N_4 "chips" into the α-Si_3N_4 powder produced (Figure 4.4).

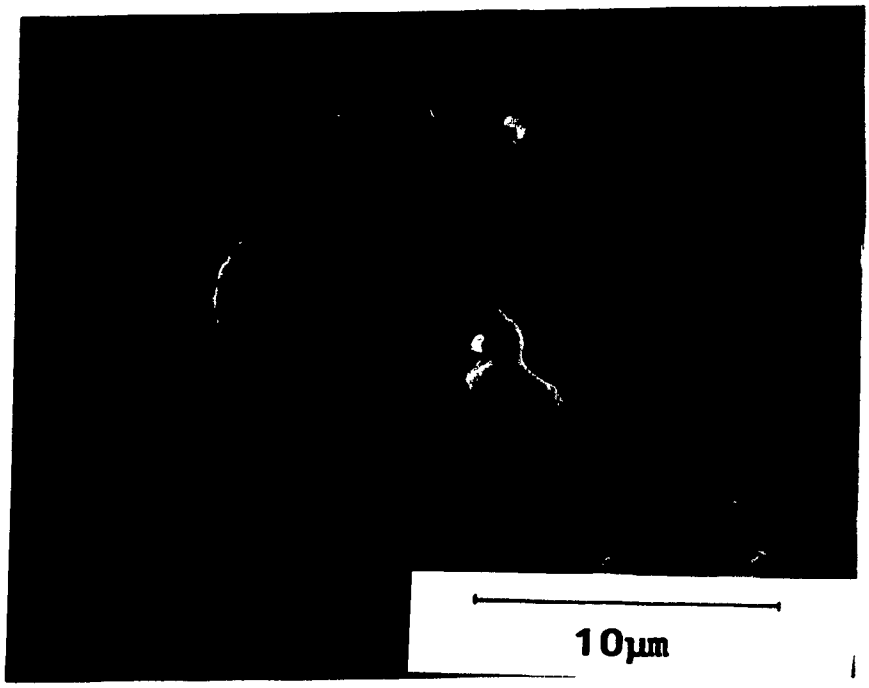

Figure 4.3 : SEM micrograph of alumina-based globules.

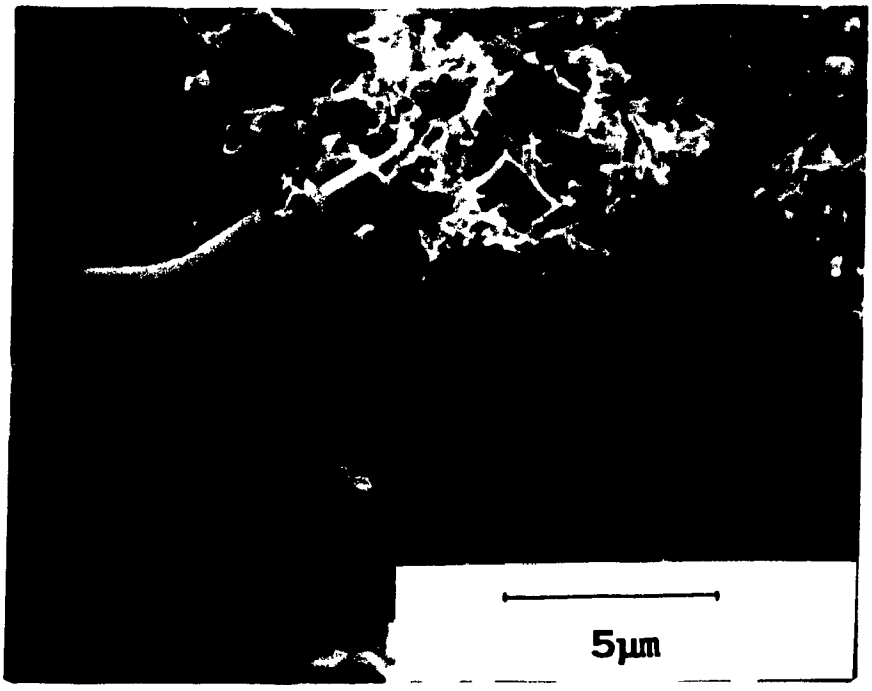

Figure 4.4 : SEM micrograph of β-Si_3N_4 "chips" resulting from the wear of the hot-pressed Si_3N_4 media after 4 hours of attrition milling.

These large "chips" of β-Si_3N_4 (high-temperature phase) will not dissolve into the liquid phase and reprecipitate (as will the α-Si_3N_4 grains) during sintering. Hence, the "chips" will remain intact in the final dense silicon nitride product where, because of their morphology, they could act as stress concentrators and therefore lower the strength of the ceramic. Also, these β-Si_3N_4 "chips" could partially inhibit the shrinkage process by hindering the movement of α-Si_3N_4 grains and creating larges pores in the final product.

ZrO_2 media balls showed the best wear performance of all, with no discernable weight loss even after 4 hours of attrition milling with a media weight:solids weight ratio of 7:1. In order for the volume of ZrO_2 media (higher density than Si_3N_4 media) to be equivalent to the volume of Si_3N_4 media used, the weight of ZrO_2 media:weight of solids ratio was increased to 13.4:1. Even with this weight (134 g of media to mill 10 g of solids), after 4 hours of attrition milling the ZrO_2 media only lost a maximum of 0.5 g for every 100 g of SiO_2 milled. Here, both the mass and the volume of media used are believed to be important factors. For a given volume of media, a higher media mass (by using a media with higher density) will mean that more energy will be imparted to each collision, and therefore result in a more efficient dispersion. On the other hand, for a given weight of media, a higher volume of media balls (more media balls having a lower density) will cause the collisions between the media and the particles to be more frequent and hence, improve the dispersion.

In order to establish the exact nature of the impurities brought about

by media wear, semi-quantitative XRF analysis was performed on Si_3N_4 powders made from precursors that were blended, attrition milled (Si_3N_4 and ZrO_2 media) and ball milled (Si_3N_4 media). The results of these analyses are presented in Table 4.1.

Table 4.1 : XRF analysis of various Si_3N_4 powders.

Precursors preparation method	Cation content (weight %)				
	Mg^{2+}	Al^{3+}	Fe^{3+}	Y^{3+}	Zr^{4+}
Mixed in blender (10 min.)	0.02	0.04	0.05	0.00	0.00
4 days ball milling (Si_3N_4 media)	0.00	0.24	0.14	3.50	0.01
4 hours attrition milling (7:1, Si_3N_4 media)	0.00	0.21	0.10	1.23	0.00
4 hours attrition milling (7:1, ZrO_2 media)	0.00	0.04	0.02	0.02	0.64

The XRF results enabled the identification of thr sintering aids used in the manufacture of the hot-pressed Si_3N_4 media (not specified by the manufacturer). The high contents of Y, Al, and Fe observed when Si_3N_4 media was used indicate that the sintering additives used were most probably Al_2O_3 and Y_2O_3. The high Fe content could also be the result of contamination from the media (i.e. from an early stage in media fabrication - milling with steel or stainless steel balls).

It was repeatedly observed that the starting materials exposed to a substantial amount of media wear (especially Si_3N_4 media) and hence containing

more impurities, had a higher tendency to form SiC and β-Si_3N_4 rather than α-Si_3N_4; an observation also shared by Bowden et al.[107]. For example, two different batches of reactants were prepared under identical conditions (attrition milled for 1 hour) with Si_3N_4 and ZrO_2. Both batches were then reacted at the same temperature (1510°C) using the same N_2 linear flow rate of 0.2 cm/s at STP. The batch of reactants made with Si_3N_4 media experienced a higher level of contamination from media wear (2 % of silica weight) than the batch milled with ZrO_2 media (no discernable wear). The silicon nitride powder produced with the "contaminated" reactants had a higher silicon carbide content (≈ 7 weight% SiC) than the "non-contaminated" one (traces of SiC). The X-ray diffraction patterns of both these powders are shown in Figure 4.5. The higher SiC content observed when precursors were exposed to Si_3N_4 media wear is believed to be related to the combined effect of Y, Al, and especially Fe impurities (Table 4.1) and strongly suggests that the iron originates from the Si_3N_4 media itself.

The effect of impurities on the thermochemistry of the Si-O-N-C system has been well studied by Siddiqi and Hendry[89] and also by Higgins and Hendry[108]. They showed that small amounts of impurities (notably iron) in the reactants have a pronounced effect on the formation of liquid phases at the reaction temperature. These liquid phases could then act as a source of silicon carbide formation, and hence catalyse and bring down the temperature at which silicon carbide starts to form (1550°C without impurities, 1320°C when 2 weight% iron is added). In Siddiqi's work, silicon carbide also formed as whiskers when contaminants

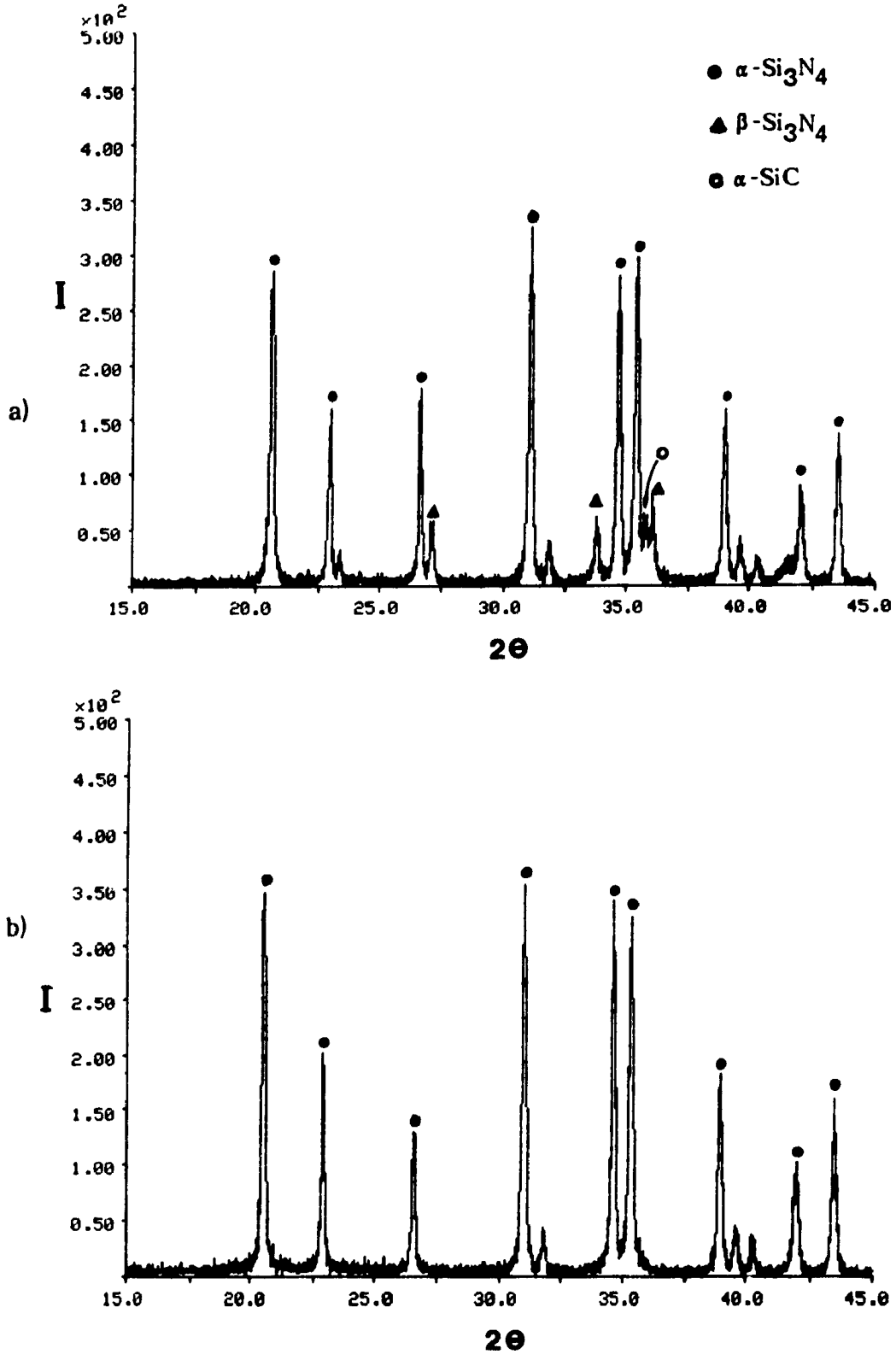

Figure 4.5 : Si_3N_4 powders produced using starting materials milled with a) hot-pressed Si_3N_4 media, b) ZrO_2 media.

were present, and the formation of liquid phases was emphasized by the presence of Fe-Si rich globules on the tip of many silicon carbide whiskers. However, in the present work no such globules were observed on the silicon carbide whiskers.

4.1.3 EFFECT OF GAS FLOW

It is generally accepted that the first step in the carbothermal reduction process is the formation of SiO gas according to equation 2.9. The SiO gas produced can then react with C (equation 2.10) or CO gas (equation 2.11) to form Si_3N_4.

However, several authors[108-112] have found that when the partial pressure of CO is too high in the reactor, the formation of silicon carbide is promoted through the following reaction (see section 4.1.5):

$$SiO_{(g)} + 3CO_{(g)} \longrightarrow SiC_{(s)} + 2CO_{2(g)} \qquad (4.1)$$

In order to lower the partial pressure of CO and hence minimize the formation of silicon carbide, pure nitrogen gas must flow continuously through the reactor bed to "flush" out the CO gas. This is the reason why flowing N_2 gas is preferred over a static nitrogen atmosphere.

A series of experiments was conducted to study the effect of varying the nitrogen flow rate through the reactor bed on the silicon carbide formation. Seeded (5 weight%) and unseeded starting materials chosen for this study were both attrition milled for 0.5 hour with a ZrO_2 media weight:solids weight ratio of 7:1. Three different nitrogen gas flows were selected; 0.1, 0.2 and 0.4 cm/sec at STP

(950, 1900 and 3800 cc/min). After the reaction (1530°C) the powders produced were decarburized and the phases present were identified by X-ray diffraction. The amount of silicon carbide in each powder was estimated with the help of a calibration curve (Appendix I). Figure 4.6 summarizes the results.

Figure 4.6 clearly shows the importance of nitrogen flow rate on silicon carbide formation. As expected, a low nitrogen gas flow of 0.1 cm/sec (at STP) was insufficient to maintain a low partial pressure of CO, and hence resulted in a silicon nitride powder with high silicon carbide contents of 9-10 weight%. Increasing the nitrogen flow rate to 0.2 cm/sec drastically reduced the levels of silicon carbide in the Si_3N_4 powders to 2-3 weight % (detection limit). Further increasing the nitrogen gas flow to 0.4 cm/sec did not result in any significant compositional changes, the levels of silicon carbide still remaining low. Also, seeding the starting materials did not seem to have any significant effects on the silicon carbide formation at the different nitrogen flow rates used.

Another interesting set of results that emerged from these experiments is the morphology of the powders produced. By visually examining the various powders with the aid of a scanning electron microscope, it was possible to note a sharp increase in the whisker content of the powders produced with a low nitrogen flow rate (950 cc/min) as opposed to that produced with a higher nitrogen gas flow (1900 and 3800 cc/min). These results are presented in Table 4.2.

Interestingly enough, the powders with the highest whisker content (produced with the lowest nitrogen flow rate) correlated with those having the

highest silicon carbide content. This further confirms that the layer of whiskers outside the reacted pellets was silicon carbide (see section 4.1.5).

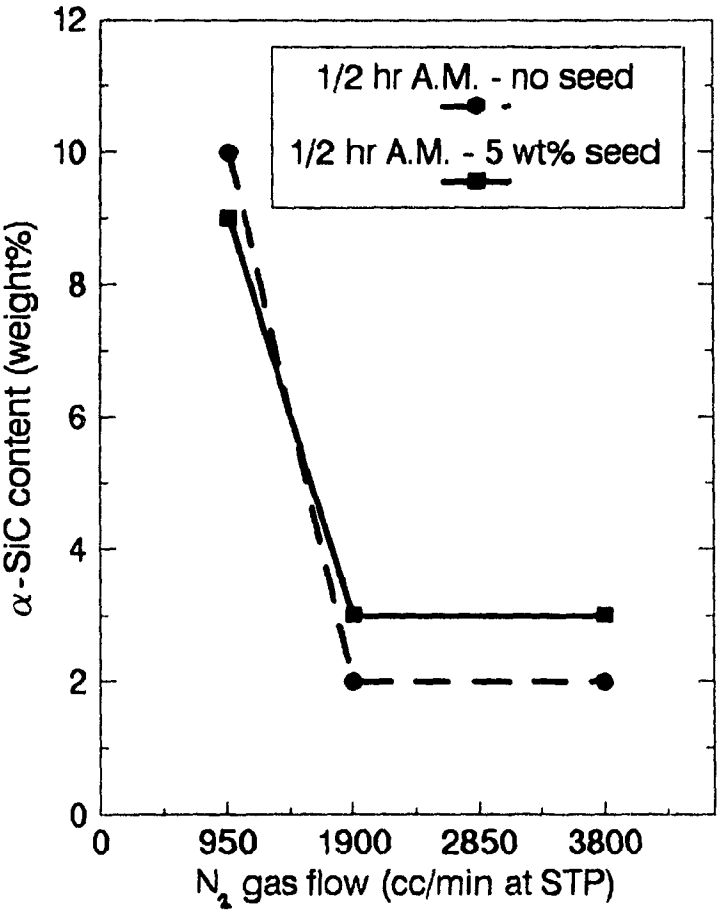

Figure 4.6 : Effect of varying the nitrogen flow rate on the silicon carbide formation.

Table 4.2 : Effect of nitrogen gas flow on whiskers content.

N_2 flow rate at STP (cc/min)	Approximate whisker content of seeded and unseeded powders	α - SiC content (weight %)
950	10-15 %	10
1900	< 5 %	2 - 3
3800	< 5 %	2 - 3

4.1.4 POSITION OF PELLETS IN THE REACTOR

The design of the reactor is such that pellets can be placed on three different levels in the reactor (Figure 4.7). About 60 grams of starting materials were placed on each of the three perforated floors. After a 5-hour reaction time at 1510°C (N_2 = 1900 cc/min at STP), the reacted pellets on each floor were separated according to their position in the reactor. On each floor, the reacted pellets located at the centre of the reactor were separated from those near the reactor wall (edge). Analysis of the silicon carbide contents of the reacted pellets from the different locations were then performed by X-ray diffraction and the results are presented in Figure 4.8.

Figure 4.8 clearly shows that the pellets located near the reactor wall on the upper floors, have a significantly higher silicon carbide content (14-15 weight %) than those on the bottom floor (6-7 weight % SiC), or even those at the centre of the upper floors (7-9 weight % SiC). This is believed to be due to a combination of two factors; the presence of "dead zones" near the reactor wall (N_2 flow was not

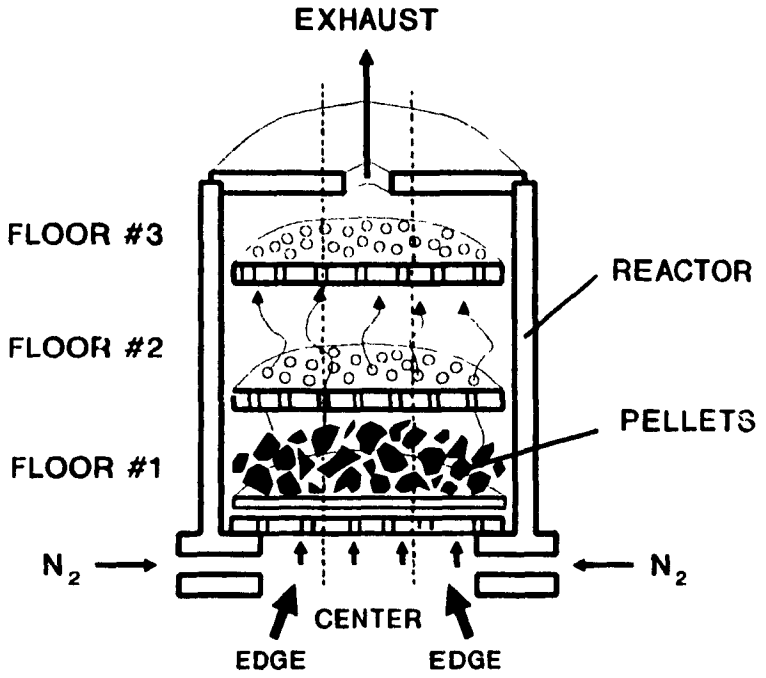

Figure 4.7 : Schematic view of reactor and position of pellets.

as efficient as in the centre of the perforated floors) and an increased partial pressure of CO for the upper floors. The later statement can be explained as follows: as the gas moves up in the reactor, the pellets on the first floor (bottom) are continuously contacted by fresh incoming pure nitrogen gas. However, the pellets on the second and third floor are not subjected to the same gaseous environment since the gaseous products (CO, CO_2, SiO) from the lower floors will eventually reach the upper ones. It has already been established that during the synthesis of α-Si_3N_4 by carbothermal reduction, relatively high partial pressures of CO can result in the formation of silicon carbide[108,112].

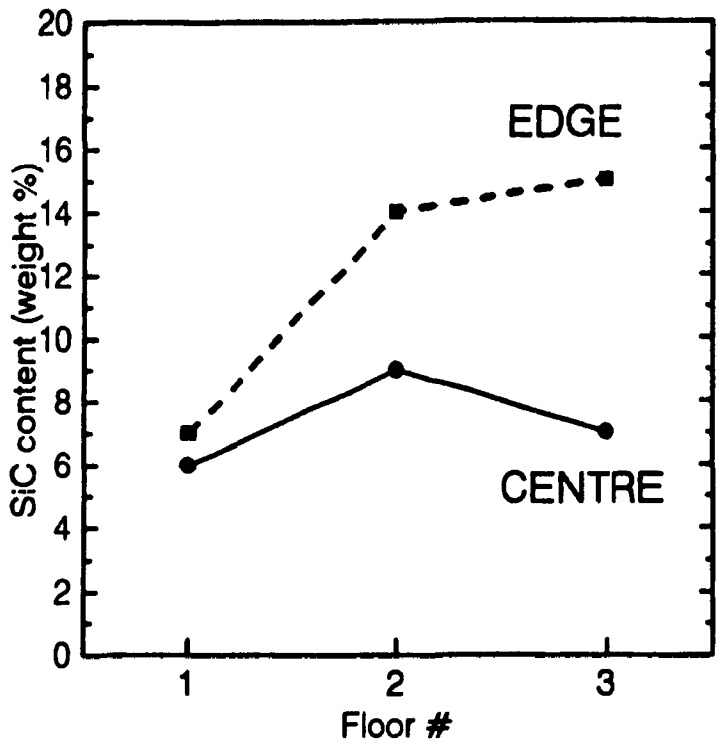

Figure 4.8 : Effect of pellet location on their silicon carbide content.

The higher silicon carbide content on the edge of the upper floors is not believed to be solely the effect of a change in gaseous environment since the pellets located at the centre of the upper floors, also subjected to high CO content, have relatively low silicon carbide levels. Also, the high silicon carbide content on the edge of the third floor cannot be caused by the presence of "dead zones" alone since, due to the symmetrical geometry of the reactor, "dead zones" on the edge of the top floors would also be present on the edge of the bottom floor. Hence, if "dead zones" alone were responsible for large differences in the silicon carbide contents between the pellets at the edge and centre of the upper floors, this difference would

also exist for the pellets on the first floor, which is not the case.

These results clearly demonstrate the importance of supplying the starting materials with an uniform and flowing supply of fresh nitrogen. Therefore, in all the subsequent experiments, the starting materials (100-150 grams) were placed only on the bottom floor. This change resulted in an overall lowering of the silicon carbide content of the α-Si_3N_4 powder produced.

4.1.5 FORMATION OF SILICON CARBIDE

It is not clear yet what effects, if any, the presence of silicon carbide in a dense Si_3N_4 part will have on its properties. Some believe that the introduction of SiC imparts thermal shock resistance to Si_3N_4[113], and that levels of SiC as high as 30 weight% do not have an effect on the oxidation resistance of Si_3N_4[114]. Others[115] have found that the presence of SiC in hot-pressed silicon nitride ceramics causes cracking during oxidation.

In this study, silicon carbide, whenever present in small quantities, was found to form a thin (<50μm) green layer on the surface of some of the reacted pellets. The composition of the layer was confirmed to be SiC by X-ray diffraction. Further SEM analysis of the silicon carbide layers, revealed that it was almost entirely composed of whiskers (Figure 4.9).

It is not clear yet why SiC forms on the outside of the pellets rather than the inside where one would expect the partial pressure of CO to be higher and the availability of C to be greater. However, this phenomenon might be explained (as just discussed) by the existence of gas flow "dead zones" in the reactor bed. The

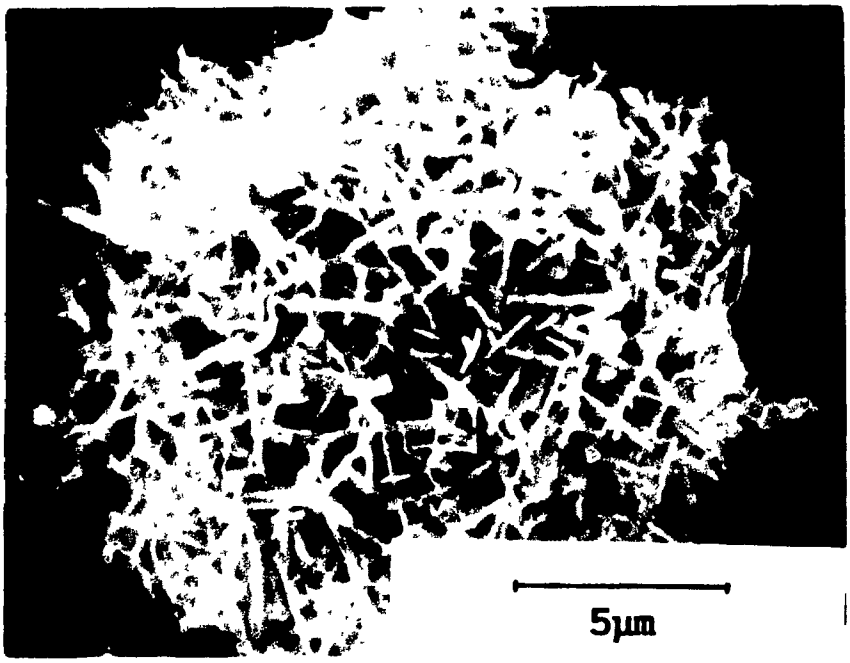

Figure 4.9 : SEM micrograph of a fragment of a silicon carbide layer (<1550°C, surface, impurity level high).

presence of these regions in the viscinity of the pellets would result in localized build-up of CO gas which could then contribute to the formation of a silicon carbide layer outside some of the pellets.

The variation in the morphologies of the silicon carbide is believed to be mainly related to the levels of impurities introduced during attrition milling of the precursors. By varying the reaction conditions (see Table 4.3) and keeping the level of impurities as low as possible, pure silicon carbide powders with a fine (0.05-0.2 µm) equiaxed (very few whiskers) morphology can be produced. These fine silicon carbide grains were, however, strongly agglomerated forming "brainlike" structures (Figure 4.10).

Silicon carbide is known to occur in some fifty or more different

Table 4.3 : Influence of various reaction parameters on the formation of silicon carbide.

Level of impurities in starting materials	Nitrogen gas flow (cm/sec)	Temperature	Relative amounts of silicon carbide	Morphology of silicon carbide present
LOW (attrition milled with ZrO_2 media, 0.5 - 4 hours)	0.10	1490 - 1550°C	5 - 10 wt%	Thick layer of whiskers (0.01-0.5 mm)
	> 0.20	1490 - 1550°C	< 3 wt%	Thin layer of whiskers (<100μm)
		> 1550°C	> 98 wt%	Mostly equiaxed grains ("brainlike")
HIGH (attrition milled with Si_3N_4 media, 1 - 4 hours)	0.10	1490 - 1550°C	80 - 90 wt%	Whisker bundles
	> 0.20	1490 - 1550°C	10 - 20 wt%	Whisker bundles
		> 1550°C	> 98 wt%	Whisker bundles
VERY HIGH (attrition milled with Si_3N_4 media, 8 - 16 hours)	> 0.20	1490 - 1550°C	50 - 90 wt%	Whisker bundles

modifications or allotropes. By comparing the X-ray diffraction patterns of the silicon carbide powders produced with the JCPDS standard diffraction patterns stored in the computer memory, it was possible to positively identify the "in-house" SiC as α-SiC, Moissanite-6H (see Appendix I). This finding is consistent with Knippenberg's observations[116] that α-SiC (hexagonal wurzite structure) is the stable modification at 1300-1600°C and that, with increasing growth temperatures,

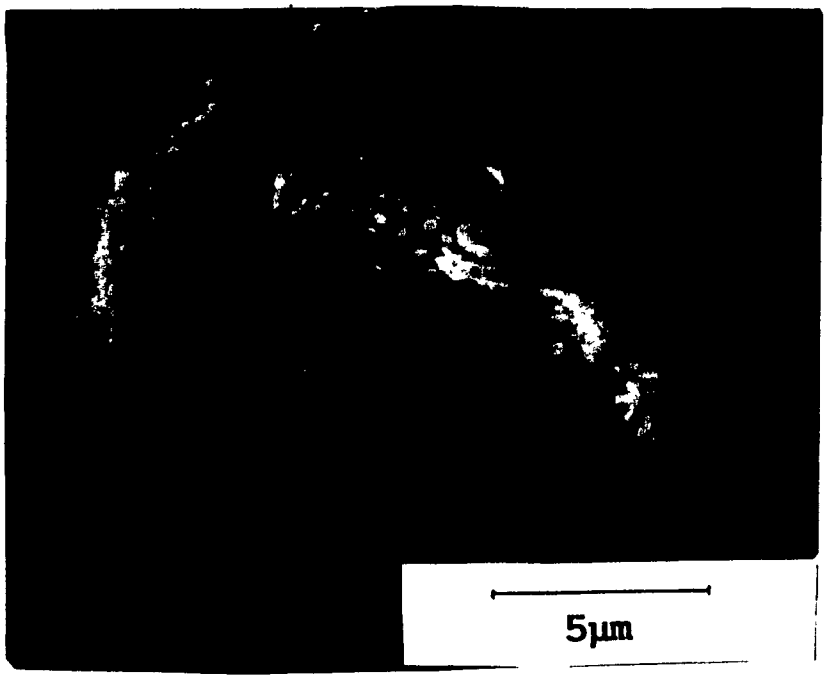

Figure 4.10 : SEM micrograph of "brainlike" silicon carbide agglomerates (>1550°C, bulk, impurity level low).

the types 4H, 15R, 6H, and 8H are found successively. Some authors[117] also claim that the 2H type (rare modification) can be stabilized by nitrogen when prepared by the Si_3N_4/C reaction. However, the only SiC polytype that was observed in this work was the commonly found[118] 6H type.

The β-SiC structure (cubic zinc blende or sphalerite structure) which is metastable at all temperatures[119] was not observed. Cho and Charles[120], working on small scale synthesis of Si_3N_4 by carbothermal reduction, claimed to have observed small amounts (< 5 weight%) of β-SiC in some of their silicon nitride powders. However, the quantities of silicon carbide produced in their experiments were insufficient to ensure proper identification of the crystalline phase (α or β-SiC) by X-ray diffraction since the main diffraction peaks for both α and β-SiC occur at the same location ($2\Theta \sim 36°$). In this work, large quantities (50 - 60 g) of pure silicon carbide powders have been synthesized by increasing the reaction temperature to ~1600°C. Whenever silicon carbide was found in large enough quantities for X-ray diffraction analysis to be conclusive (> 2 weight%), the analysis revealed α-SiC, rather than β-SiC. Figure 4.11 compares the X-ray diffraction patterns of the pure silicon carbide powder and that of a silicon nitride powder containing ~ 5 weight % SiC (both powders McGill synthesized) with the JCPDS standard diffraction patterns for both α and β-SiC. The identification of the crystalline phase of SiC (α or β) is made difficult when SiC is present in Si_3N_4 in small quantities (<10 weight %). Since in Figure 4.11 a) SiC occurs as a "green layer" surrounding the reacted lumps of α-Si_3N_4, it was possible to physically separate this

layer. The pieces of SiC "layers" were collected (with some α-Si_3N_4 present) and analyzed by X-ray diffraction. The diffraction pattern obtained is presented in Figure 4.11 b) where it becomes clearer that the small quantity of SiC present in a) was in fact α-SiC. Figure 4.11 clearly shows how α-SiC can easily be mistaken for β-SiC by X-ray diffraction, when only small amounts of SiC are available for analysis.

The reaction temperature can have a dramatic effect on the formation of silicon carbide. Previous work done at McGill University[85] showed that the synthesis of Si_3N_4 by carbothermal reduction of SiO_2 only occurs over a narrow temperature range (1500-1550°C). This study showed that for a 5 hour reaction time, a temperature below 1450°C yielded very little α-Si_3N_4 (very slow reaction) while above 1550°C, silicon carbide was the stable solid phase. These results are in good agreement with Szweda's work[121]. In order for the reaction to achieve completion within a reasonable amount of time, and also avoid the presence of silicon carbide in the Si_3N_4 powder produced, the reaction temperature should be carefully controlled and kept roughly between 1500°C and 1550°C. It is, however, important to note that these values are only valid for high purity starting materials. The presence of impurities can considerably lower this temperature "window" or, even make it very difficult to avoid SiC formation[89,120].

Table 4.3 summarizes qualitatively the observations made during this work, with respect to the effects of impurities (picked up mainly from media wear), temperature and gas flow on the SiC morphology and content in the α-Si_3N_4 powder

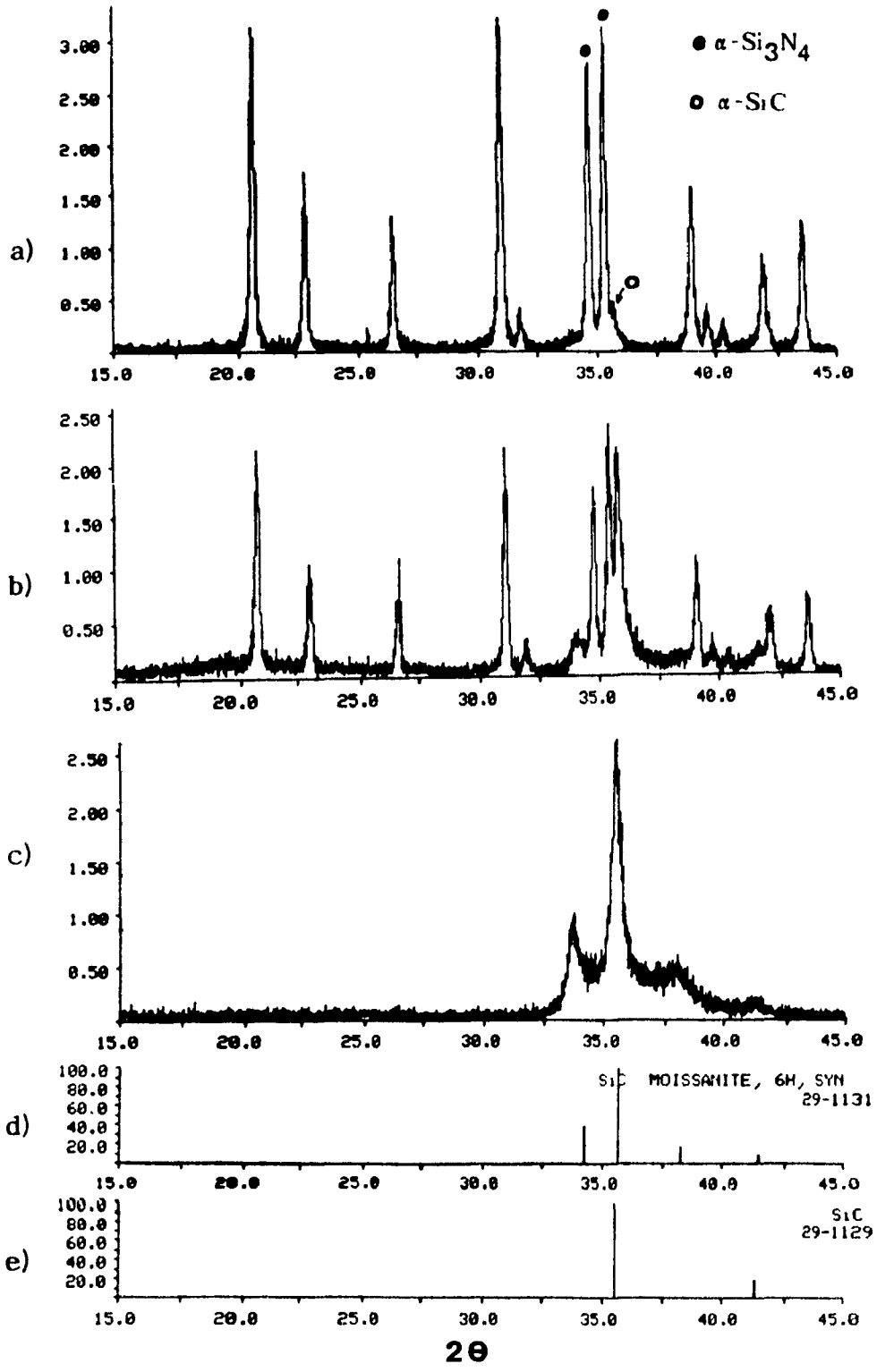

Figure 4.11 : X-ray diffraction patterns of: a) Si_3N_4 powder containing ~ 5 weight % SiC, b) "green layer" collected in a), c) Pure silicon carbide powder, d) JCPDS standard for α-SiC, e) JCPDS standard for β-SiC.

produced.

Large increases in the silicon carbide levels could be seen whenever the starting materials were heavily contaminated. Also, for the cases where the silicon carbide content reached > 90 weight%, the powder morphology was quite different; an equiaxed or "brainlike" morphology (see Figure 4.10) for starting materials with low impurities, and whisker bundles for those with high levels of contaminants (see Figure 4.9).

4.1.6 SUMMARY OF OPTIMUM PRECURSOR PREPARATION METHOD

In summary, the optimum precursor preparation method was:

Mixing Method : Attrition Milling (0.5 - 4 hours)

Media : ZrO_2 (7:1, 13.4:1)

while the optimum reaction conditions were found to be:

Temperature : 1490 - 1540 ^{o}C

N_2 Gas Flow : 0.2 cm/sec

Position of pellets : Bottom Floor.

4.2 EFFECT OF PRECURSOR PREPARATION ON SILICON NITRIDE FORMATION

Although the C and SiO_2 particles are extremely fine (10-40 nm), they both tend to agglomerate. The degree of intimacy between the C and SiO_2 particles will therefore depend to a great extent on the ability of the mixing process (attrition milling with ZrO_2 media) to break down these agglomerates. This section

will investigate the effect of the degree of intimacy between the precursors and the nucleation and growth behaviour of silicon nitride.

4.2.1 PARTICLE SIZE

A series of experiments was conducted in order to study the effect of varying the attrition milling time of the starting materials, on the morphology and size of the silicon nitride powders produced. The silica and carbon (without silicon nitride seed) were mixed for 0.5, 1, 2 and 4 hours using ZrO_2 media, after which, these four different batches of reactants were nitrided under the same reaction conditions (T=1510°C, N_2=1900 cc/min at STP). The reacted products were then decarburized and the morphology of the α-Si_3N_4 particles was studied with the aid of the SEM. Figure 4.12 (a) and (b) are micrographs of the powders produced from the 1/2-hour and 4-hour attrition milled starting materials.

These micrographs illustrate the bimodal size distribution of the powders. All four powders had a more or less similar appearance, with variations in the size of the large and small particles, as well as the relative amount of each size class present. Quantifying these results was, however, difficult without the aid of the particle size analyzer (section 3.4.3.2), which experienced problems with the dispersion of the silicon nitride particles. The size analysis of the small and large grains was finally performed on SEM micrographs using techniques described in Appendix II, while the relative amount of each size class was semi-quantitatively obtained from SEM observations (section 3.4.4). These results, together with surface area measurements are presented in Table 4.4.

(a)

(b)

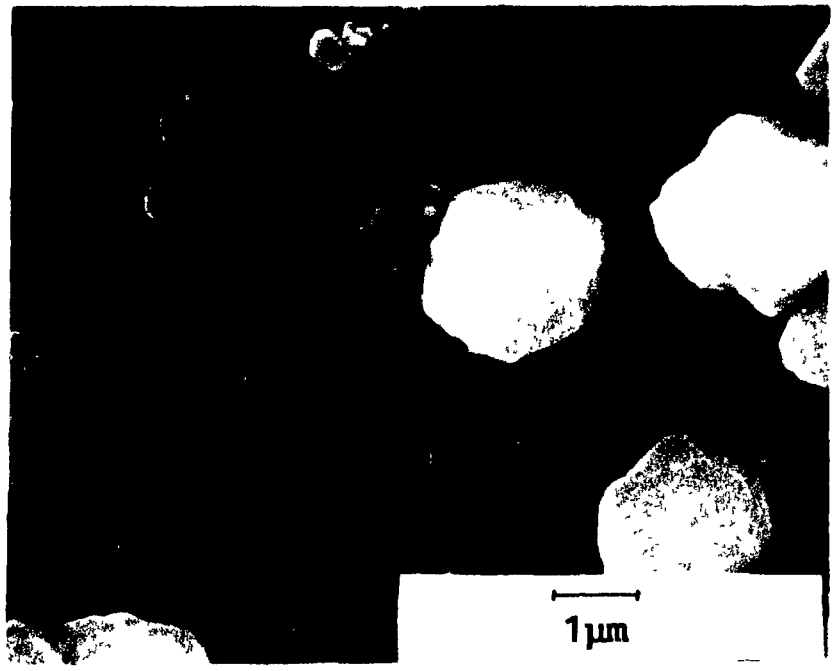

Figure 4.12 : SEM micrograph of powder produced from unseeded starting materials (7:1, weight of ZrO_2 media:weight of solids) attrition milled for a) 1/2 hour b) 4 hours.

The values presented in Table 4.4 clearly indicate that, although the calculated weighted average diameters stay fairly constant (1.4-1.5 μm) even for increased attrition milling time, the surface area of the powders goes up from 8.92 m^2/g for the 1/2 hour attrition milled precursors to 12.30 m^2/g when the milling time is increased to 4 hours. This is the result of a larger proportion of finer particles. The 1/2 hour attrition milled unseeded precursors yielded a Si_3N_4 powder composed mostly of coarse particles with ~ 60 vol% of 0.75 μm grains and ~ 40 vol% of 2.5 μm grains. Increasing the milling time to 1 hour resulted in a decrease of the size of larger grains (from 2.5 μm to 1.45 μm) and the formation of finer grains. Further increases in the milling time did not bring about significant changes in the average diameter of the fine grains, but did raise the proportion of fines from 2 vol% for 1 hour A.M. to 35 vol% for 4 hours A.M.. Some of the variations in particle size distributions observed in Table 4.4 are difficult to explain, and might be attributed to the sensitivity of the reaction conditions which have been shown to play an instrumental role in determining the particle's morphology (see section 4.4.1).

Table 4.4 : Relative amounts of large and small silicon nitride particles as a function of attrition milling time of unseeded starting materials (7:1, weight of ZrO_2 media:weight of solids).

Attrition milling time of unseeded starting materials	Calculated average diameter of SMALL particles (μm)	Approx. content of SMALL particles (vol %)	Calculated average diameter of LARGE particles (μm)	Approx. content of LARGE particles (vol %)	Calculated weighted average diameter (μm)	BET Surface area (m^2/g)
1/2 hour	0.75	60	2.5	40	1.5	8.92
1 hour	0.4 - 0.6	~ 2	1.45	~ 98	1.5	11.57
2 hours	0.54	10	1.45	90	1.4	12.13
4 hours	0.53	35	1.96	65	1.5	12.30

4.2.2 NUCLEATION BEHAVIOUR

The trends presented in Table 4.4 can be explained by the nucleation and growth behaviour of α-Si_3N_4. Zhang and Cannon[86] suggested that the growth of Si_3N_4 takes place via the gas-phase reaction (4.5) and that nucleation of Si_3N_4 occurs either on the silica or the carbon surface through the solid-phase reaction (4.6).

gas-phase $3SiO_{(g)} + 3CO_{(g)} + 2N_{2(g)} \longrightarrow Si_3N_{4(s)} + 3CO_{2(g)}$ (4.5)

$\Delta G = 8.4$ J/mol

solid-phase $3SiO_{(g)} + 3C_{(s)} + 2N_{2(g)} \longrightarrow Si_3N_{4(s)} + 3CO_{(g)}$ (4.6)

$\Delta G = 12.3$ J/mol

$SiO_{2(s)} + C_{(s)} + \text{Flowing } N_{2(g)} \longrightarrow SiO_{(g)} + CO_{(g)} + \text{Flowing } N_{2(g)}$ (4.7)

$\Delta G \approx -60\ 000$ J/mol

The ΔG of both reaction 4.5 and 4.6 are only slightly positive (close to zero). By looking at reaction 4.7 one can understand better why the gas phase reaction (4.5) is favoured. The highly negative ΔG of reaction 4.7 indicates that it will be the first reaction to occur, producing large amounts of SiO and CO gases. Since these products are the reactants for reaction 4.5, they will hence drive it to the right.

Previous work done at McGill University[90,92] on the growth of Si_3N_4 on various substrates also confirmed these results, and indicated that growth of Si_3N_4 on pre-existing α-Si_3N_4 grains by the gas-phase reaction was by far favoured

over nucleation of Si_3N_4 on carbon by the solid-phase reaction. In other words, α-Si_3N_4 preferred to grow on pre-existing α-Si_3N_4 nuclei rather than to form new nuclei. However, in Durham's work[92], the reactant concentration near the substrates surfaces might not have been high enough to promote nucleation of α-Si_3N_4 on carbon. La Mer[122] described a process (Figure 4.13) whereby a burst of nucleation is followed by growth. In this process, nucleation only occurs when the concentration of reactants has reached a high enough level, termed super-saturation (see section 4.3.1). When the nucleation reaction has used up the reactants to the

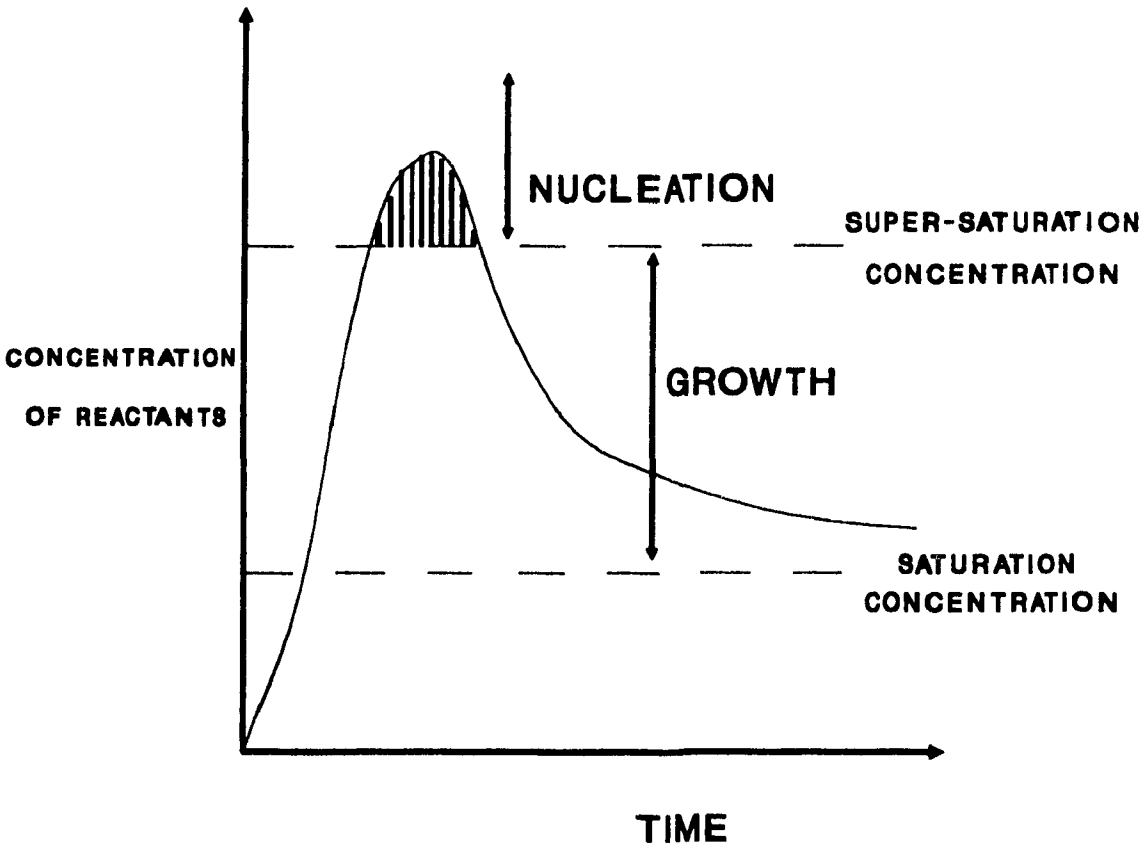

Figure 4.13[122] : Schematic of the ideal nucleation-growth process.

point where their concentration is below the super-saturation level, growth of Si_3N_4 then occurs.

A similar curve for the evolution of CO gas during carbothermal reduction was obtained (Figure 4.14) when a CO analyzer was connected to the off-gases of the furnace. Monitoring the CO gas evolution during the reaction is also an efficient way to monitor the SiO gas since the concentration of SiO and CO are closely related to one another; the main source of CO production being the reaction between SiO_2 and C and/or CO (equations 4.7 and 2.12) or between C and CO_2 (equation 2.13).

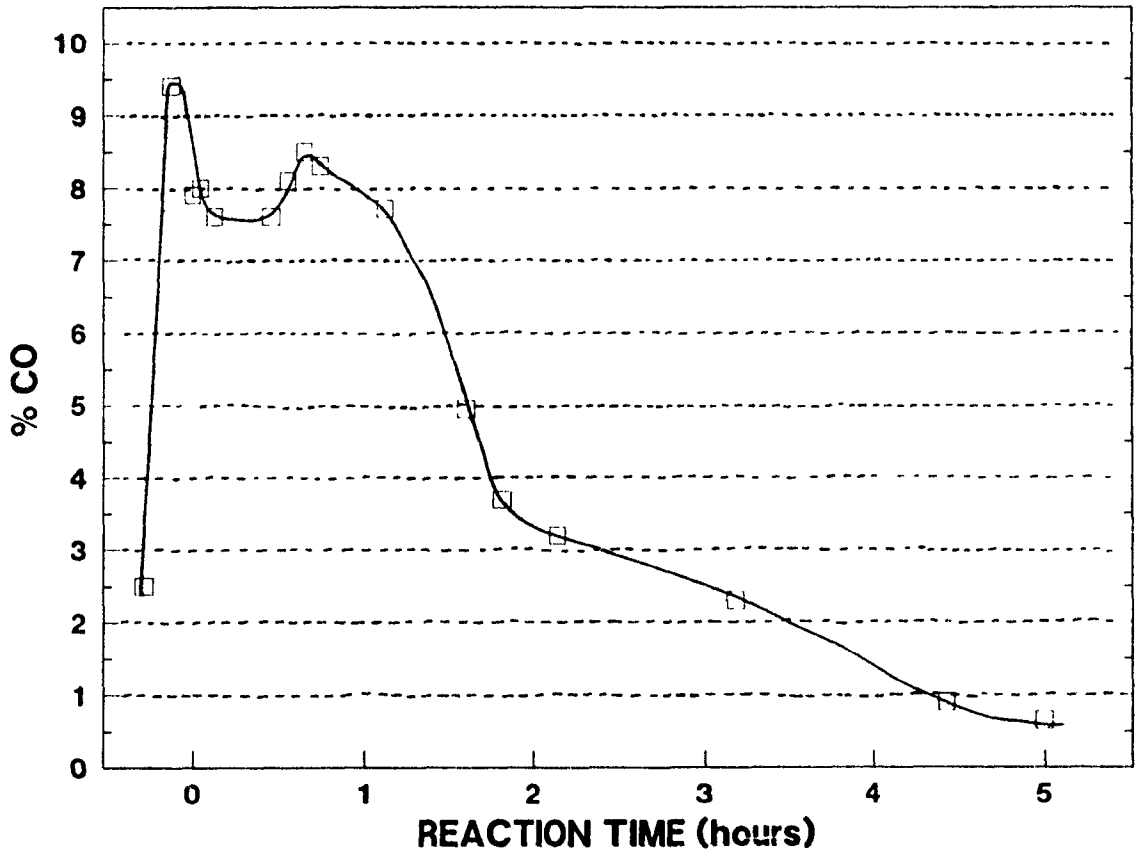

Figure 4.14 : CO evolution during carbothermal reduction of SiO_2 at 1530°C.

The Si_3N_4 powders in Table 4.4 are, in the main, composed of large particles. This is believed to be directly related to the very small number of nuclei present (unseeded starting materials), or formed at the beginning of the reaction. The limited number of sites initially present for growth to take place resulted in a few nuclei growing to large dimensions (1-5 μm). Since a large fraction of the total volume of reactants (notably SiO gas) is used up rapidly at the beginning of the reaction, insufficient SiO gas is left for further growth on the nuclei produced some time after the initial burst of CO and SiO.

With regard to the bimodal size distribution, nucleation is believed to take place throughout the reaction; i.e. on a global basis at the beginning of the reaction and, after the initial burst of reactants, on a more limited scale in local regions where the starting materials are especially well mixed. Even though attrition milling is an aggressive mixing method, the starting materials from which these Si_3N_4 powders were produced had, overall, an insufficient number of "well mixed" regions to cause a widespread formation of α-Si_3N_4 nuclei. However, increasing the attrition milling time is believed to have resulted in a larger number of these "well-mixed" regions, and therefore a greater amount of nucleation for the 4 hours A.M. than for the 1/2 hour A.M. starting materials, explaining why the volume fraction of fines tends to go up with longer attrition milling times.

4.2.3 REACTION USING A SOLUBLE FORM OF CARBON

A series of experiments was conducted in order to study both the feasability of the use of a soluble form of carbon and the morphology and particle

size of the silicon nitride powder produced. Indeed, the size and size distribution of the silicon nitride particles provide key indications on the nucleation and growth behaviour that has taken place during the reaction. Various soluble forms of carbon exist such as furfuryl alcohol used by Silverman[123] for the carbothermal synthesis of aluminum nitride, poly-acrylonitrile (PAN) which is soluble in dimethylformamide (DMF), ethyl cellulose, starch and sugar to name a few. Because of its wide availability, low cost and high purity, refined sugar (sucrose) was used in these experiments. Extensive work has been done at McGill University on the use of sugar as a carbon source for the synthesis of AlN by carbothermal reduction[124]. From this work, an optimized pyrolysis cycle was developed (Figure 4.15) and the actual carbon yield from the pyrolysis of sugar was estimated to be around 20-25% (100 grams of sugar will yield 20-25 grams of carbon).

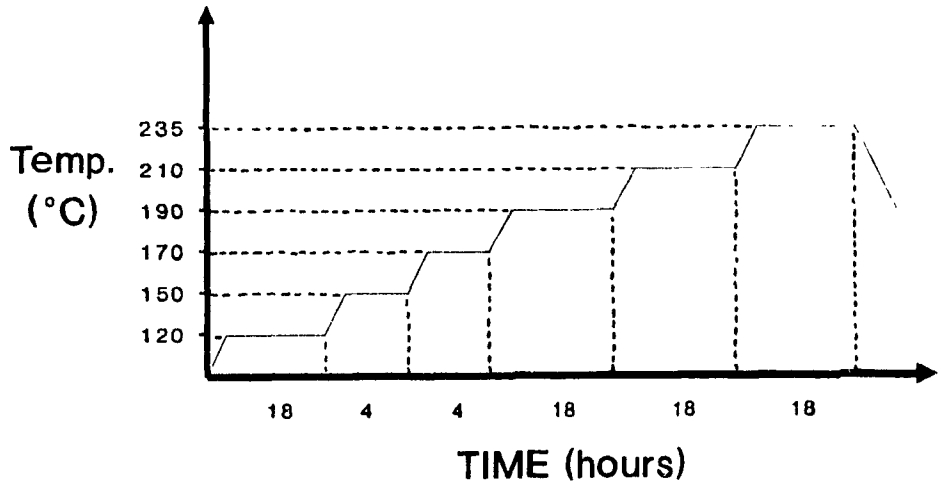

Figure 4.15 : Pyrolysis cycle used for the "burn-out" of sugar.

The reactants for the synthesis of silicon nitride powders were prepared using the following amounts of precursors (Table 4.5) :

Table 4.5 : Amounts of precursors used for the synthesis of silicon nitride using sugar as a carbon source.

Starting materials	Weight (grams)
Sugar	114.1
SiO_2	35.1
H_2O	310

The precursors together with ~ 1 kilogram of ZrO_2 media balls (weight of ZrO_2 media:total weight of solids ratio of 7:1) were placed in a polyethylene bottle in which they were ball milled for 24 hours and then, pyrolyzed into pellets. These pellets were reacted at a temperature of 1510-1520°C for 5 hours under a N_2 flow rate of 1900 cc/min at STP. The silicon nitride powder produced (Figure 4.16) was extremely fine (20-50 nm) with a surface area of 85.2 m^2/g. The addition of seeds to the starting materials did not seem to have a significant effect on the particle size, since the vast majority (>99%) of the particles observed by electron microscopy had a size well below that of the seed (0.2 μm).

The X-ray diffraction pattern of the decarburized silicon nitride powder (Figure 4.17) indicates that, although the peaks present are those of α-Si_3N_4, the powder is not fully crystalline (shown by amorphous background below the peaks). The amorphous background is the result of residual amounts of both carbon (~ 5 weight%) and silica (oxygen ~ 9.5 weight%). Although a high oxygen

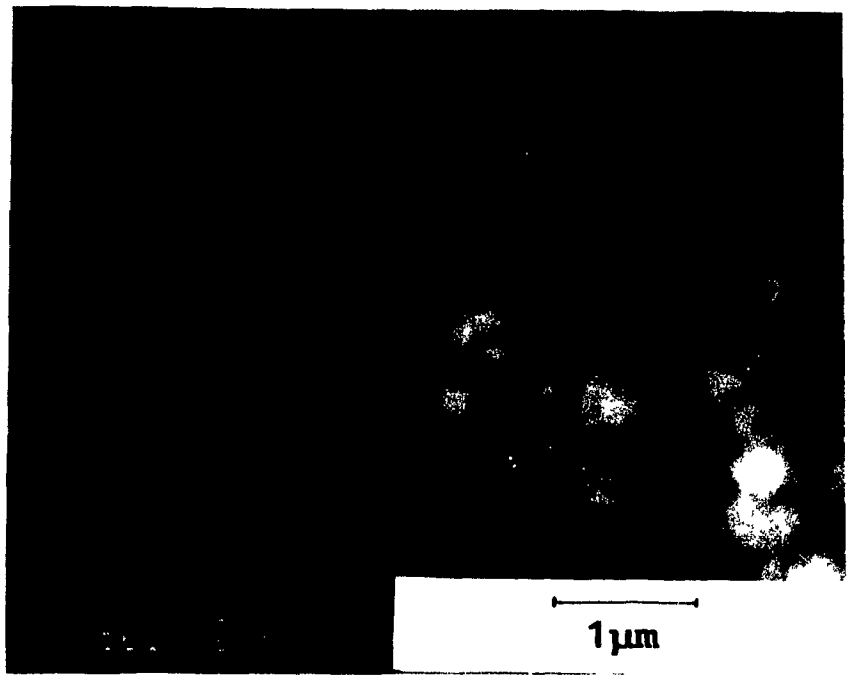

Figure 4.16 : SEM micrograph of silicon nitride powder produced with sucrose.

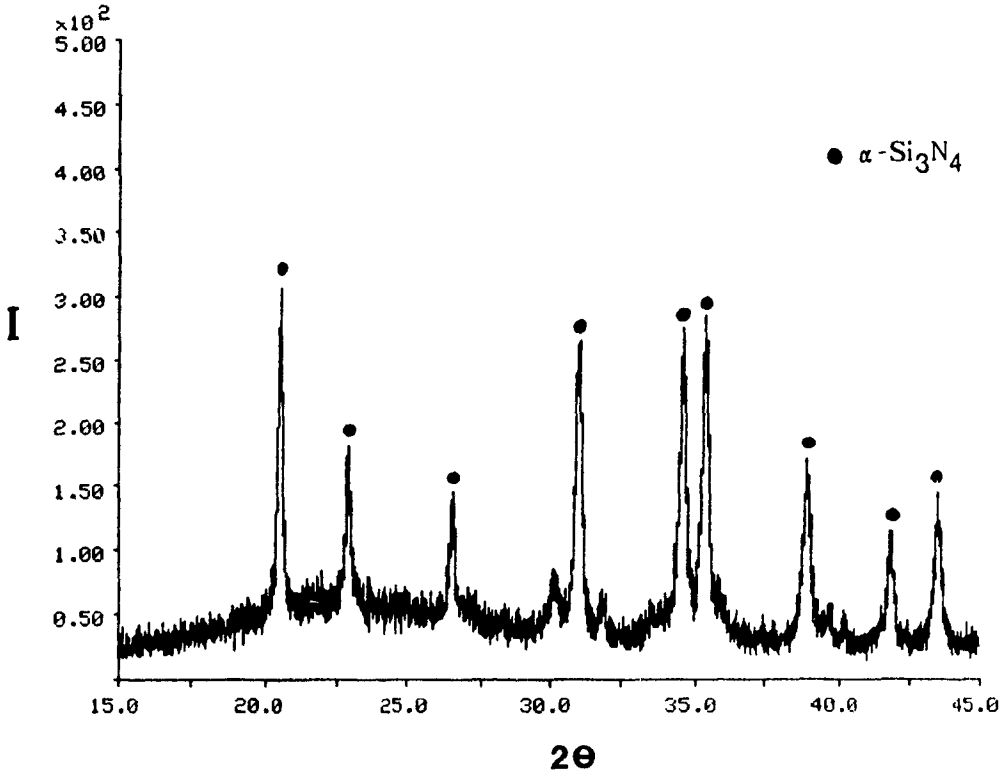

Figure 4.17 : X-ray diffraction pattern of the silicon nitride powder produced with sugar.

content was expected for such a fine powder, levels of oxygen well above 5 weight% clearly indicate that not all of the SiO_2 converted into Si_3N_4. The lack of conversion is thought to be due to pellets of reactants being insufficiently porous to allow for adequate diffusion of nitrogen. The density of pellets was measured by the Archimedian method using mercury. The pellets made with sugar had a density of 1.2 - 1.5 g/cm^3, compared with a density of 0.6 - 0.7 g/cm^3 for the pellets made with carbon black. The high density of the material even after reaction would also explain why the normal decarburization cycle (2 hours at 750°C in still air) was unable to bring the final carbon content down to normal levels (0.5 -1.5 weight%). Optimizing pellet densities, as well as the various parameters involved in the use of a soluble form of carbon is, however, beyond the scope of this work. The only information that was sought here was to see the effect of replacing C black by sugar (hence maximizing the intimacy between the precursors) and observing its influence on the particle size of the silicon nitride powders.

A higher degree of intimacy between the carbon and silica particles, brought about by longer attrition milling times will result, at least on a local basis, in a faster release of reactants (SiO and CO gases). This will then cause the concentration of reactants to locally exceed the super-saturation concentration and will hence, with the help of a sufficently high number of carbon particles or other appropriate nucleation sites in close proximity, result in a burst of nucleation.

The use of longer attrition milling times to achieve a better intimacy between the precursors is limited in its efficiency, and even with ZrO_2 media,

extremely long milling times can cause serious contamination problems. As will be seen in section 4.3, combining the effects of moderate attrition milling time together with the introduction in the reactants of fine α-Si_3N_4 particles as seed is a viable way to produce fine equiaxed α-Si_3N_4 powders.

Another interesting way to produce a fine Si_3N_4 powder is to maximize the contact between the carbon and silica by having either one, or both of these in a water soluble form during mixing. However, upon drying a soluble form of silica (i.e. no evidence of solids) might agglomerate and form small pockets of silica (even with an excess amount of carbon). These regions would tend to sinter before the reaction temperature is reached, forming relatively large silica globules (1 - 10μm). Because of mass transfer considerations, such globules might not convert into Si_3N_4 as efficiently, resulting in high oxygen contents for the final α-Si_3N_4 powder. On the other hand, upon drying and pyrolyzing, a soluble form of carbon, the result would also be carbon rich regions in the reactants (especially since carbon is used in excess). However, these regions do not represent a problem since carbon does not sinter under these reaction conditions.

When a soluble form of carbon is mixed with an extremely fine particulate silica powder, such as the fumed silica used in this study, the carbon bearing molecules surround the silica particles. After pyrolyzing, the carbon particles left behind will actually coat each silica particle, hence maximizing the contact between the carbon and the silica. Such an intimate contact between the precursors will result locally, in an extremely rapid rate of SiO and CO gas evolution

at the reaction temperature yielding concentrations well above the super-saturation level discussed earlier. This will in turn cause a widespread burst of Si_3N_4 nucleation to occur, resulting in a very fine powder.

Such a fine powder with a narrow size distribution is not the result of heterogeneous nucleation. The size characteristics of this powder clearly indicate that homogeneous nucleation (nuclei forming almost everywhere at the same time) played a major role in the formation of the silicon nitride by carbothermal reduction. This is proof that as the intimacy between the carbon and the silica is improved (either by using a soluble form of carbon and/or by increasing the attrition milling time (section 4.2.1)), a greater degree of nucleation occurs. This in turn results in a finer silicon nitride powder.

4.3 EFFECT OF SEEDING

Several authors[92,125,126] have already established the importance of seeding of carbon/silica mixtures in reducing the final particle size of the silicon nitride powder. Also, it will be shown in section 4.4 that seeding ensures a faster conversion of SiO_2 to α-Si_3N_4.

Previous work done at McGill University by Shanker et al.[90] showed that as the amount of seed is increased from 5 to 50 % of the weight of silica, the particle size decreases and tends towards that of the seed (0.2μm) material. However, in their work, the starting materials were not attrition milled but were mixed in a blender for 15 minutes in iso-propanol.

Although submicron silicon nitride powders can be synthesized by using

large amounts of seed, it is not a commercially viable option. Shanker et al. also reported that increasing the seed content causes a greater agglomeration of the final powder. Hence, if seeding is used, it should be limited to small quantities. The next section will deal with the combined effects of small additions of α-Si_3N_4 seed together with an increased intimacy between the carbon and silica achieved through attrition milling.

4.3.1 INFLUENCE OF ATTRITION MILLING TIME

Figure 4.18-19 are SEM micrographs of the α-Si_3N_4 powders produced from seeded and unseeded starting materials attrition milled for 0.5 and 4 hours respectively, using carbon black.

The addition of 5 % by weight of seed to the raw materials, combined with attrition milling as a means of improving the precursor intimacy, resulted in submicron α-Si_3N_4 powders with narrow size particle size distributions. As seen in Figures 4.18-19, the most dramatic difference between the seeded and unseeded powders lies in their particle size distributions. The seeded precursors resulted in fairly monosized powders, unlike the unseeded ones which resulted in the formation of powders with bimodal size distributions (see section 4.2.1). The bimodal size distributions observed in the unseeded powders is thought to be the result of very few nucleation/growth sites being available at the beginning of the reaction concurrent with the large SiO release. Initially, this translates into the formation of few nuclei which will then grow to large dimensions (1.5 - 5 μm) since the growth process is favoured over nucleation under these conditions. However, in the case of

(a)

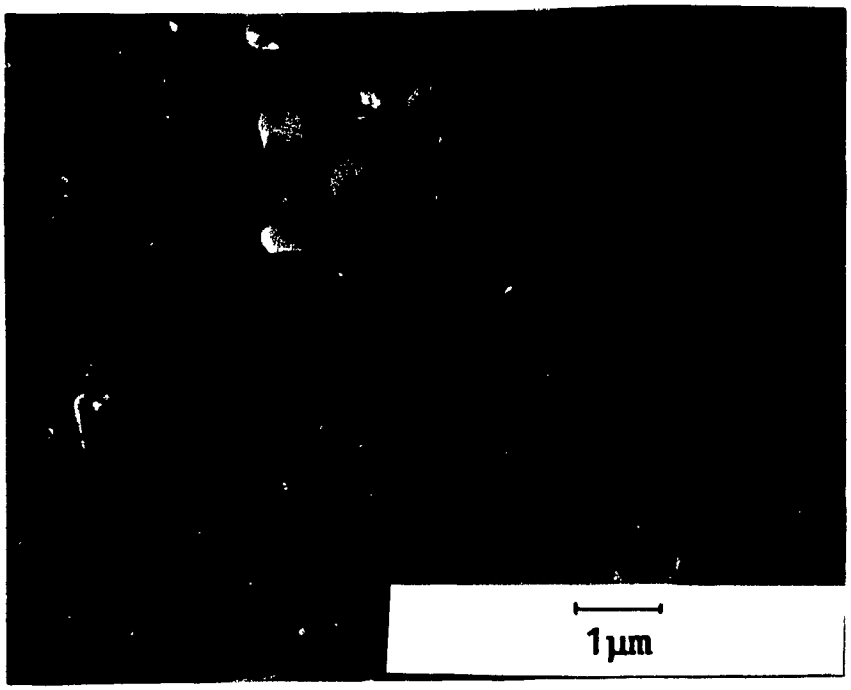

(b)

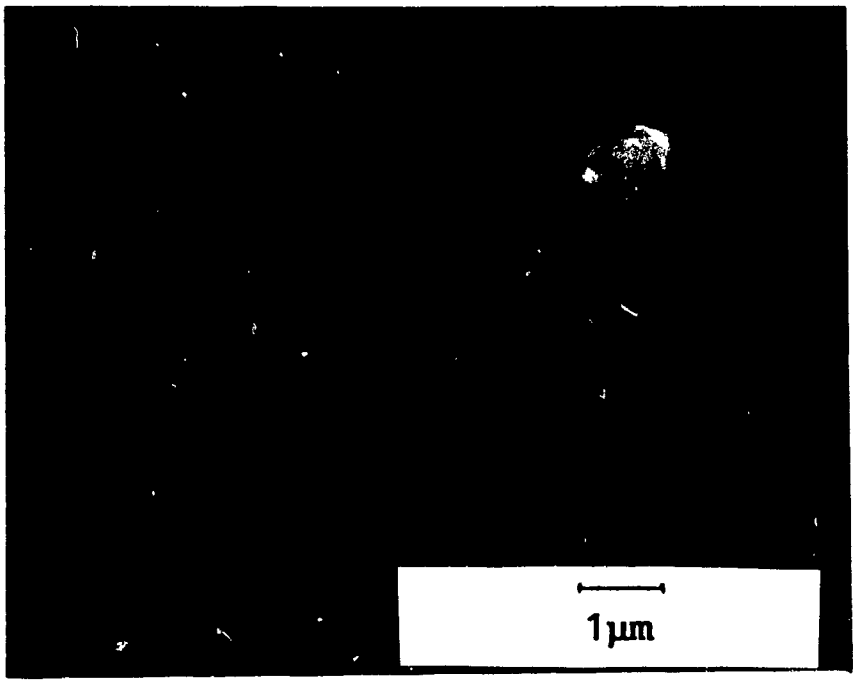

Figure 4.18 : SEM micrographs of α-Si_3N_4 powders produced (~1510°C) from starting materials attrition milled (7:1, weight of ZrO_2 media: weight of solids ratio) for 0.5 hour,
a) unseeded, b) seeded.

(a)

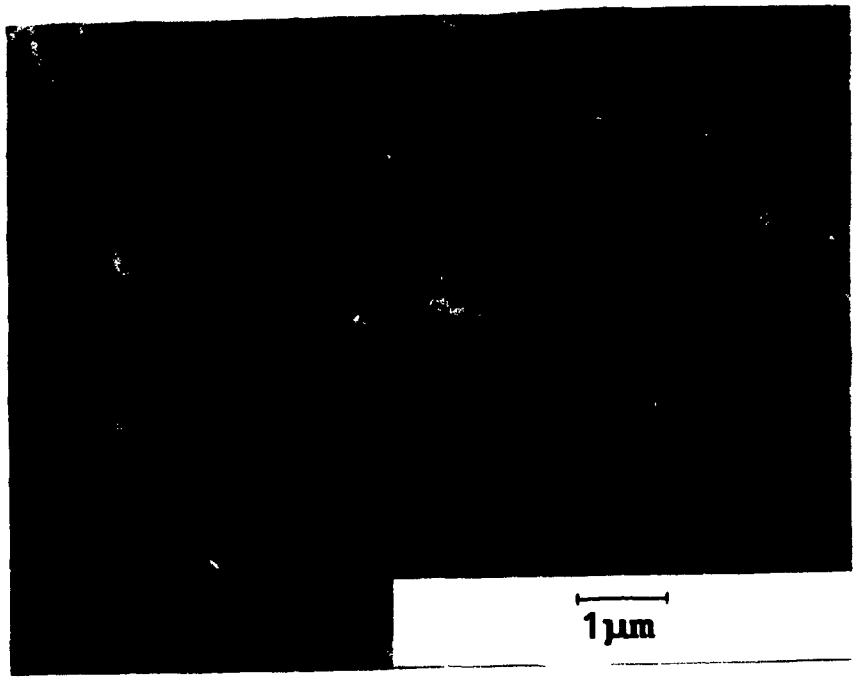

(b)

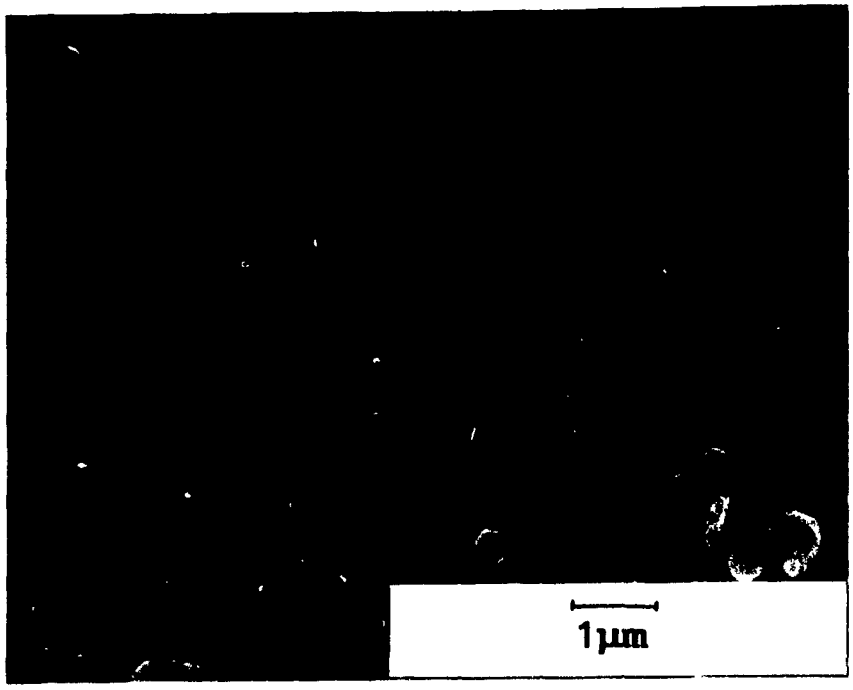

Figure 4.19 : SEM micrographs of α-Si_3N_4 powders produced (~1510°C) from starting materials attrition milled (7:1, weight of ZrO_2 media:weight of solids ratio) for 4 hours, a) unseeded, b) seeded.

the seeded powders, the fine α-Si_3N_4 particles present allowed the initial SiO burst of nucleation and growth to take place on a larger number of nucleation sites, hence resulting in an α-Si_3N_4 powder with narrow size distribution.

The particle size analysis performed on the powders produced from both the seeded and unseeded starting materials are presented graphically in Figure 4.20 (data for unseeded material presented in Table 4.4).

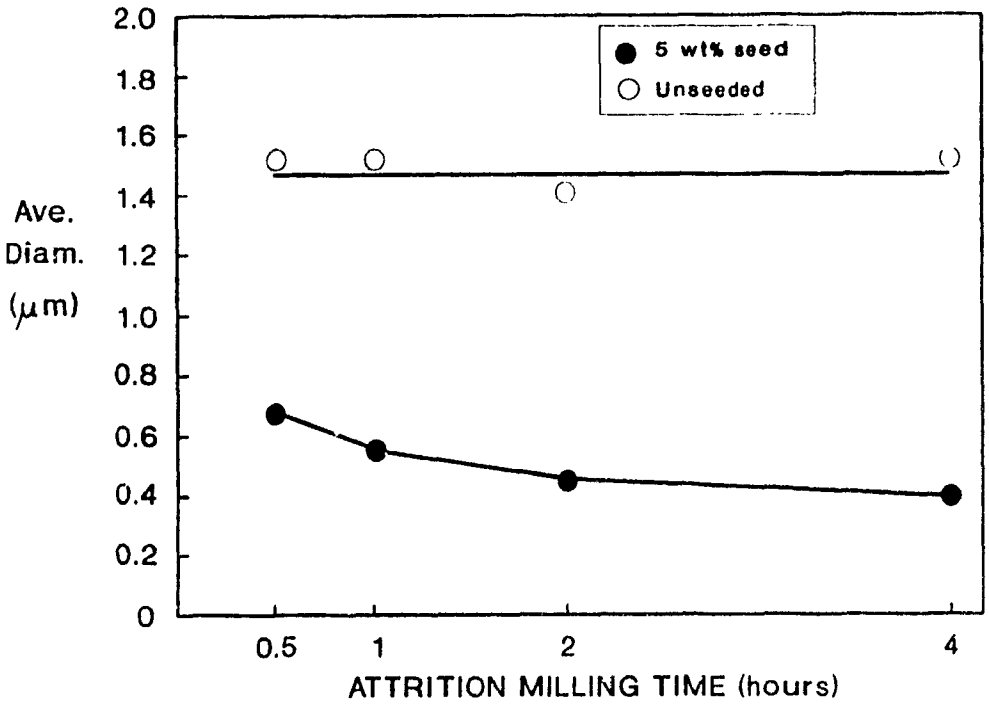

Figure 4.20 : Effect of seeding and attrition milling of the starting materials on the particle size of α-Si_3N_4 powders (T~1510°C, N_2 = 1900 cc/min, RX time = 5 hours, 7:1 weight of ZrO_2 media:weight of solids ratio).

In Figure 4.20, the weighted average of the particles for the unseeded powders is represented by hollow circles, while the solid circles represent the

narrow size distributions observed in the seeded powders. Although it is difficult to establish any trend for the unseeded powders, the seeded powders clearly show a reduction in silicon nitride particle size with increasing attrition milling time of the precursors. The decrease in particle size observed for the seeded powders could be attributed to two factors. The first is the same one that was responsible for an increase in surface area for the unseeded powders (see section 4.3). Mixing the starting materials for longer periods of time increases the number of regions where there is good intimacy between the carbon and silica particles. This in turn causes a larger amount of nucleation to take place and hence, results in a finer α-Si_3N_4 powder since growth takes place on existing nuclei (e.g. seed material) while concurrently, nucleation occurs in regions defficient of nuclei. The second factor that could also play an important role in reducing the α-Si_3N_4 particle size is the actual milling of the seed itself. As the attrition milling time is increased, the particles and the agglomerates in the α-Si_3N_4 seed which is added prior to milling get broken down more and more by the media, hence providing smaller and more numerous sites on which growth and nucleation can occur.

4.3.2 INCREASING THE MEDIA:SOLIDS RATIO

In the previous section it was shown that the addition of 5 weight% seed to the starting materials resulted in fine monosized Si_3N_4 powders and, that increasing the intimacy between the starting materials with longer attrition milling time resulted in a decrease of the average particle size. Another way to improve the intimacy between the starting materials is to increase the aggressiveness of the

milling process by having a higher media:solids weight ratio. A series of experiments was therefore conducted where the ZrO_2 media:solids ratio was increased from 7:1 to 13.4:1. These experiments were carried out at 1500°C for 5 hours with a nitrogen flow rate of 0.2 cm/sec at STP. The results of the particle size analysis are presented in Table 4.6 and Figure 4.21.

Figure 4.21 shows that the powders synthesized from starting materials milled with a ZrO_2 media:solids ratio of 13.4:1 had an average particle diameter about 0.1 μm smaller than those milled with a 7:1 media:solids ratio. This is due to the fact that having a higher media:solids ratio is in fact equivalent to transferring more "milling energy" into breaking the small silica and carbon agglomerates (as well as the seed) and increasing the dispersion. This, in turn, translates into a better intimacy between the precursors, and more homogeneously disperses the seed particles; this was shown to be responsible (see above) for the formation of fine particles and narrow size distributions. The values of standard deviation in Table 4.6 confirm that as the intimacy between the precursors is improved, the particle size distribution becomes narrower (indicated by a decrease in the absolute value of the standard deviation). SEM micrographs of the powder made from starting materials attrition milled for 4 hours with 13.4:1 media:solids ratio are shown in Figure 4.22. Attrition milling the seeded (5 weight %) starting materials for 4 hours, using a 13.4:1 ZrO_2 media:solids ratio, proved to be the optimum preparation technique developed for the production of very fine unagglomerated α-Si_3N_4 powders.

Table 4.6 : Effects of attrition milling time and media:solids ratio on particle size.

ZrO_2 media:solids weight ratio	Attrition milling time (hours)	Calculated average diameter (μm)	Standard deviation, σ (μm)
7:1	0.5	0.73	0.32
	1	0.56	0.11
	2	0.50	0.09
	4	0.40	0.06
13.4:1	0.5	0.58	0.19
	1	0.47	0.14
	2	0.37	0.12
	4	0.28	0.12

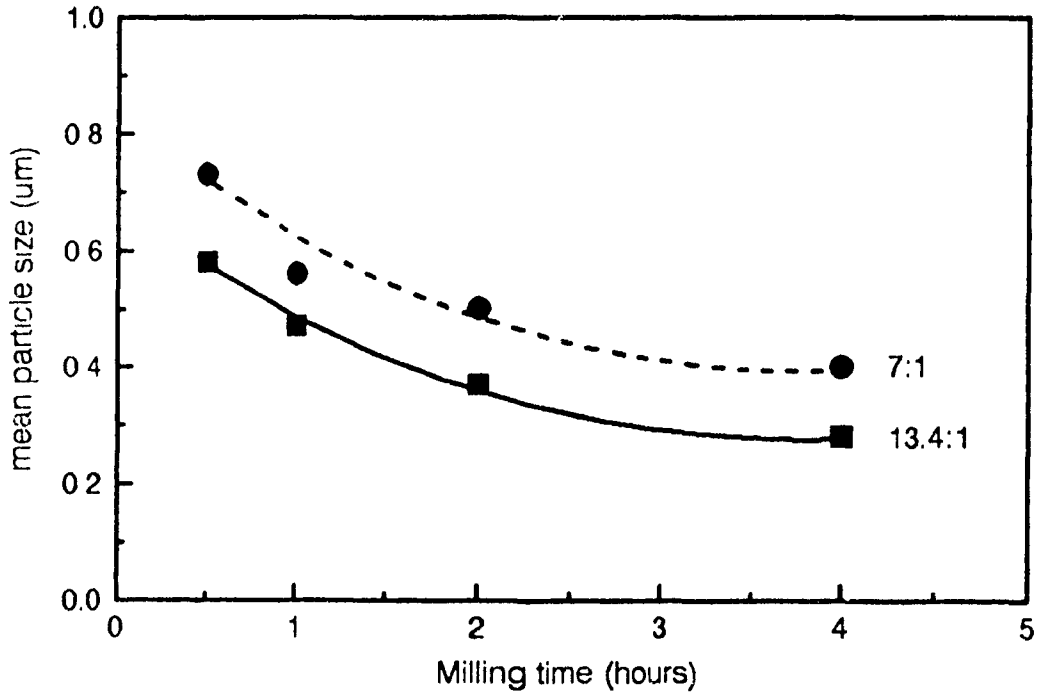

Figure 4.21 : Effects of attrition milling time and media:solids ratio on particle size.

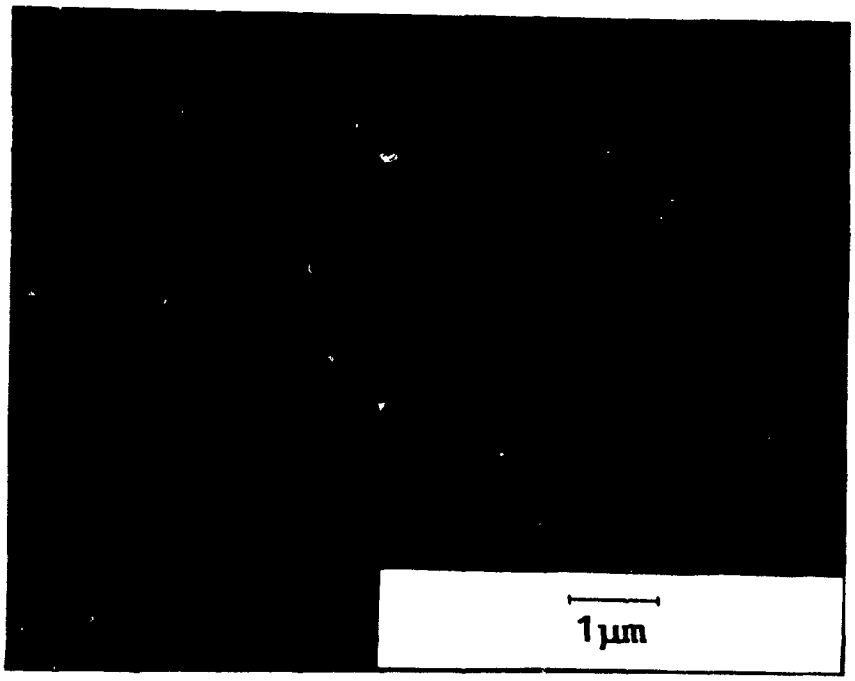

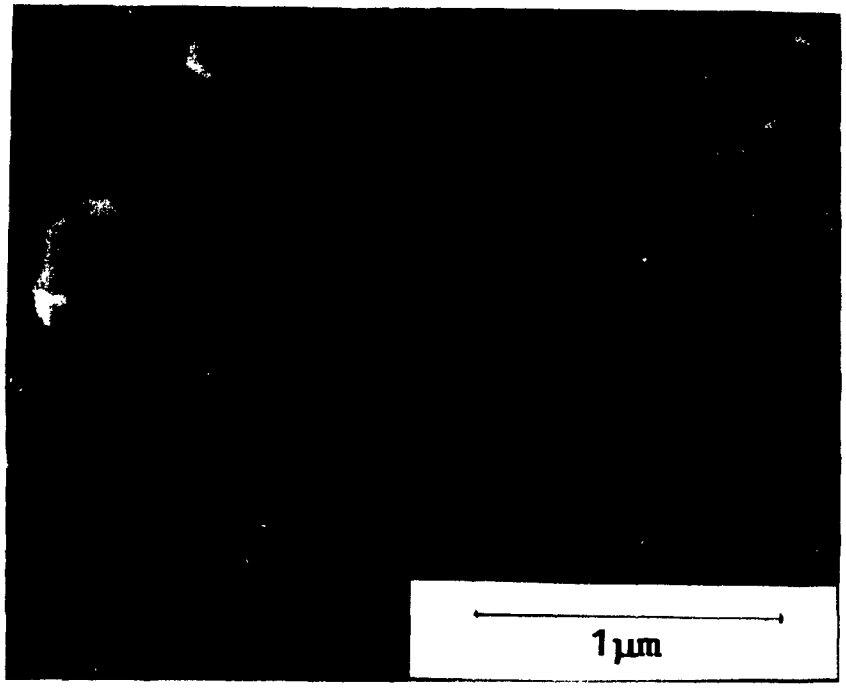

Figure 4.22 : SEM micrographs of silicon nitride powder (4 hours A.M.- 13.4:1 ZrO_2 media:solids - 5 weight % seed - T = 1510°C - N_2 = 0.2 cm/sec.).

4.4 EFFECT OF REACTION TIME AND TEMPERATURE ON CONVERSION OF SiO_2

A series of experiments was conducted to study the effect of reaction time and temperature on the formation of Si_3N_4. The degree of conversion of silica can be evaluated by several methods. Measuring the weight loss which occurred during the reaction is an easy and efficient way to estimate the extent of conversion. It was experimentally observed that after reaction, a weight loss of ~ 36% (for 7:1 carbon black:fumed silica ratio) translates, after decarburization, into a powder composed of > 97% silicon nitride. However, one has to be careful and not rely solely on weight losses for conversion studies. X-ray diffraction should always be used to identify the presence of crystalline phases other than silicon nitride. For example, large quantities of SiC (>10 weight%) in the final product will increase the weight losses since the conversion of SiO_2 into SiC (100%) was experimentally observed to result in weight losses of 47-50%.

As seen in section 4.1.5, the complete conversion to Si_3N_4 occurs only over a narrow temperature range. These experiments were conducted at 1490°C for various lengths of time and at 1540°C (upper end of range) for 5 hours. The choice of temperatures was based on the formation of large amounts of SiC being observed above 1540°C and below 1490°C the formation of Si_3N_4 is very slow. The reactants used in this study were attrition milled for 0.5 hour (seeded and unseeded) and 4 hours (seeded). Figure 4.23 summarizes the weight loss results and indicates that, at a temperature of 1490°C, a reaction time of at least 8 hours was necessary in order for the seeded starting materials to fully convert into Si_3N_4. However, for the

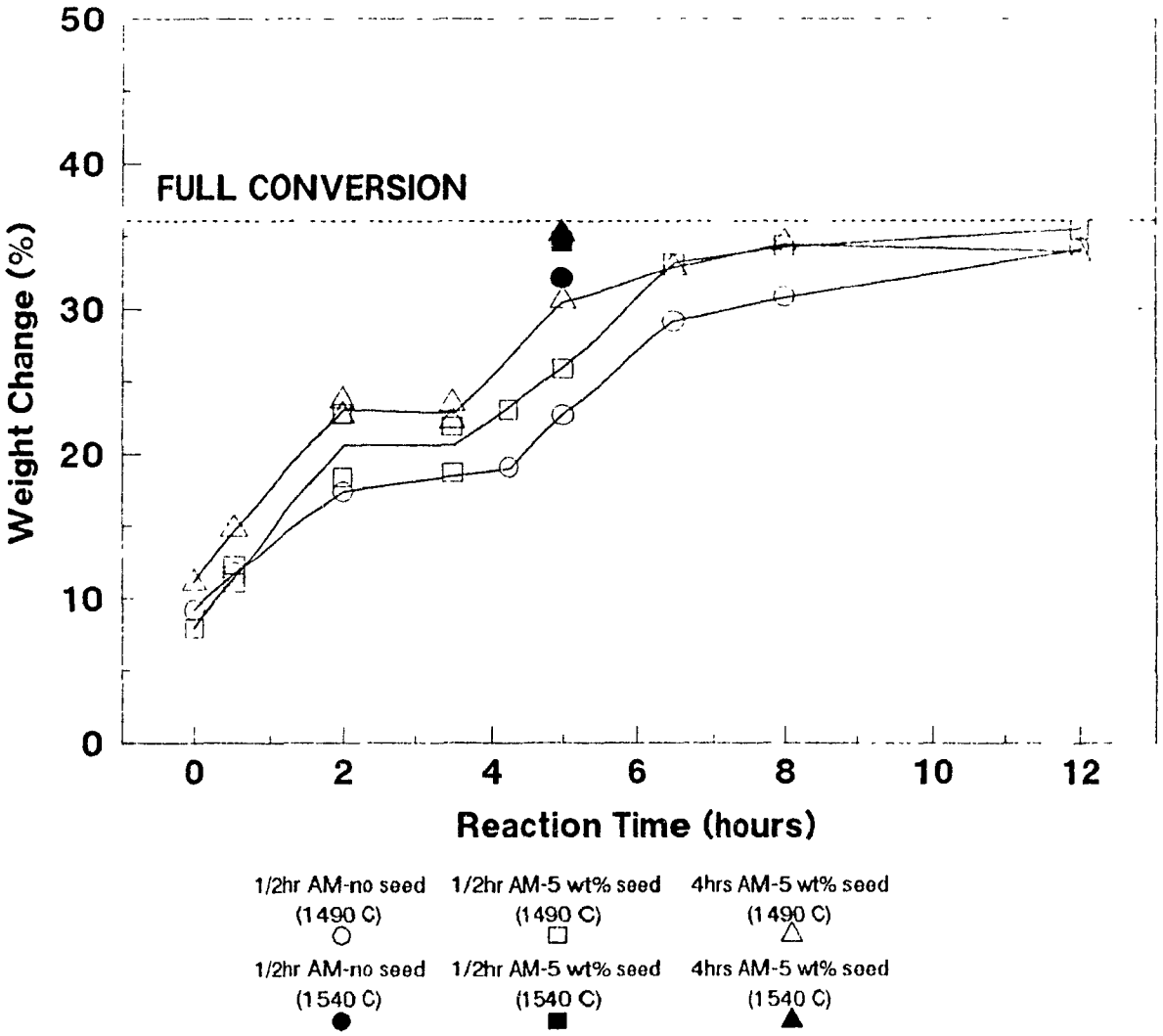

Figure 4.23 : Effect of reaction time on the weight losses of various reactants.

unseeded precursors, conversion was incomplete, even after 12 hours at 1490°C. On the other hand, at a reaction temperature of 1540°C and a reaction time of 5 hours, the unseeded starting materials were > 90% converted while the seeded ones achieved complete conversion showing, once again, the dramatic effect of temperature on the kinetics of the process. In general, the strong influence of

temperature reaction rates has been described extensively by the Arrhenius equation[102,127,128].

The extent of conversion of SiO_2 into Si_3N_4 can be visualized more clearly by looking at Figure 4.24 which gives the oxygen and nitrogen contents of the undecarburized powders after reaction. It is interesting to note, in Figures 4.23 and 4.24, that the presence of a discontinuity in reaction between 2 and 4 hours, renders an "S" shape to all three curves. To verify the existence of this discontinuity, the 2 and 3 1/2 hour experiments were repeated, yielding similar results.

The elongated "S" shape of the curve observed in Figure 4.23 is known to occur in a few systems, and is one of the four main reaction kinetics models[129] which follows Avrami's equation[130-2]:

$$x = 100*[1 - \exp(-k\,t^n)] \qquad 4.2$$

Where x = Degree of conversion (0 - 100%)
k = Rate constant
t = Time
n = Avrami exponent

Developing this equation further by taking double logarithms we obtain:

$$\ln(-\ln(1 - x)) = \ln k + n \ln t \qquad 4.3$$

Therefore according to equation 4.3, plotting $ln(-ln(1-x))$ vs $ln\ t$ should result in a linear relationship if the model is obeyed. Figure 4.25 indicates a good

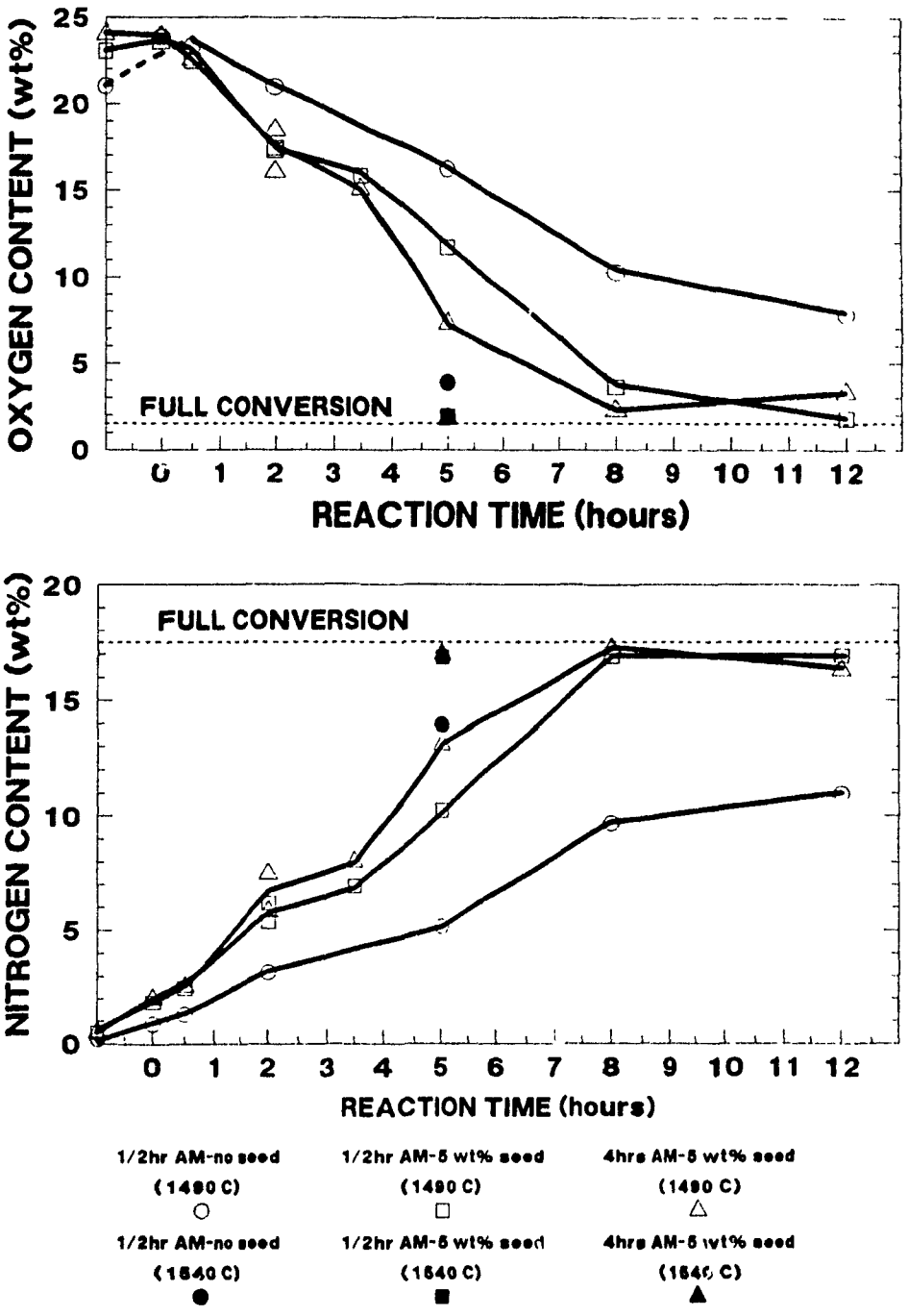

Figure 4.24 : Oxygen and nitrogen contents in the undecarburized Si_3N_4 powders as a function of reaction time.

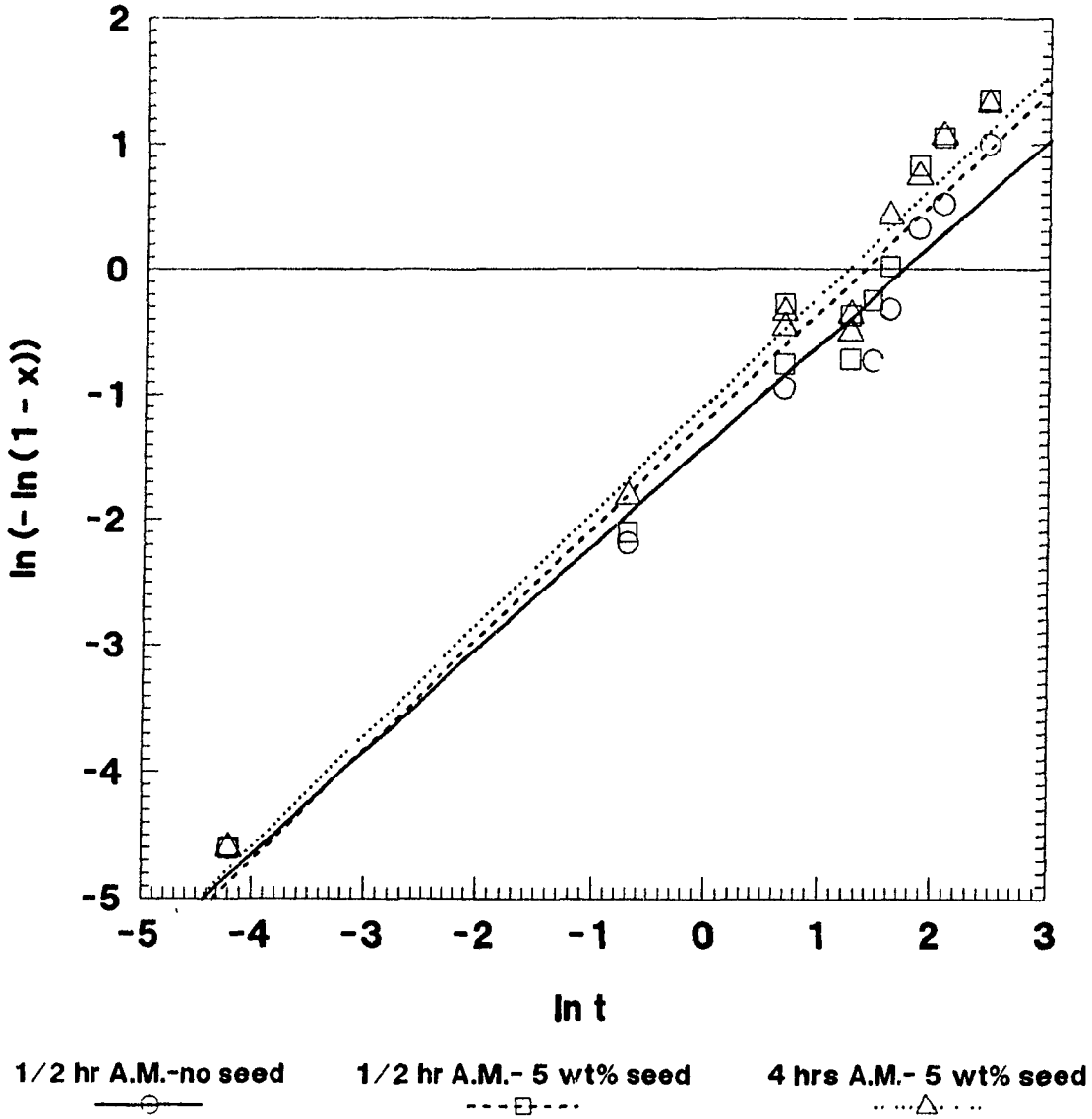

Figure 4.25 : Graphical representation of conversion versus time using the Avrami model.

fit of the data with correlation coefficient of ≥ 0.95 for the linear regression analysis (Table 4.7). The values of *k* and *n* that were calculated from that graph are also presented in Table 4.7. The conversion vs time data that was used to build both Figures 4.23 and 4.25 are presented in Appendix III.

The value of *n* (an integer which varies from 1 to 4) can reflect the

Table 4.7 : Values of *n* and *k* derived from Figure 4.25.

	n	k	Coefficient of linear regression, r^2
1/2 hr A.M.-no seed	0.81	0.25	0.97
1/2 hr A.M.-5 wt% seed	0.87	0.30	0.95
4 hrs A.M.-5 wt% seed	0.88	0.34	0.97

geometry and dimensionality of the growth process[133]. As seen in Table 4.7, the calculated values of *n* are very close to unity. Under these conditions, the growth is said to proceed in a rodlike fashion from instantaneous nuclei i.e., most of the nuclei being formed initially at the start of reaction. Interestingly enough, the results obtained in this work tend to support the fact that both an initial burst of nucleation occurs (see section 4.2.2), and that the growth of the Si_3N_4 grains at 1490°C does seem to occur in a rodlike fashion (see section 4.4.1). The values of *k* presented in Table 4.7 indicate that the rate of reaction is slightly faster for the seeded starting materials compared with the unseeded, and also faster for the precursors attrition milled for longer periods of time (better contact between the silica and carbon particles). Both confirm the evidence presented in earlier sections.

Very few authors have worked on the reaction kinetics of carbon:silica mixtures at high temperature. Among those who did, Blumenthal et al.[134] and Biernacki and Wotzak[135] have both found that a discontinuity (at certain temperatures and for specific C:SiO_2 ratios) does appear somewhere in the middle of the reaction kinetics curves, giving them the appearance of an elongated "S".

Blumenthal et al. attributed the presence of this discontinuity to the formation of SiC (reaction 4.8) as an intermediate product. The SiC would then proceed to react with SiO_2 to form CO and SiO gases according to reaction 4.9.

$$SiO_2 + 3\ C \text{ ---> } SiC + 2\ CO \qquad 4.8$$

$$SiC + 2\ SiO_2 \text{ ---> } 3\ SiO + CO \qquad 4.9$$

However, the results obtained in this work do not support their theory. X-ray diffraction patterns for various reaction times (Figure 4.26) do not show the presence of any SiC at 1490°C before, during, or after after the discontinuity. Zhang and Cannon[86] also studied the reaction kinetics of the formation of Si_3N_4 but they did not find any discontinuity. Their measurements were, however, obtained over long time intervals (3, 5, 7, and 14 hours reaction time), making it difficult to observe or confirm the presence of such changes. Using the ratio of intensities of an α-Si_3N_4 peak (20.6°) and the amorphous background (highest intensity of unreacted SiO_2 between 15^o and 35^o) in the diffraction patterns obtained after different reaction times at 1490°C, it was possible to get an even more direct measurement of conversion (Figure 4.27).

Figure 4.27 clearly shows how sluggish the conversion of unseeded materials is, compared with the seeded precursors. This demonstrates the importance of possessing a sufficiently large number of nucleation sites if the reaction is to go to completion within a reasonable period of time. In order to try to explain the presence of the discontinuity also found in Figure 4.27, continuous

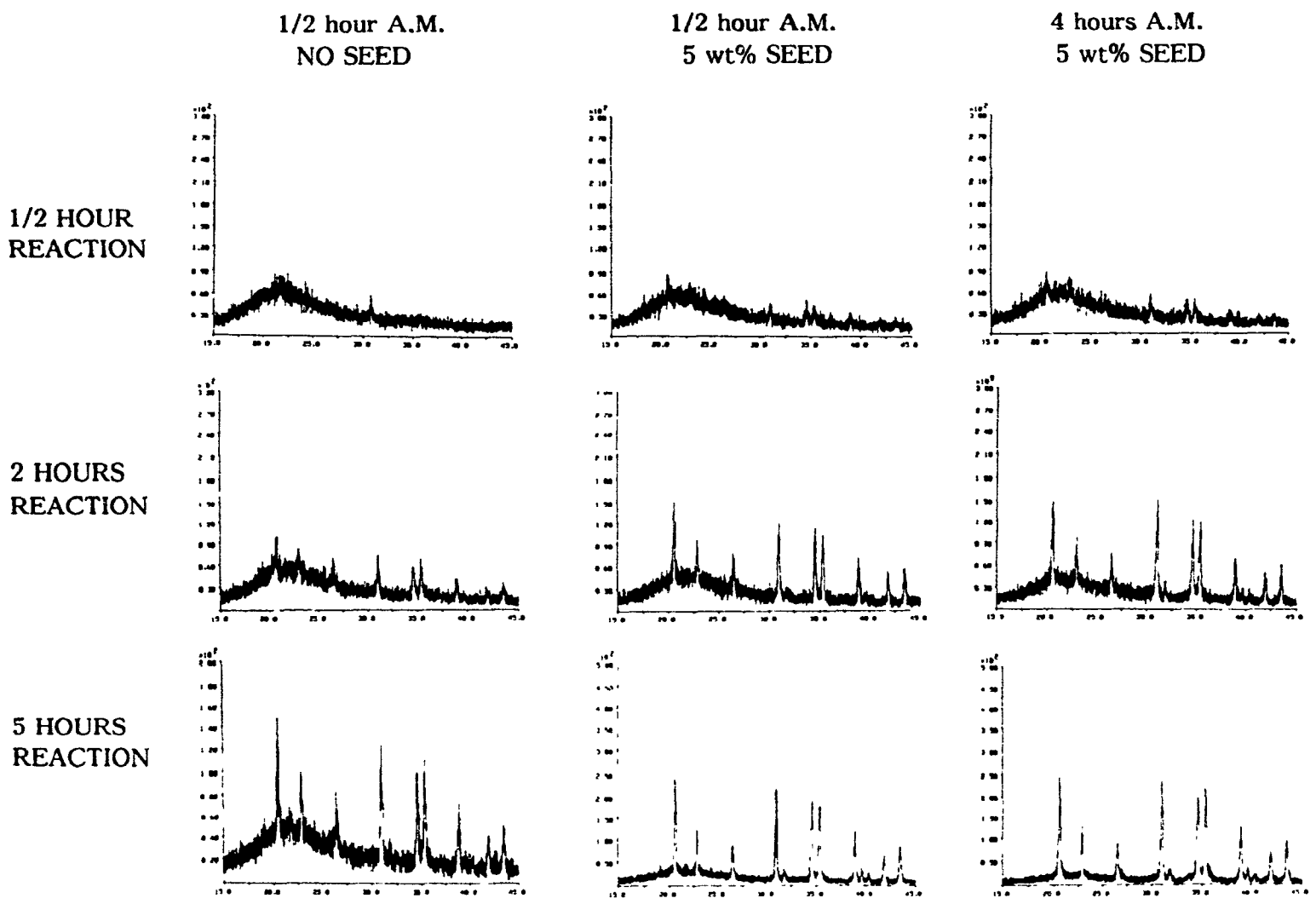

Figure 4.26 : X-ray diffraction patterns of Si_3N_4 powders synthesized at 1490°C (continue on next page).

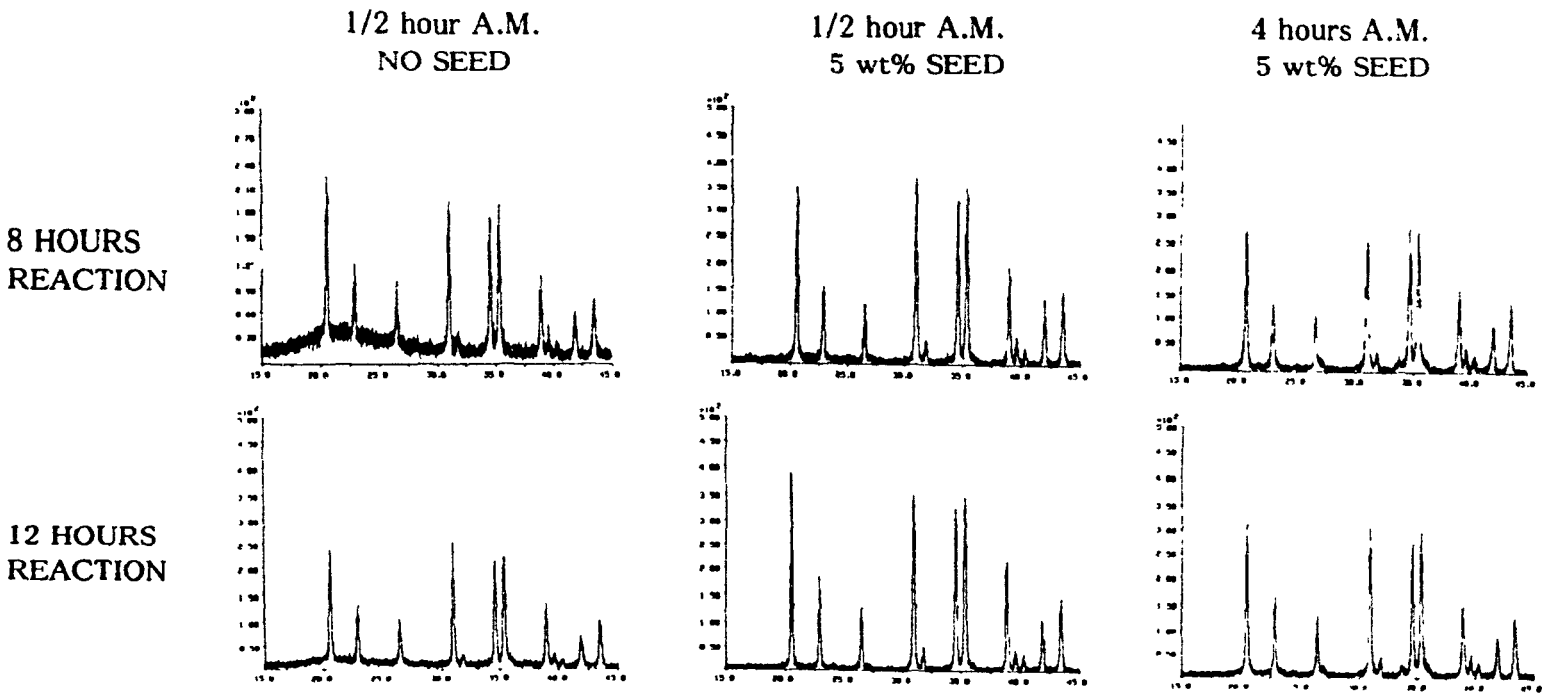

Figure 4.26 : X-ray diffraction patterns of Si_3N_4 powders synthesized at 1490°C.

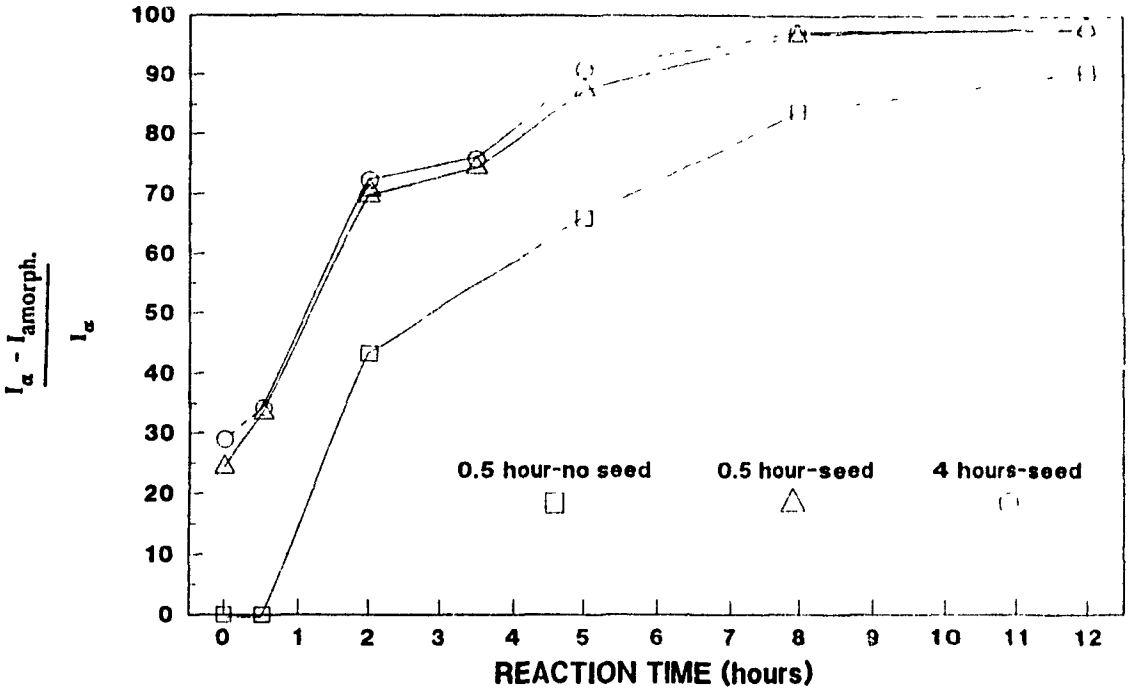

Figure 4.27 : Ratios of X-ray diffraction peaks intensity vs reaction time.

measurements of CO gas evolution were obtained on two separate occasions during the carbothermal reduction of a given starting material (1/2 hour A.M.- 5 wt% seed). The results obtained from these experiments are presented in Figure 4.28. As expected, in both cases the CO contents reached a maximum at the beginning of the reaction, and dropped rapidly after only several minutes. This burst of CO gas is the

result of the fast reaction between the C and SiO_2 particles (see sections 4.2.2 and 4.3.1) which are initially in good contact with each other. Because of mass transfer considerations, once the intimate contact between the C and SiO_2 is no longer present, the amount of CO gas produced will decrease dramatically.

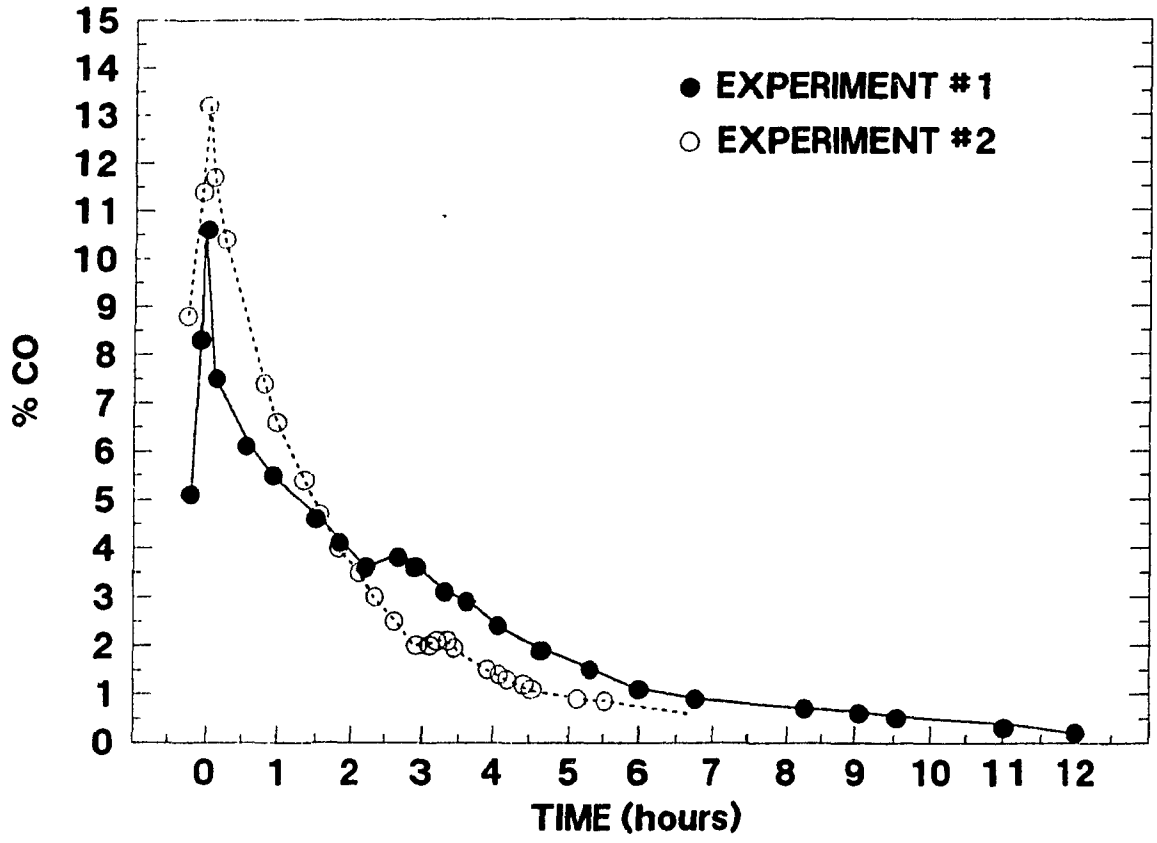

Figure 4.28 : CO evolution as a function of reaction time (1490°C) for the carbothermal reduction of 1/2 h A.M.-5 wt% seed precursors.

Interestingly enough, in Figure 4.28, between 2 and 4 hours (location of the discontinuity) a small but definite increase in the CO content can be observed. An explanation has been put forward in order to try to explain the presence of a small "burst" of CO gas a few hours after the initial burst. It is

suggested that this phenomenon might be caused by a partial sintering of the unreacted SiO_2 agglomerates. As the SiO_2 agglomerates densify into globules, they bring in their path carbon particles, establishing once again good contact between them. This causes the reaction to accelerate again and in turn results in a "secondary" burst of CO gas. Since this secondary burst of CO gas is thought to be the result of the reaction between C and SiO_2 (equation 2.9), a burst of SiO should also be generated leading to an increase in the conversion rate (observed in Figures 4.23, 24, 26 and 27). The sintering of silica agglomerates, taking place during the initial period of the reaction (0 - 4 hours), could explain why the net weight losses observed between 2 and 4 hours reaction times (Figure 4.23) were so small. It would also explain why the reacted pellets showed 20 - 30 % shrinkage after reaction. Evidence that sintering took place was obtained when the reacted mixture containing α-Si_3N_4 and amorphous silica after a 2 hour reaction at 1490°C was decarburized and observed by SEM (Figure 4.29). This micrograph clearly shows that the silica particles have now sintered together, forming large porous globules. The presence of these silica globules was expected since the reaction temperature used in this study is equivalent to ~ 90% of the melting point of pure silica (1710°C).

Figure 4.30 is a schematic representation of the phenomenon described above. Prior to the reaction, the carbon and silica agglomerates are in physical contact with each other. The regions where the C and SiO_2 touch each other will react rapidly, leading to rapid evolution of CO and SiO. Since the C and SiO_2 agglomerates react together to form gaseous products, the solid particles are no

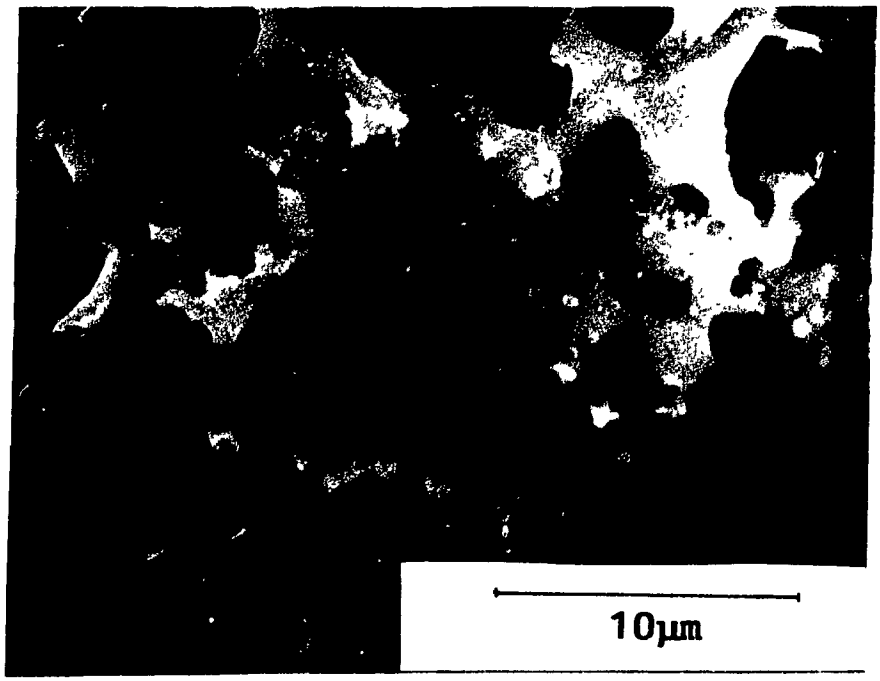

Figure 4.29 : SEM micrograph of sintered silica agglomerates present after a 2 hours reaction at 1490°C.

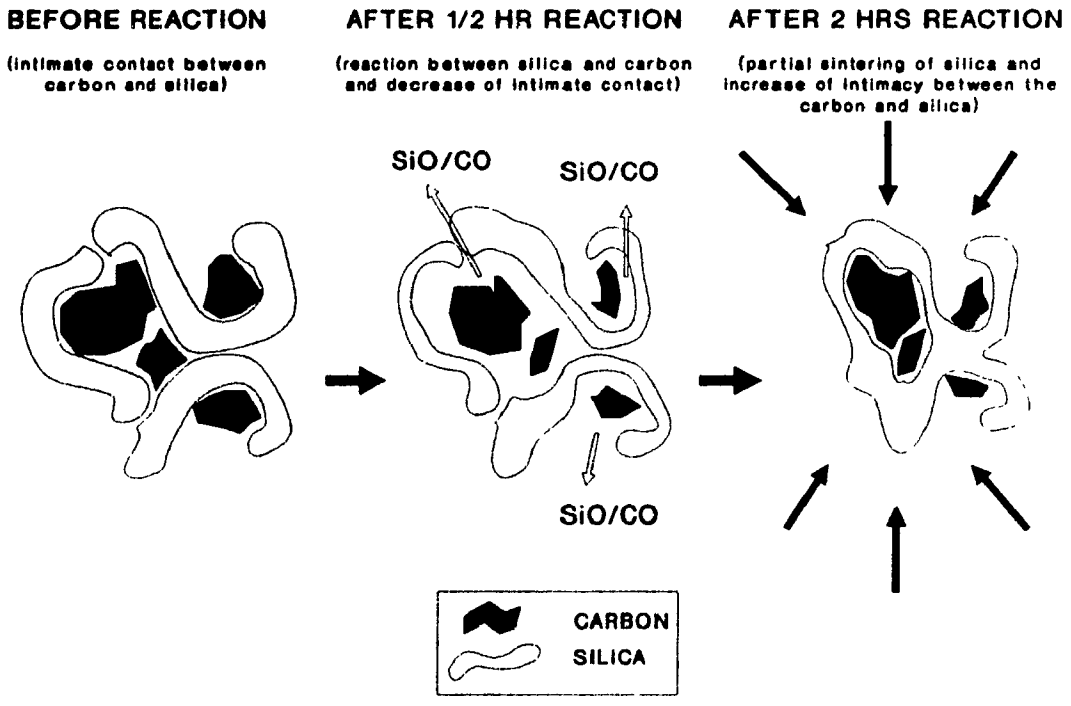

Figure 4.30 : Schematic representation of the partial sintering of SiO_2 agglomerates.

longer in good contact with each other and hence, the rate of evolution of CO/SiO slows down. When the silica agglomerates sinter together, they bring once again the C and SiO_2 particles in good contact with each other, resulting in a "secondary" burst of SiO and CO gases.

4.4.1 EFFECT OF TEMPERATURE ON MORPHOLOGY OF Si_3N_4 POWDER

In the previous section, it was shown that temperature played an important role in establishing the time required for complete conversion of SiO_2 into Si_3N_4. Temperature was also seen to be a key parameter responsible for the presence of compounds other than silicon nitride; Si_2O_2N at low temperature (<1490°C) and SiC at high temperature (>1550°C). It has also been observed that temperature played a role in establishing the type of growth which occurs. There was a drastic difference between the morphology of the α-Si_3N_4 grains produced at 1490°C and the material produced at 1540°C. The effect of a 50°C temperature difference in the reaction temperature is shown in Figure 4.31. The SEM micrographs clearly illustrate that the α-Si_3N_4 particles produced at 1490°C have a much larger aspect ratio than those synthesized at 1540°C. The difference in morphology is believed to be related to the time available for growth. For the seeded precursors, at 1540°C, less than 5 hours are required for complete conversion, as opposed to roughly 10 hours at 1490°C. In the case of slower growth of α-Si_3N_4 grains the rate determining step becomes the availability of growth/nucleation sites on pre-existing α-Si_3N_4 nuclei (grains). Previous work done

at McGill[92] showed that at low temperature, a preferred growth along the c-axis takes place. At higher temperature, the gaseous species are more abundant, hence

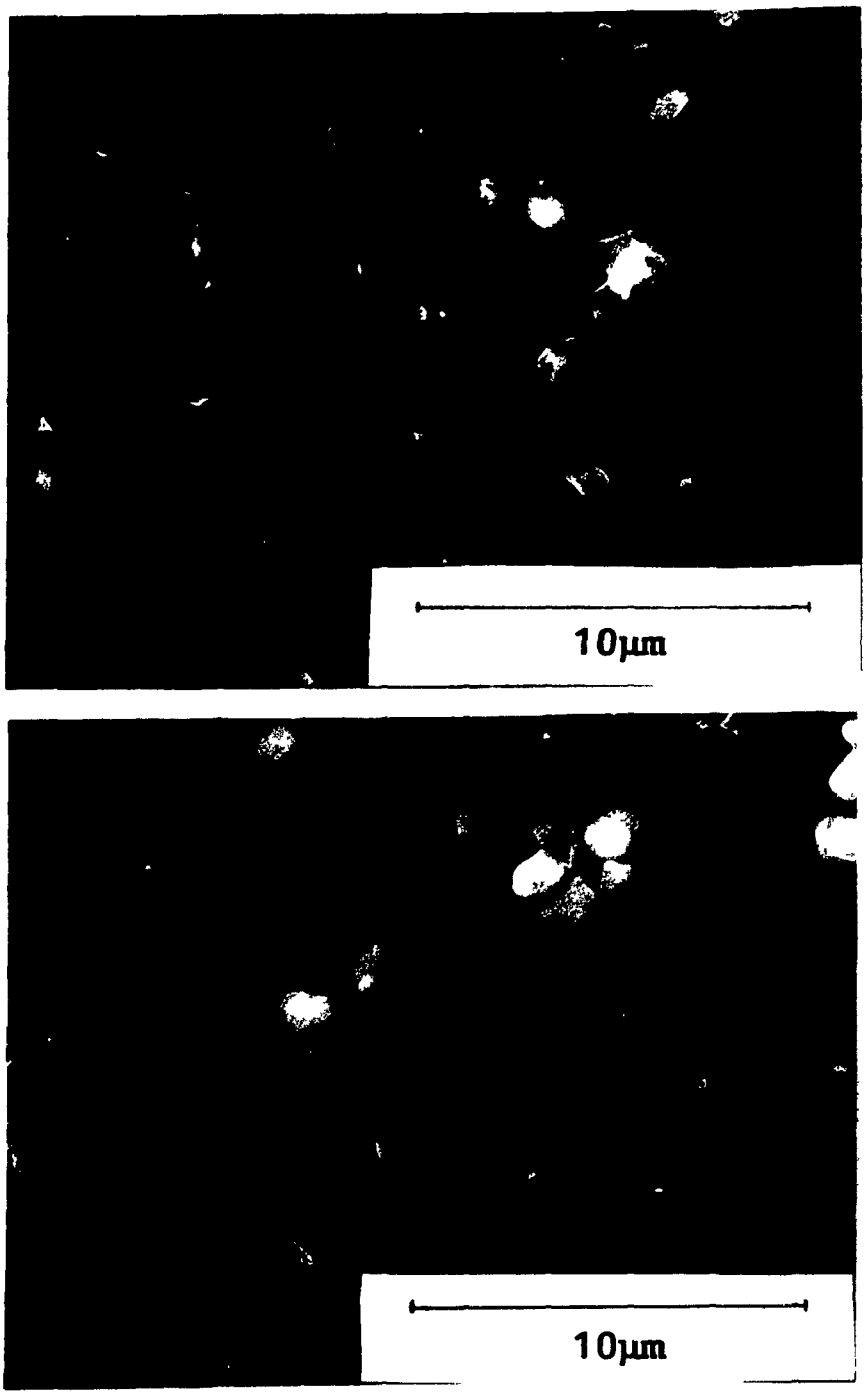

Figure 4.31 : SEM micrographs of α-Si_3N_4 powders produced from precursors (1/2 hour A.M. - no seed) reacted at a) 1490°C, b) 1540°C.

increasing the driving force for the growth to occur on several sites rather than only along the c-axis. Hence, the grains that have grown at a lower temperature will be more prismatic in appearance, and will tend to grow in a rodlike fashion. This last observation was predicted by an Avrami exponent of near unity (see section 4.4). On the other hand, a fast growth rate indicates that the sites on which α-Si_3N_4 can grow are more numerous and hence, the grains will tend to exhibit an equiaxed appearance (almost spherical in shape).

4.5 SINTERING AND MECHANICAL PROPERTIES

The quality of ceramic powders is often evaluated in terms of its sinterability and the mechanical properties of the final product. In order to evaluate the quality of the Si_3N_4 powders produced by carbothermal reduction, two large batches (~ 100 grams) of powders produced at McGill were compared to the best commercially available Si_3N_4 powder; UBE SN-E10 (imide process). The two Si_3N_4 powders synthesized at McGill were made from seeded precursors attrition milled for 0.5 and 4 hours using a ZrO_2 media:solids ratio of 13.4:1. The carbothermal reaction temperature for these two powders was 1540°C. Such a temperature enabled a relatively rapid conversion of SiO_2 (within 5 hours) while limiting both, the presence of SiC observed at higher temperatures (> 1550°C), and the formation of large quantities of α-Si_3N_4 whiskers seen at lower temperatures (~ 1490°C).

The UBE powder, along with the two carbothermic powders were pressed into bars, sintered, and then fractured to study their mechanical properties.

4.5.1 SINTERING BEHAVIOUR

Table 4.8 summarizes the various densities obtained for the Si_3N_4 powders. The first interesting thing to notice is the difference in surface area between the carbothermally produced powders. By simply varying the length of attrition milling of the precursors, it is possible to create a powder with the

Table 4.8 : Relative densities and surface area of carbothermic and commercial Si_3N_4 powders.

Si_3N_4 Powders		Surface Area (m^2/g)	Average relative density* (%)			
			Tap density	After uniaxial pressing	After iso-static pressing	After sintering
Carbothermal process	0.5 hour A.M.	7.4	17	43	51	93.0
	4 hours A.M.	15.3	15	41	49	95.0
Imide process	UBE	10.6	21	41	50	96.1

* The theoritical density of the Si_3N_4 powders with the additives (4 weight % Al_2O_3, 6 weight % Y_2O_3) was calculated to be = 3.321 g/cm^3.

desired surface area. It was mentioned in sections 2.1.2.3 and 2.1.3.2 that the driving force behind sintering was the reduction in surface area. Therefore, it is not surprising that the final sintered density is higher for the 4 hour A.M. powder (high surface area) than it is for the 0.5 hour A.M.(low surface area). The 4 hour A.M. powder was, however, expected to have a higher sintered density than the UBE since

its surface area is 2/3 that of the 4 hour A.M.. The presence of small amounts of SiC whiskers and free carbon in the carbothermic powders is thought to have partially inhibited the sintering process.

The relative density of the sintered UBE powder was similar to that obtained in previous work (pressureless sintering) done at McGill[136]. In their work, Pugh and Drew achieved a relative density of 96.3% for UBE and of 94.0% for Toshiba, a commercial Si_3N_4 powder synthesized by carbothermal reduction.

4.5.2 MECHANICAL PROPERTIES

The mechanical properties of the sintered bars are listed in Table 4.9. The highest average bend strength was obtained with the bars made from UBE powder (637 MPa), followed closely by the 0.5 hour A.M. (577 MPa) and the 4 hours A.M. (507 MPa). Although these strength values are similar, the same test performed at high temperature (1250°C) could have well resulted in much higher values for the carbothermal powders than for the UBE powder (imide process). It is known that chloride impurities present in imide powders (0.005 - 0.1 wt%) have a strong adverse effect on the high temperature properties of sintered products[137]. The bend strength observed for the UBE bars is in good agreement with values previously obtained (650-700 MPa)[136] by Pugh and Drew using a similar densification and strength testing procedure. In their work they also studied the densification behaviour of other commercial powders such as Toshiba A-200, a powder produced by carbothermal reduction. The average bend strength obtained from the densified Toshiba powder was 510 MPa with a Weibull modulus of 9. Both

Table 4.9 : Mechanical properties of sintered bars.

Si_3N_4 Powders		Mechanical Properties			
		Average 4-points bend strength (MPa)	Number of bars	K_{Ic} ($MNm^{-3/2}$)	Weibull modulus
Carbothermal Process	0.5 hour A.M.	576 ± 33*	10	5.8	11.5
	4 hours A.M.	507 ± 16*	9	4.9	22.0
Imide Process	UBE	637 ± 24*	11	4.1	16.2

* These values represent the 95% confidence interval.

the 0.5 and 4 hour A.M. powders resulted in bars with much higher Weibull modulus and strength values similar or better than those of the Toshiba.

The Weibull modulus values presented in Table 4.9 were obtained by calculating the slope of the curve in Figure 4.32. The Weibull modulus "m" is an indication of the reliability of the ceramic product (a value of m > 10 is usually considered good). The 4 hour A.M. series exhibited the best Weibull modulus (m = 22.0), followed by UBE (m = 16.2) and the 0.5 hour A.M. powder (m = 11.5). The high value of "m" obtained for the 4 hour A.M. bars might indicate that although the internal flaws present are more numerous (lower sintered density and strength), they are also probably more uniform in size than the UBE series since a large variation in critical defect size will result in a wide range of strength values. The Weibull modulus values obtained for the 0.5 and 4 hours A.M. series are also far superior to

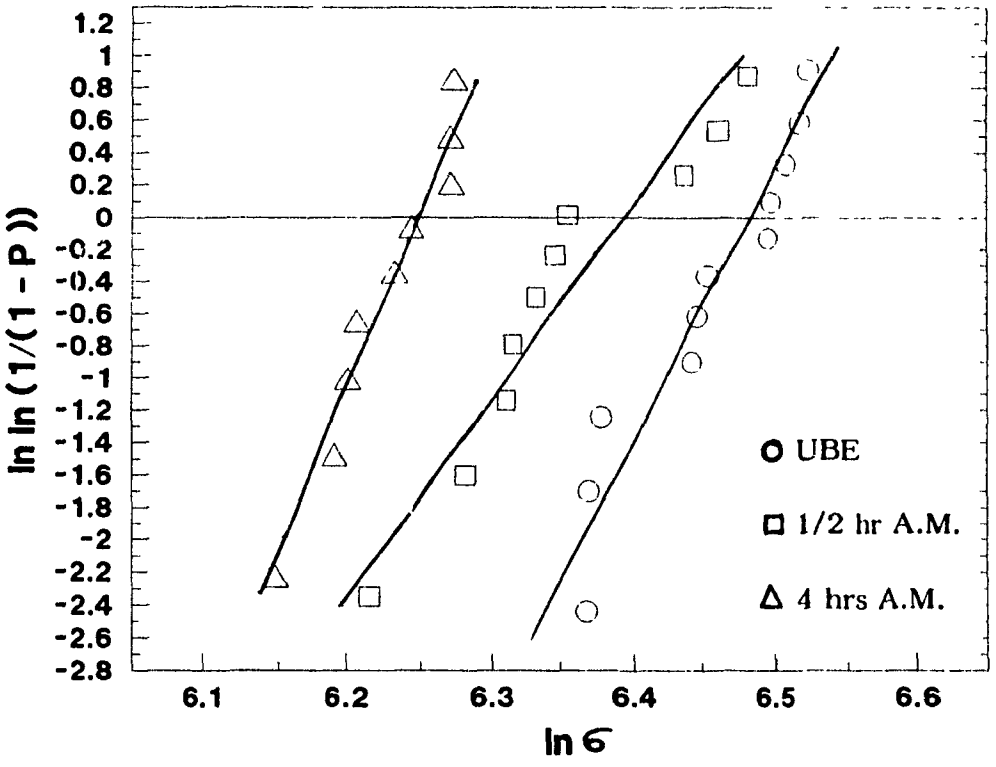

Figure 4.32 : Weibull plot for the sintered powders.

The K_{Ic} values reported in Table 4.9 gave a measure of the materials relative toughness. The highest K_{Ic} was obtained for the 0.5 hour A.M. series (5.8 $MNm^{-3/2}$), while UBE had the lowest value with 4.1 $MNm^{-3/2}$. Although it is difficult to compare these values due to their low sintered densities (pores help arrest cracks), they are still in good agreement with the values obtained by Henshall et al.[138] (4.5 - 5.1 $MNm^{-3/2}$), Nose and Jujii[139] (4.8 - 6.4 $MNm^{-3/2}$) and Evans and Charles[140] (4.9 $MNm^{-3/2}$) for similar material.

5. CONCLUSIONS

The research work into the formation of Si_3N_4 powder by carbothermal reduction of SiO_2 was carried out in order to optimize the conditions to produce a high quality, sinterable powder.

A) PREPARATION METHOD OF PRECURSORS

(1) A high degree of intimacy for the starting materials (C, SiO_2) was found to be essential to obtain a high surface area powder.

(2) Attrition milling the starting materials to achieve an intimate mixing of the precursors, proved to be superior over blending or ball milling.

(3) ZrO_2 media were found to have a much lower wear rate than Si_3N_4 or Al_2O_3 media and hence contributed to maintain a low contamination level.

B) EFFECT OF SEEDING

(1) The addition of 5 weight % seed material (UBE - 0.2 μm) to the starting materials resulted in Si_3N_4 powders with narrow particle size distribution and much finer average grain size than for the unseeded precursors.

(2) The addition of seed was also observed to improve the reaction kinetics.

C) REACTION CONDITIONS

(1) The flow of N_2 through the reactor during reaction was found to be very important in keeping the SiC contents in the final powder low. For this reason, a linear gas flow rate $\geq$ 0.2 cm/sec was used in this study.

(2) The pellets in the reactor should not be located where the N_2 flow is poor (near the walls) or where the partial pressure of CO might be high (upper levels of reactor) if low SiC contents are desired.

(3) The SiC synthesized in this work was α-SiC, a crystallographic phase rarely reported in carbothermic powders. Other authors have reported the presence of β-SiC in their powders but, it may have been misidentified since large quantities (>10 weight % SiC in Si_3N_4 powders) are required in order to differentiate between the α and β phases with X-ray diffraction techniques.

(4) The reaction temperature was found to be extremely important. Only reaction temperatures between 1490°C and 1550°C resulted in a relatively pure Si_3N_4 powder. Below 1490°C the reaction kinetics are very slow (unconverted SiO_2 present after 5 hours reaction) and above 1550°C large quantities of SiC are produced.

(5) The Si_3N_4 grains produced at 1490°C were found to be acicular in nature, while those produced at 1540°C were equiaxed.

(6) A burst of CO gas was seen to occur a short time after the reactants reached the reaction temperature. This burst of CO gas was seen to be of great importance in trying to explain the nucleation phenomena and the reaction mechanisms.

D) SINTERING AND MECHANICAL PROPERTIES

(1) Average relative densities of 93.0 and 95.0% (pressureless sintering) were obtained for the carbothermic powders produced in this work, while a slightly higher relative density was obtained for the UBE powder (imide process).

(2) For the sintered bars made from carbothermic powders, very good strengths (507 and 577 MPa) and excellent Weibull modulus (16 and 22) were obtained. These results clearly show that carbothermal powders can be used to produce high strength ceramic materials.

6. FUTURE WORK

1 - Lower the final O_2 content of the Si_3N_4 powder by:

a) making sure that the SiO_2 is completely reduced by using a CO analyzer to monitor the progress of reaction.

b) limit the amount of oxidation brought about by the decarburization stage, by removing the carbon in NH_3 rather than in dry air.

2 - Improve the physical and chemical characterization procedures for Si_3N_4 powders:

a) find a proper carbon analysis method that can distinguish between free carbon and carbon from SiC.

b) use automated Image Analysis techniques to characterize the particle size and size distribution parameters in a statistically rigorous manner.

3 - Do a complete study on the reaction kinetics of the carbothermal reduction of SiO_2 into Si_3N_4 and examine the effects of various parameters such as:

a) higher temperatures (1515°C, 1540°C).

b) effect of pellet size on weight losses observed.

c) effect of higher N_2 gas flow on conversion time.

4 - Optimize the pyrolysis cycle when sugar is used as a carbon source, and vary the density of the pellets to study if the diffusion of gaseous species in and out the pellets is indeed the rate determining step.

5 - Study the sinterability of other powders such as those synthesized at lower temperature (1490°C), as well as the unseeded ones. Find the optimum sintering cycle and compare the synthesized powders with commercial powders made by carbothermal reduction (Starck) and processed under identical conditions.

6 - Build a small continuous carbothermal reactor (rotating graphite tube) for the synthesis of Si_3N_4 powders.

REFERENCES

1. R.W.Rice, "Capabilities and Design Issues for Emerging Tough Ceramics", Ceram. Bull., Vol.63, No.2, (1984), pp.256-62.

2. E.J.Kubel Jr., "Structural Ceramics: Materials of the Future", Adv. Mater. & Processes, Vol.8, (1988), pp.25-33.

3. L.M.Sheppard, "A Global Perspective of Advanced Ceramics", Ceram. Bull., Vol.68, No.9, (1989), pp.1624-33.

4. G.Ziegler,J.Heinrich,G.Wotting, "Review:Relations Between Processing, Microstructure and Properties of Dense and Reaction-Bonded Silicon Nitride", J.Mater.Sci., Vol.22, (1987),pp.3041-86.

5. A.W.J.M.Rae,N.E.Cother,P.Hodgson, "Nitride Ceramics - Their Availability and Commercialization", First European Symp. on Engineering Ceram..(1985), pp.1.

6. H.S.C.Deville,F.Wohler, Liebeg's Ann., Vol.104, (1857), pp.256.

7. J.F.Collins,R.W.Gerby, "New Refractory Uses for Silicon Nitride Reported", J. Metals, Vol.17, (1955), pp.612-5.

8. CRC Handbook of Chemistry and Physics, Weast 66th Edition, CRC Press, (1985-6), pp.B7,B14.

9. W.Alexander, A.Street, "Metals in the Service of Man", Eighth Edition, Pelican Books, (1982),pp.72,122.

10. ASM Metals Handbook, 8th Edition, Vol.1, (1961).

11. K.H.Jack, "Review:Sialons and Related Nitrogen Ceramics", J.Mater.Sci., Vol.11,(1976),pp.1135-58.

12. R.A.L.Drew, "Silicon Nitride and Sialons Ceramics-A Review", Can.Metal.Quater., Vol.27, No.1, (1988),pp.59-64.

13. T.B.Troczynski,D.Ghosh,S.D.Gupta, "Advanced Ceramic Materials for Metal Cutting", Proceed. of the International Symp. on Adv. Struc. Mater., Montreal, Canada, Ed. D.S.Wilkinson, Pergamon Press, (1988), pp.157-168.

14. R.Wertheim, "Improved Tool Life With Silicon Nitride", Machine and Tool Blue Book, Vol.81, No.1, Jan.,(1986), pp.66-68.

15. S.W.Korthals-Altes, "Does the Space Plane Have the Right Stuff?", Tech.Review, Jan.(1987), pp.41-51.

16. S.Natansohn, "Silicon Nitride, A Material for Tommorow's Engines?", Proceed. of the ACS, Div. of Polymeric Sci. and Eng., Vol.53, Publ. by ACS, (1985), pp.297.

17. M.D.Pugh,R.A.L.Drew, "Fabrication of Si_3N_4 Valve Discs", Proceed. of the International Symp. on Adv. Struc. Mater., Montreal, Canada, Ed. D.S.Wilkinson, Pergamon Press, (1988), pp.139-148.

18. R.F.Coe,R.T.Lumby,M.F.Pawson, "Some Properties of Hot-Pressed Silicon Nitride", Proceed. 5^{th} Symp. Special Ceram.,BCRA, Ed.P.Popper, (1972), pp.361-76.

19. R.N.Penny, Science Journal, April, (1970), p.54.

20. E.J.Kubel Jr.,"Good Opportunities for Advanced Ceramics", Adv. Mater. & Processes, Vol.9, (1989), pp.55-60.

21. D.W.Richerson, "Modern Ceramic Engineering", Ed.M.Dekker, (1982), p.219.

22. B.Vassiliou,F.G.Wild, "A Hexagonal Form of Silicon Nitride", Nature, Vol.179, (1957), p.435.

23. S.N.Ruddlesden,P.Popper, "On the Crystal Structures of the Nitrides of Silicon and Germanium", Acta.Cryst., Vol.11, (1958), pp.465.

24. E.T.Turkdogan,P.M.Bills,V.A.Tippett, "Silicon Nitrides: Some Physico-Chemical Properties", J.App.Chem., Vol.8, (1958), p.296.

25. R.Marchand,Y.Laurent,J.Lang, "Structure du Nitrure de Silicium α", Acta.Cryst., Vol.B25, (1969), pp.2157-60.

26. D.Hardie,K.H.Jack, "Crystal Structures of Silicon Nitride", Nature, Vol.180, (1957), pp.332-3.

27. I.Colquhoun,S.Wild,P.Grieveson,K.H.Jack, "Thermodynamics of the Silicon-Nitrogen-Oxygen System", Proc. Brit. Ceram. Soc., Vol.22, (1973), p.207.

28. A.Hendry,K.H.Jack, "Special Ceramics 6", ed. F.L.Riley, (1977), p.183.

29. S.Wild,P.Grieveson,K.H.Jack,"The Thermodynamic and Kinetics of Formation of Phases in the Ge-N-O and Si-O-N Systems",(Special Ceramics 5), Ed.P.Popper, B.C.R.A., Stoke-on-Trent,(1972),pp.271-87.

30. P.Grieveson,K.H.Jack,S.Wild, "Special Ceramics 4", ed. P.Popper, BCRA, Stoke-on-Trent, (1968), p.237.

31. H.Feld,P.Ettmayer,I.Petzenhauser, Ber.Deut.Keram.Ges., Vol.51, (1974), p.127.

32. H.F.Priest,F.C.Burns,G.L.Priest,E.C.Skaar, J.Am.Ceram.Soc., Vol.56, (1973), p.395.

33. A.J.Edwards,D.P.Elias,M.W.Lindley,A.Atkinson,A.J.Moulson, J.Mater.Sci., Vol.9, (1974), p.516.

34. K.Kijima,K.Kato,Z.Inoue,H.Tanaka, J.Mater.Sci.,Vol.10,(1975),p.362.

35. D.R.Messier,F.L.Riley,R.J.Brook, "The α/β Silicon Nitride Phase Transformation", J.Mater.Sci., Vol.13, (1978), pp.1199-1205.

36. S.Nathansohn,V.K.Sarin, Proc.2nd Int. Symp. on Ceramic Powder Processing Science, Oct.(1988), Berchtesgaden, Germany.

37. R.P.Seelig, "The Physics of Powder Metallurgy", Ed. W.E.Kingston, Published by McGraw-Hill Book Company, N.Y., p.344.

38. P.Duwez, L.Zwell, AIME Tech. Publ. 2515, Metals Trans., No.1, Vol.137, (1949).

39. W.D.Kingery, "Pressure Forming of Ceramics", in Ceramic Fabrication Processes, Ed. W.D.Kingery, MIT Press, Cambridge, Mass., (1963), pp.55-61.

40. See ref.21, p.186.

41. C.M.Lambe, "Preparation and Use of Plaster Molds", in Ceramic Fabrication Processes, Ed. W.D.Kingery, MIT Press, Cambridge, Mass., (1963), pp.31-40.

42. P.D.S.St-Pierre, "Slip Casting Nonclays Ceramics", on Ceramic Fabrication Processes, Ed. W.D.Kingery, MIT Press, Cambridge, Mass., (1963), pp.45-51.

43. H.Okuda, "Present Situation in the Field of Ceramics", 2nd International Symp. on Ceramic Materials and Components for Engines, Ed. W.Bunk, H.Hausner, (1986), pp.139-46.

44. S.Wada, Y.Oyama, "Thermal Extraction of Binder Components From Injection-Molded Bodies", 2nd International Symp. on Ceramic Materials and Components for Engines, Ed. W.Bunk, H.Hausner, (1986), pp.225-33.

45. Y.Hattori, Y.Tajima, K.Yabuta, J.Matsuo, M.Kawamura, T.Watanabe, "Gas Pressure Sintered Silicon Nitride Ceramics for Turbocharger Application", 2nd International Symp. on Ceramic Materials and Components for Engines, Ed. W.Bunk, H.Hausner, (1986), pp.165-172.

46. J.White, "Basic Phenomena in Sintering", Science of Ceramics, Vol.1, Ed. G.H.Stewart, (1962), pp.1-19.

47. W.Symons,K.J.Nilsen,R.Riman,S.C.Danforth, 2nd Int. Conf. on Powder Processing Science, Oct. (1988), Berchtesgaden, Germany.

48. W.Symons,K.J.Nilsen,S.C.Danforth, "Synthesis, Characterization, and Dispersion of Laser-Synthesized Silicon Nitride Powders", Ultrastructure Process. of Adv. Ceramics, Ed. J.D.Mackenzie, D.R.Ulrich, (1988), pp.907-17.

49. T.Vasilos, R.M.Spriggs, Proc. Brit. Ceram. Soc., Vol.3, (1967), pp.195-221.

50. M.H.Leipold, "Treatise on Materials Science and Technology", Ceramic Fabrication Processes, Vol.9, Ed. F.F.Y.Wang, Academic Press, Inc., New York, Vol.9, (1976), p.361.

51. C.R.Terwilliger, J.Am.Ceram.Soc., Vol.57, No.1, (1974), pp.48-9.

52. E.S.Hodge, Mater. Des. Eng., Vol.61, (1965), pp.92-7.

53. W.D.Kingery, H.K.Bowen, D.R.Uhlmann, "Introduction to Ceramics", 2nd Ed., John Wiley & Sons Inc., N.Y., (1976), pp.476.

54. See Ref.27, p.155.

55. J.P.Singh, Advanced Ceramic Materials, Vol.3, (1988), pp.18.

56. E.Barringer, N.Jubb, B.Fegley, R.L.Pober, H.K.Bowen, Ultrastructure Processing, Ed. L.L.Hench and D.Ulrich, (1984).

57. R.M.German, "Particle Packing Characteristics", Published by Metal Powder Industries Federation, New Jersey, (1989), pp.93.

58. A.R.Dexter, D.W.Tanner, "Packing Density of Ternary Mixtures of Spheres", Nature Physical Science, Vol.230, (1971), pp.177-9.

59. R.K.McGeary, "Mechanical Packing of Spherical Particles", J.Am.Ceram.Soc., Vol.44, (1961), pp.513-22.

60. K.E.Meiners, R.F.Geisendorfer, B.C.Mutsuddy, D.M.Bigg, "First Progress Report on Complex Metal Powder Shapes by Injection Molding", Battelle Columbus Laboratories, Columbus, OH, August, (1980).

61. D.J.Cumberland, R.J.Crawford, "The Packing of Particles", Elsevier Science, Amsterdam, The Netherlands, (1987).

62. F.F.Lange, "Silicon Nitride Polyphase Systems: Fabrication, Microstructure, and Properties", International Metals Review, No.1, Review 247, (1980), pp.1-20.

63. W.Braue, G.Wotting, G.Ziegler, "Influence of Impurities in Different Processed Si_3N_4-Powders on High-Temperature Properties of Sintered Materials", Brit.Ceram.Proc., No.37, "Special Ceramics 8", Oct., (1986), pp.71-80.

64. D.R.Clarke, J.Am.Ceram.Soc., Vol.65, (1982), p.C21.

65. J.L.Iskoe, F.F.Lange, E.S.Diaz, J.Mater.Sci., No.11, (1976), p.908.

66. J.R.G.Evans, J.Mater.Sci., No.2, (1983), p.19.

67. W.-M.Shen,R.V.Sara, "Characteristics and Processability of Gas Phase Synthesized and Direct Nitridation Si_3N_4 Powders", Conf. paper pres. at 1st Intl. Conf. on Ceram. Powder Process. Sci., Orlando, Florida, Nov.1-4,(1987), pp.1-12.

68. J.M.Schoenung, "Silicon Nitride Powders: Investigating the Costs of Production", Intl. Symp. Fine Particles, Montreal, (1988), pp.1-11.

69. D.Segal,"Chemical Synthesis of Advanced ceramic materials",Cambridge University Press,(1989),p.129.

70. B.G.Durham,M.J.Murtha,G.Burnet,"Si_3N_4 by the Carbothermal Ammonolysis of Silica",Adv.Ceram.Mat.,Vol.3,No.1,(1988),pp.45-8.

71. G.Schwier,G.Nietfeld,G.Franz, "Production and Characterization of Silicon Nitride Powders", Mat.Sci.Forum, Vol.47,(1989),pp.1-20.

72. G.Schwier,"Progress in Nitrogen Ceramics",Ed.F.L.Riley,(1983),pp.157-166.

73. M.B.Trigg,J.Drennan, "Synthesis of Silicon Nitride Powders", Proc. Aust. Ceram. Conf.,12^{th}, (1986), pp.54-8.

74. K.S.Mazdiyasni,C.M.Cooke,"Synthesis, Characterization, and Consolidation of Si_3N_4 Obtained from Ammonolysis of $SiCl_4$", J.Am.Ceram.Soc., Vol.56, No.12,(1973),pp.628-33.

75. K.Ishizaki,T.Egashira,K.Tanaka,P.B.Celis,"Direct Production of Ultra-Fine Nitrides (Si_3N_4 and AlN) and Carbides (SiC, WC and TiC) Powders by the Arc Plasma Method", J. Mater. Sci., Vol.24, (1989), pp.3553-9.

76. W.Symons,K.J.Nilsen,S.C.Danforth, "Synthesis and Processing of Laser Synthesized Silicon Nitride Powders", 2^{nd} International Symp. on Ceramic Materials and Components for Engines, Ed.W.Bunk, H.Hausner, (1986), pp.39-54.

77. J.Canteloup,A.Mocellin,"Special Ceramics 6",Stoke on Trent, B.C.R.A., (1975), pp.209-22.

78. R.Bachelard, "La Synthèse des Poudres Céramiques Non-Oxides Par Réduction Carbothermique", Matériaux et Techniques, Dec., (1987), pp.461-5.

79. F.K.Dijen, R.Metselaar, C.A.M.Siskens, Sprechsaal, Vol.117, No.7, (1984), pp.627-9.

80. Mehnar, German Patent, #88999, (1895).

81. BASF, German Patent, #234128, (1909).

82. A.Sinding-Larzen, Storm, German Patent, #229638, (1909).

83. Lindblud, US Patent, #1311568, (1918).

84. Bichowsky, US Patent, #1415280, (1921).

85. S.J.P.Durham,K.Shanker,R.A.L.Drew, "Carbothermal Synthesis of Silicon Nitride: Effect of Reaction Conditions", J.Am.Ceram.Soc.,Dec.(1988).

86. S.Zhang, W.R.Cannon, "Preparation of Si_3N_4 From SiO_2", J.Am.Ceram.Soc., Vol.67, No.10, (1984), pp.691-5.

87. J.G.Lee, P.D.Miller, I.B.Cutler, "Reactivity of Solids", Ed. J.Wood, O.Linquist, N.G.Vannenberg, Plenum Press, N.Y., (1977), pp.707.

88. M.Mori,H.Inoue,T.Ochiai, "Progress in Nitrogen Ceramics", ed. F.L.Riley, (The Hague, Martinus Nijhoff), (1983), pp.149-56.

89. S.A.Siddiqi, A.Henry, "The Influence of Iron on the Preparation of Silicon Nitride From Silica", J.Mater.Sci., Vol.20, (1985), pp.3230-8.

90. K.Shanker,S.J.P.Durham,S.Grenier,R.A.L.Drew, "Carbothermal Synthesis of Sub-Micron Silicon Nitride Powders", submitted to J.Am.Ceram.Soc., April (1991).

91. F.K.van Dijen, J.Pluijmakers, "The Removal of Carbon Residues From Ceramic Powders or Greenware with Ammonia", J.Eur.Ceram.Soc., Vol.5, (1989), pp.385-90.

92. S.J.P.Durham, "Carbothermal Reduction of Silica to Silicon Nitride Powder", Ph.D. Thesis, McGill University, June 1989.

93. C.P.Gazzara, D.R.Messier, "Determination of Phase Content of Si_3N_4 by X-Ray Diffraction Analysis", Ceram.Bull., Vol.56, No.9, (1977), pp.777-80.

94. S.Prochazka,C.D.Greskovich, "Development of a Sintering Process for High-Preformance Silicon Nitride", AMMRC TR 78-32, (1978).

95. G.Wotting, Thesis, TU Berlin, (1983).

96. S.Brunauer,P.H.Emmett,E.Teller, "Adsorption of Gases in Multimolecular Layers", J.Am.Chem.Soc., Vol.60, (1938), pp.309-319.

97. D.W.Budworth, "An Introduction to Ceramic Science", Pergamon Press, (1970), p.158.

98. L.L.Hench,R.W.Gould, "Characterization of Ceramics", Ed.M.Dekker, (1971), p.360.

99. See Ref.28, p.248.

100. R.E.Loehman,D.J.Rowcliffe, "Sintering of Si_3N_4-Y_2O_3-Al_2O_3", J.Am.Ceram.Soc., Vol.63, No.3-4, (1980), pp.144-8.

101. C.Chatfield,T.Ekstrom,M.Mikus, "Microstructural Investigation of Alpha-Beta Yttrium Sialon Materials", J.Mater.Sci., Vol.21, (1986), pp.2297-307.

102. J.L.Latham, "Elementary Reaction Kinetics", Published by Butterworth & Co.Ltd., 2nd edition, (1969), p.79.

103. J.T.Neil,A.E.Pasto,L.J.Bowen, "Improving the Reliability of Silicon Nitride: A Case Study", Adv. Ceram. Mat., Vol.3, No.3, (1988), pp.225-30.

104. A.E.Pasto,J.T.Neil,C.L.Quackenbush, "Microstructural Effects Influencing Strength of Sintered Silicon Nitride", Ultrastructure Processing of Ceramics, Glasses and Composites, ed. L.Hench, D.Ulrich, (1984), pp.476-89.

105. D.Muscat, "Silicon Nitride/Silicon Nitride Whisker-Reinforced Composites", M.Eng. Thesis, McGill University, Aug. 1990.

106. M.T.Laugier, J. Mater. Sci. Letters, No.6, (1987), pp.355-6.

107. M.E.Bowden, K.J.D.MacKenzie, J.H.Johnston, "Reaction Sequence During the Carbothermal Synthesis of β'-Sialon From a New-Zealand Halloysite", Ceramic Developments, Ed. C.C.Sorrell, B.Ben-Nissan, Vol.34-36, (1988), pp.599-603.

108. I.Higgins, A.Hendry, Proc.Brit.Ceram.Soc., Vol.38, (1986), p.163.

109. H.Wada, L.Wang, "Effect of Gas Phase Composition on SiC and Si_3N_4 Formations", Ceram.Eng.Sci.Proc., Vol.11, (1990), pp.1463-79.

110. L.Wang, H.Wada, Presented at the Third International Conference on Ceramic Powder Processing Science, Am.Ceram.Soc., February, (1990).

111. H.Wada, "Silicon Nitride and Silicon Carbide Ceramic Whiskers Synthesis and Phase Stability", Proceedings of the International Symposium on Advanced Structural Materials, Montreal, Canada, Ed.D.S.Wilkinson, Pergamon Press, (1988), pp.149-56.

112. S.J.P.Durham, K.Shanker, R.A.L.Drew, "Thermochemistry of the Si-O-N-C System With Relation to the Formation of Silicon Nitride", Can. Metall. Quarterly, Vol.30, No.1, (1991), pp.39-43.

113. G.A.Gogotsi, "Strength of Machine-Building Nitride-Based Ceramics", Institute for Problems of Strength, Academy of Sciences, UkrSSR, Kiev, (1982), p.59.

114. Y.G.Gogotsi, V.A.Laurenko, "The Effect of Carbide and Nitride Additives on the Oxidation Resistance of Silicon Nitride Ceramics", High Temperature Technology, Vol.6, No.2, May (1988), pp.79-86.

115. H.Knoch, G.E.Gazza, J.Am.Ceram.Soc., Vol.62, (1979), p.634.

116. W.F.Knippenberg, Philips Res. Reports, Vol.18, (1963), p.271.

117. M.M.Patience, P.J.England, D.P.Thompson, "Ceramic Alloys of Silicon Carbide With Aluminum Nitride and Nitrogen", Proceedings of the International Symp. on Ceramic Components for Engines, (Hakone, Japan, 1983), Ed. S.Somiya, E.Kanai, K.Ando, KTK Scientific, Tokyo, Japan, (1984), pp.473-9.

118. D.C.Apperley, R.K.Harris, "Nuclear Magnetic Resonance Studies of Silicon Carbide Polytypes", J.Am.Ceram.Soc., Vol.74, No.4, (1991), pp.777-82.

119. A.H.G.Mesquita, "Refinement of the Crystal Structure of SiC Type 6H", Acta Cryst., Vol.23, (1967), pp.610-7.

120. Y.M.Cho, J.A.Charles, "Synthesis of Nitrogen Ceramic Powders by Carbothermal Reduction and Nitridation. Part I Silicon Nitride", Mater. Sci. & Technology, Vol.7, April, (1991), pp.289-98.

121. A.Szweda, A.Henry, K.H.Jack, "Special Ceramics 7", Proc.Brit.Ceram.Soc., No.31, Ed. J.Taylor, P.Popper, (1981), p.107.

122. V.K.La Mer, R.H.Dinegar, "Theory, Production and Mechanism of Formation of Monodispersed Hydrosols", J.Am.Chem.Soc., Vol.72, No.11, (1950), pp.4847-54.

123. L.D.Silverman, "Carbothermal Synthesis of Aluminum Nitride", Adv. Ceram. Mater., Vol.3, No.4, (1988), pp.418-9.

124. Y.Baik, "Carbothermal Synthesis of AlN Using Sucrose", M.Eng. Thesis, McGill University, August (1991).

125. H.Inoue,K.Komeya,A.Tsuge, "Synthesis of Silicon Nitride Powder From Silica Reduction", J.Am.Ceram.Soc., Vol.65, (1982), p.C-205.

126. V.Figusch,T.Licke, "Synthesis of Silicon Nitride Powder by Carbothermal Nitriding of Silica", High Tech. Ceramics, ed. P.Vincenzini, Elsevier Press, Holand, (1987), p.517.

127. S.Arrhenius, Z.Phys.Chem. (Leipz), Vol.4, (1889), p.226.

128. M.J.Pilling, "Reaction Kinetics", Clarendon Press, Oxford, (1975), p.14.

129. G.Pannetier,P.Souchay, "Chemical Kinetics", Elsevier Publishing Co. Ltd., (1967), p.387.

130. M.Avrami, "Kinetics of Phase Change. I", J. Chemical Physics, Vol.7, December, (1939), pp.1103-12.

131. M.Avrami, "Kinetics of Phase Change. II", J. Chemical Physics, Vol.8, February, (1940), pp.212-24.

132. M.Avrami, "Kinetics of Phase Change. III", J. Chemical Physics, Vol.9, February, (1941), pp.177-84.

133. J.M.Shultz, "Treatise on Materials Science and Technology", Academic Press Publishing Co. Ltd., Vol.10, (1977), pp.247-51.

134. J.L.Blumenthal,M.J.Santy,E.A.Burns, "Kinetics Studies of High-Temperature Carbon-Silica Reactions in Charred Silica-Reinforced Phenolic Resins", J. Amer. Institute of Areonautics & Astronautics, Vol.4, No.6, (1966), pp.1053-7.

135. J.J.Biernacki,G.P.Wotzak, J.Am.Ceram.Soc., Vol.72, (1989), p.132.

136. M.D.Pugh and R.A.L.Drew, "Processing Improvements in a Sintered Si_3N_4 Material", Report prepared for CUICAC, (1988).

137. J.E.O.Ovri,T.J.Davies, "Effect of Surface Condition on the Flexural Strength of Sintered Silicon Nitride", J.Mater.Sci.Letters, Vol.6, (1987), pp.849-50.

138. J.L.Henshall,D.J.Rowcliffe,J.W.Edington, "The Fracture Toughness and Delayed Fracture of Hot-Pressed Silicon Nitride", Brit.Ceram.Soc., "Special Ceramics 6", (1984), pp.185-98.

139. T.Nose,T.Fujii, "Evaluation of Fracture Toughness for Ceramic Materials by a Single-Edge-Precracked-Beam Method", J.Am.Ceram.Soc., Vol.71, No.5, (1988), pp.328-33.

140. A.G.Evans,E.A.Charles, "Fracture Toughness Determinations by Indentation", J.Am.Ceram.Soc. Discussion and Notes, Vol.59, No.7-8, (1976), pp.371-2.

APPENDICES

APPENDIX I

X-RAY DIFFRACTION CALIBRATION CURVES

In order to estimate the α-SiC and the β-Si_3N_4 content in a α-Si_3N_4 powder, calibration curves were generated (Fig.I-1). In both cases, the curves were obtained by adding known amounts of pure α-SiC (in-house synthesis) or β-Si_3N_4 (from fully sintered commercial powder*) to an α-Si_3N_4 powder* (the small amount of β-Si_3N_4 present in the α-Si_3N_4 powder was taken into account in the measurement and calculation). In order to have complete calibration curves, this procedure was repeated with different amounts of α-SiC and β-Si_3N_4. These very fine (<325 mesh) powders were mixed with a mortar and pestle, and then, put into a XRD sample holder. X-ray diffraction patterns were then taken for the various mixtures of α-SiC/α-Si_3N_4 and β-Si_3N_4/α-Si_3N_4.

For each of the α-SiC, α-Si_3N_4, and β-Si_3N_4 diffraction patterns, a single peak was selected (Table I-1). The selection criteria for each peak was based on factors such as their high relative intensity, and whenever possible, their lack of overlap with peaks of the other phases. The JCPDS standard diffraction pattern for α-SiC that was used in this study was 29-1131 (Moissanite-6H).

The XRD calibration curves are given as a plot of the net relative intensity (total intensity - background) ratio of the selected peaks (Eqn.I-1) versus weight% content of the phase of interest.

Table I-1 : Selection of diffraction peak angle for calibration curves.

	ANGLE 2θ SELECTED (MILLER INDICES)		
Calibration curve	α-Si_3N_4 phase	β-Si_3N_4 phase	α-SiC phase
β-Si_3N_4/α-Si_3N_4	31.0^o (201)	27.1^o (200)	——
α-SiC/α-Si_3N_4	20.6^o (101)	——	35.8^o (102)

* SN-E-10, UBE Industries LTD.

$$(I\text{-}1) \qquad \text{Ratio} = \frac{(I_{\text{phase 1}} - \text{BKG})}{(I_{\text{phase 1}} - \text{BKG}) + (I_{\text{phase 2}} - \text{BKG})}$$

Where . BKG = Background intensity

I_i = Intensity of selected peak i

a

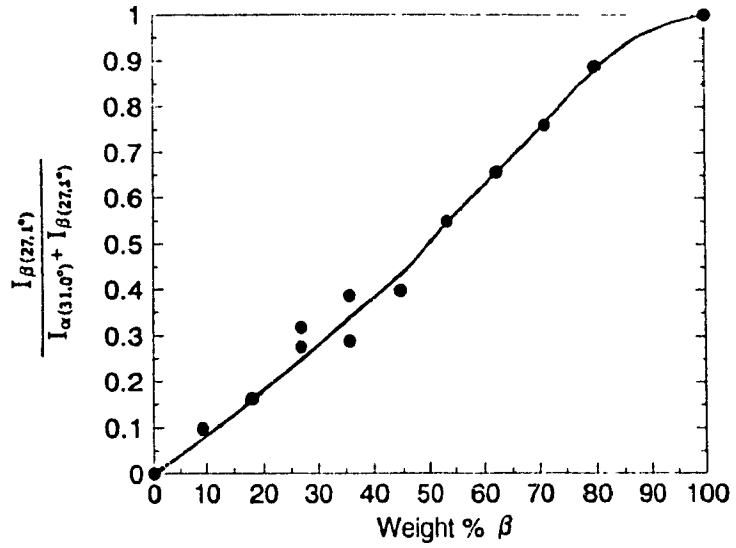

b

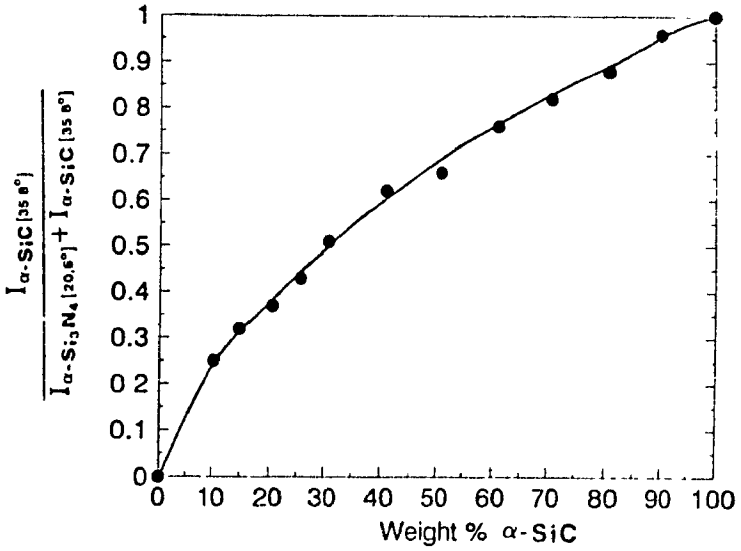

Figure I-1 : XRD Calibration curves; (a) β-Si_3N_4/α-Si_3N_4
(b) α-SiC/α-Si_3N_4

APPENDIX II

COMPARISON BETWEEN PARTICLE SIZE OBTAINED WITH THE DLS TECHNIQUE AND THOSE OBTAINED BY SEM

Table II-1 compares the average diameters (d) calculated with SEM micrographs (expressed on a % number basis), with the average diameters obtained with the DLS technique (expressed on both a % number and a % volume basis).

Table II-1 : Average diameter of seeded α-Si_3N_4 powders (7:1 weight of ZrO_2 media:weight of solids).

Attrition milling time of precursors (hours)	$\bar{d}$, calculated with SEM micrographs (μm) % number	$\bar{d}$, obtained with DLS technique* (μm)	
		% number	% volume
0.5	0.73	0.762	0.847
1	0.56	0.556	0.602
2	0.50	0.566	0.599
4	0.40	0.481	0.517

Both techniques showed relatively good agreement, with a maximum difference of ~ 0.08 μm (at 4 hours A.M.) for the average diameters on a % number basis. The small discrepency between the two values is thought to be related to the difficulty in obtaining a good dispersion of particles for the DLS technique. The lack of dispersion results from the formation of soft agglomerates and these being seen as larger particles, thus yielding average diameters that are usually slightly larger than those calculated with SEM micrographs.

* The DLS results represent an average of 3-4 measurements.

APPENDIX III

WEIGHT LOSS vs REACTION TIME DATA

Table III-1 contains the *weight loss* vs *reaction time* data that was used to build the graphs in Figures 4.23 and 4.25 (see section 4.4).

Table III-1 : Weight loss and % conversion as a function of reaction time (1490°C for various precursors).

	Precursors					
	0.5 hour A.M.- no seed		0.5 hour A.M.- 5 weight% seed		4 hours A.M.- 5 weight% seed	
Reaction time (hours)	Wt loss (%)	Extent of conversion (%)	Wt loss (%)	Extent of conversion (%)	Wt loss (%)	Extent of conversion (%)
0*	9.2	~ 1	7.9	~ 1	11.1	~ 1
0.5	11.5	10.6	11.1	11.4	14.8	14.9
2	17.4	32.1	18.4	37.4	22.7	46.6
	---	---	22.8	53.0	23.7	50.6
3.5	---	---	21.9	49.8	23.5	49.8
4.25	19.1	38.3	23.1	54.1	---	---
5	22.7	51.5	25.9	64.1	30.6	78.3
6.5	29.2	75.2	33.2	90.0	32.9	87.6
8	30.9	81.4	34.4	94.3	34.6	94.4
12	34.2	93.4	35.4	97.9	33.8	97.6

* A reaction time of 0 hours was approximated by stopping the experiment as soon as the starting materials reached the reaction temperature.

The weight loss data was obtained by measuring the difference in weight of the precursors before, and after the reaction, while the extent of conversion data was derived from O_2 and N_2 analysis performed on the reacted products.